ANL-6912

ANL-6912

Argonne National Laboratory

REACTOR DEVELOPMENT PROGRAM

PROGRESS REPORT

June 1964

LEGAL NOTICE

This report was prepared as an account of Government sponsored work. Neither the United States, nor the Commission, nor any person acting on behalf of the Commission:

A. Makes any warranty or representation, expressed or implied, with respect to the accuracy, completeness, or usefulness of the information contained in this report, or that the use of any information, apparatus, method, or process disclosed in this report may not infringe privately owned rights; or

B. Assumes any liabilities with respect to the use of, or for damages resulting from the use of any information, apparatus, method, or process disclosed in this report.

As used in the above, "person acting on behalf of the Commission" includes any employee or contractor of the Commission, or employee of such contractor, to the extent that such employee or contractor of the Commission, or employee of such contractor prepares, disseminates, or provides access to, any information pursuant to his employment or contract with the Commission, or his employment with such contractor.

Price **$2.25** *. Available from the Office of Technical Services, Department of Commerce, Washington 25, D.C.*

ANL-6912
Reactor Technology
(TID-4500, 31st Ed.)
AEC Research and
Development Report

0545

ARGONNE NATIONAL LABORATORY
9700 South Cass Avenue
Argonne, Illinois 60440

REACTOR DEVELOPMENT PROGRAM PROGRESS REPORT

June 1964

Albert V. Crewe, Laboratory Director
Stephen Lawroski, Associate Laboratory Director

Division	Director
Chemical Engineering	R. C. Vogel
Idaho	M. Novick
Metallurgy	F. G. Foote
Reactor Engineering	L. J. Koch
Reactor Physics	R. Avery
Remote Control	R. C. Goertz

Report Coordinated by
R. M. Adams and A. Glassner

Issued July 21, 1964

Operated by The University of Chicago
under
Contract W-31-109-eng-38
with the
U. S. Atomic Energy Commission

FOREWORD

The Reactor Development Program Progress Report, issued monthly, is intended to be a means of reporting those items of significant technical progress which have occurred in both the specific reactor projects and the general engineering research and development programs. The report is organized in a way which, it is hoped, gives the clearest, most logical over-all view of progress. The budget classification is followed only in broad outline, and no attempt is made to report separately on each sub-activity number. Further, since the intent is to report only items of significant progress, not all activities are reported each month. In order to issue this report as soon as possible after the end of the month editorial work must necessarily be limited. Also, since this is an informal progress report, the results and data presented should be understood to be preliminary and subject to change unless otherwise stated.

The issuance of these reports is not intended to constitute publication in any sense of the word. Final results either will be submitted for publication in regular professional journals or will be published in the form of ANL topical reports.

The last six reports issued in this series are:

December 1963	ANL-6810
January 1964	ANL-6840
February 1964	ANL-6860
March 1964	ANL-6880
April 1964	ANL-6885
May 1964	ANL-6904

TABLE OF CONTENTS

TABLE OF CONTENTS

TABLE OF CONTENTS

TABLE OF CONTENTS

I. BOILING WATER REACTORS

A. BORAX-V

1. Operations

At the end of June, BORAX-V had been operated at power with the peripheral superheater core, PSH-1, for a total of 121 megawatt-days. Of the 36 reactor startups and shutdowns this month, sixteen cycles included draining and flooding of the superheater. The reactor vessel was above 400°F throughout each 5-day work week, and pressure was reduced to atmospheric on the weekends.

Transfer function measurements were made at zero power, 5, 10, 15, and 18.1 MWt. Experiments at 18.1 MWt were not completed due to apparent failure in the rotating oscillator or drive shaft within the reactor vessel.

Flux wires were irradiated at four power levels to determine the neutron flux and cadmium ratio distribution in the core. The flux wires were inserted in thimbles projecting into coolant channels in the core. Flux distribution and cadmium ratio measurements at four power levels were also made by using miniature fission ionization chambers in thimbles which project into boiling fuel rod positions in the core.

Radiation levels throughout the plant have remained at low values (see Table I).

Table I. Radiation Levels of BORAX-V during Operation with Peripheral Superheat Core PSH-1

	mr/hr			
Power Level, MWt	5	10	15	20
Main Steam Line, Reactor Bldg.*	20-30	50-90	85-100	100
Turbine Building Main Floor**	1-3	7-18.5	14-27	35-43
Condenser Hotwell	1-5	10-35	23-75	105-110
Air Ejector Exhaust Absolute Filter	1-5	4-28	28-48	27-110
Air Ejector Exhaust Charcoal Filter	1-5	5-22	12-31	17-155
Reactor Water Line to Bypass Demineralizer	8-26	23-80	34-90	95-100

*Monitor located about 5 ft from the main steam pipe line. The pipe line distance from the reactor vessel is about 50 ft.

**Monitor located about 10 ft from main steam pipe line. The pipe line distance from the reactor vessel is 300 ft.

2. Experiments

a. Power Split Experiment. According to reactor design, 19% of the core power should be produced in the superheater and 81% in the boiler. From flux wire irradiations at zero power and room temperature, the fraction of the power produced in the superheater was about 17% with all 9 control rods banked.

Some control of this power split should be effected by changing the position of the control rods in the superheating region in relation to the position of the control rods in the boiling region. To determine the extent of such control, the control rod positions were changed while maintaining approximately the same power level. Table II shows that for these conditions the power in the superheater can be varied from 16 to 18.3% of the total power.

Table II. Change in Superheater-boiler Power Split by Control Rod Manipulation with Core PSH-1 in BORAX-V

Power Level (MWt)	Superheater Exit Steam Temp (°F)	Control Rod Positions (in.)			Percent Power Produced in Superheater
		Central	Intermediate Gang	Outside Gang	
8.1	820	19.80	19.80	19.80	17.9
7.6	830	17.50	19.80	25.00	18.3
7.4	790	25.00	19.80	16.00	16.9
7.3	765	25.00	25.00	12.00	16.0

For one full working week, the reactor was operated continuously without a shutdown, the power level being maintained at maximum for most of the time. Due primarily to the buildup of fission product poisoning, the maximum possible power with control rods fully withdrawn was reduced from about 18.0 MWt to 10.5 MWt. The reactor water cleanup demineralizer was kept at the same flow, 36 gpm. At the start of the run (power level of 17.6 MWt), the power produced in the superheater was 17.9%; at the end of the run (10.5 MWt), 16.7% of the power was being produced in the superheater.

b. Low-power Oscillations. On several occasions while using a combination of electric and low-power nuclear heating to raise the reactor with core PSH-1 to operating temperature and pressures, the usually random boiling noise on a neutron flux trace has exhibited cyclic characteristics. This phenomenon has occurred only at low pressures in a range of 150-220 psig with reactor powers of 50-100 kW and with the external electric preheat system furnishing 254 kW. During this heating operation, the coolant channels in the superheater were flooded and the superheater interpass plenum chambers were interconnected to the steam dome and steam

line via the pressure-equalizing valves. All steam line valves were closed, and feedwater was supplied only by in-leakage of control rod drive and auxiliary pump seal water. The seal water system flowmeters indicated a steady flow rate.

The oscillations, as observed on the linear neutron flux recorder, had a cycle time of about 10 sec. The period meter indicated ±10 sec. Maximum amplitude observed was ±17% of average power. The amplitude decreased as the pressure increased for a given power, but the amplitude increased when power was raised. Above about 220 psig, the linear flux trace reverted to random boiling noise. Figure 1 shows a typical portion of the linear flux trace.

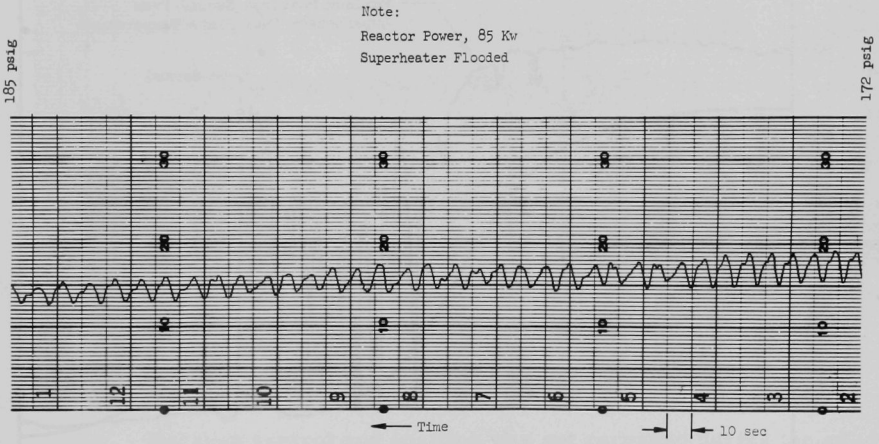

Figure 1. Low-pressure Oscillations with Core PSH-1 of BORAX-V

c. Superheater Wetting Experiment. It has been predicted that flooding of an integral nuclear superheater while the reactor was operating at power would be retarded by the flashing of the water to steam on the high-temperature superheater fuel elements and that the resulting change in reactivity would be slow. This theory has been at least partially confirmed by an unplanned experiment with the core containing peripheral superheater PSH-1, which occurred as follows:

During operation on June 8, the reactor had leveled off at 20 MWt at 1030 hr. At about 1034, the steam line and superheater fuel plate temperatures began to decrease rapidly, as shown in Figure 2. At about 1035, the reactor operator started to insert control rods slowly to maintain a constant power. At about 1039 and 50 sec, the operator started to insert control rods rapidly to reduce power, and at about 1040 the reactor

was scrammed by a signal indicating high reactor water level. The incident was caused by the sticking of the reactor water-level recorder which controls the feedwater flow. The reactor water-level recorder indication rose from 11 ft to 13 ft 2 in. immediately after the scram. The feedwater flow rate increased steadily throughout the experiment and went off scale on the recorder at 150 gpm about 2 min before scram. Reactor pressure remained constant at 600 psig, but indicated steam flow rate increased from 45,000 to about 50,000 lb/hr. The superheater pressure drop increased from 15 to 24 psi during the experiment.

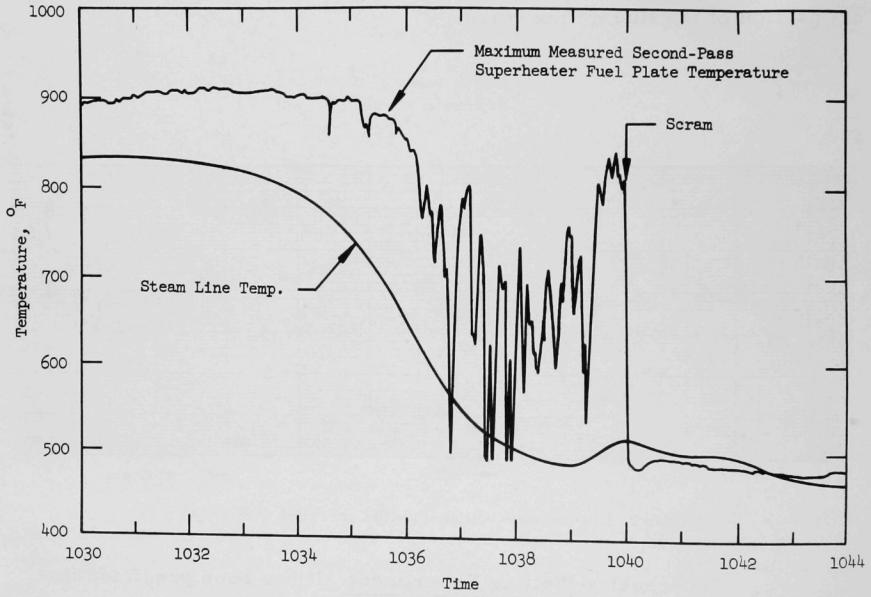

Figure 2. Superheater Fuel and Steam Line Temperatures vs. Time in Superheater Wetting Experiment with Core PSH-1 of BORAX-V

The reduction in steam line and superheater fuel temperatures shown in Figure 2 is believed to have been caused by carryover of steam-water foam into the superheater due to the high reactor water level and the extreme turbulence of the steam-water mixture at 20 MWt. The actual steam-foam interface at an indicated level of 13 ft 2 in. is estimated to be about 1 to 2 ft higher, while the height of the superheater inlets is 14 ft 5 $\frac{1}{2}$ in. to 14 ft 7 $\frac{1}{2}$ in. The minimum amount of moisture carried over into the superheater required to reduce the steam line temperature from 830°F to saturation at 489°F is calculated to be about 9,000 lb/hr.

The effect of the moisture carryover into the superheater on the boiling noise can be seen on the linear neutron flux trace shown in Figure 3, where the noise begins to increase at about 1036 hr.

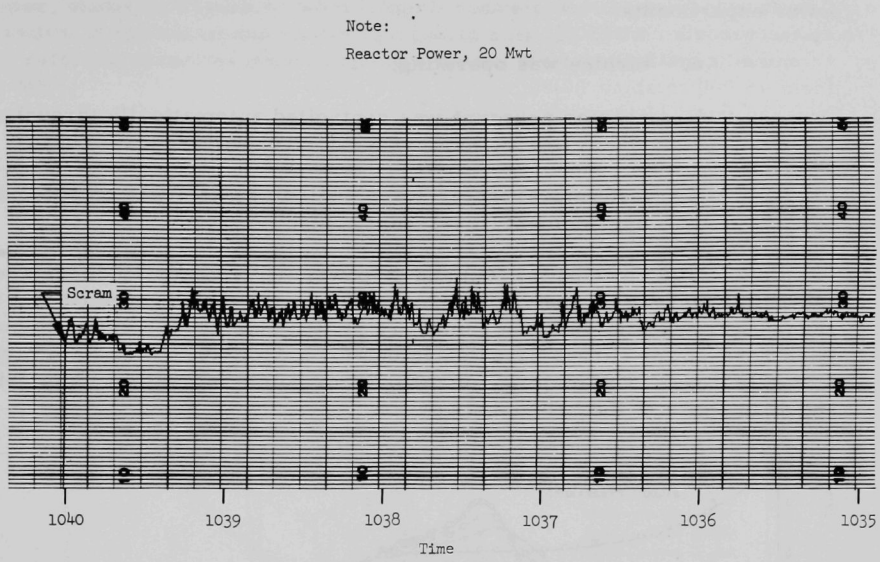

Figure 3. Linear Neutron Flux Plot in Superheater Wetting Experiment with Core PSH-1 of BORAX-V

Because control rod position was not recorded during the experiment and because of the uncertainty of control rod worth at high powers, no accurate estimate of the actual reactivity addition or rate of addition, due both to moisture in the superheater coolant channels and higher inlet subcooling due to the excessive feedwater flow, can be made. However, the observed reactivity values were low and the addition rate slow. During this operation, the reactor power level and the 5-sec period reactor scram circuits were in effect.

d. Measurements of Reactor Transfer Function. Measurements of reactor transfer function were made at zero power, 5, 10, 15 and 18.1 MWt to determine the stability of the PSH-1 core. The fueled oscillator, with a rotor made of U-Zr and hafnium, was located in the reflector just outside the core. The cross-correlation analog computer transfer function measuring equipment was essentially the same as that for core B-2. New Donner Model 3200 analog computer components were used in the computing section.

The overall frequency response was measured at about 22 frequency points at each power level, except for a power level of 18.1 MWt, for which only 13 points were taken. All transfer functions were measured at reactor conditions of 489°F and 600 psig, and, in addition for the at-power experiments,

a. turbine was operating;

b. reactor pressure was controlled automatically through the steam line back-pressure control valve;

c. feedwater-reactor-level control system was on automatic one-element (level only) control.

The zero-power (G_0) and at-power (G) transfer functions are shown in Figure 4 for the various power levels. It should be noted that the zero-power transfer function points are plotted along with a set of calculated zero-power curves based on values for a $\tilde{\beta}$ of 0.0071 and for ℓ^* of 3.22×10^{-5} sec. The majority of zero-power points fell within 1% in gain and 1° in phase of the calculated curves.

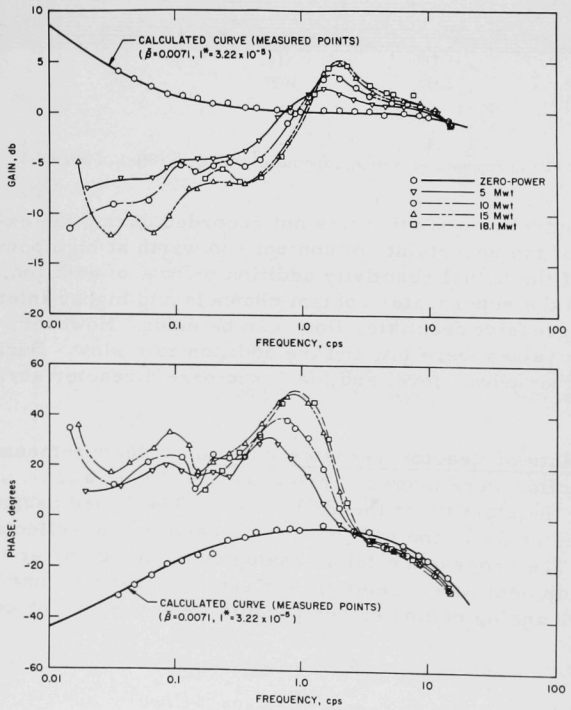

Figure 4

Overall Gain and Phase vs. Frequency for Various Power Levels with Core PSH-1 of BORAX-V

The open-loop (G_0H) Nyquist diagrams at the various power levels are shown in Figure 5. Although all the loci do cross the 180° axis into the second quadrant, a great margin of stability is apparent since none comes close to encircling the -1,0 point. The gain and phase margins vs. power, shown in Figure 6, more clearly indicate the large margin of reactor stability at the maximum power reached to date (22 MWt). Extrapolation of the gain and phase margins suggests a power level instability at about 39 MWt.

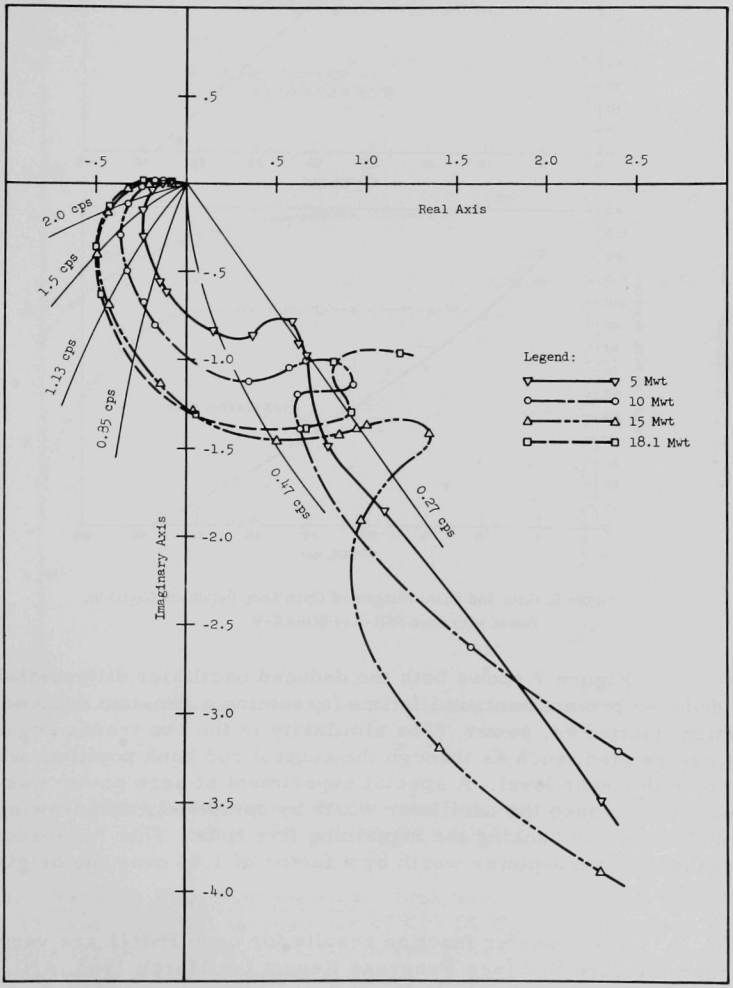

Figure 5. Open Loop Response (G_0H) for Various Power Levels with Core PSH-1 of BORAX-V

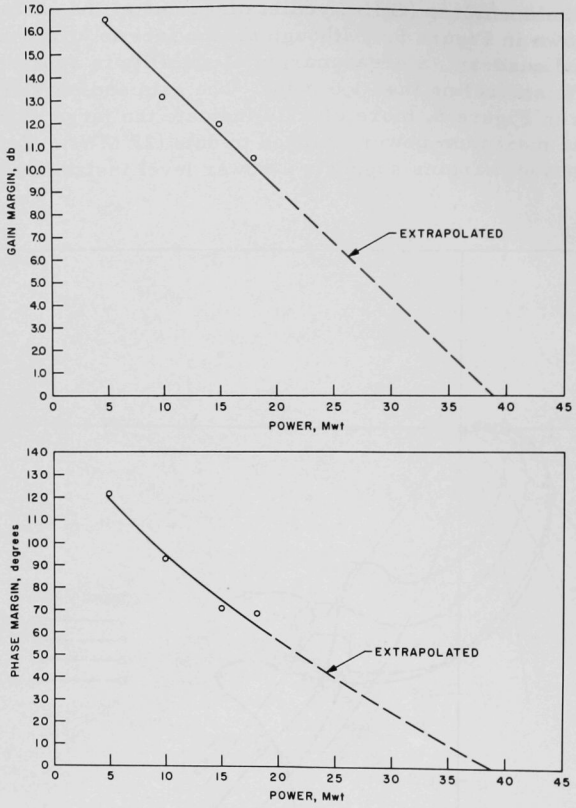

Figure 6. Gain and Phase Margins of Open Loop Feedback (G_oH) vs. Power with Core PSH-1 of BORAX-V

Figure 7 shows both the deduced oscillator differential worth and deduced prompt neutron lifetime (assuming a constant delayed neutron fraction) plotted vs. power. The similarity in the two trends suggests that they are related, such as through the control rod bank position, which varies with power level. A special experiment at zero power was performed to increase the oscillator worth by completely withdrawing the four outer T-rods and banking the remaining five rods. This "unshadowing" increased the zero-power worth by a factor of 1.44 over the original value of 2.8¢.

The transfer function results for core PSH-1 are very similar to those for core B-2 (see Progress Report for March 1963, ANL-6705). The resonance peaks have similar values versus power, and the trend of resonance frequency with power is almost identical.

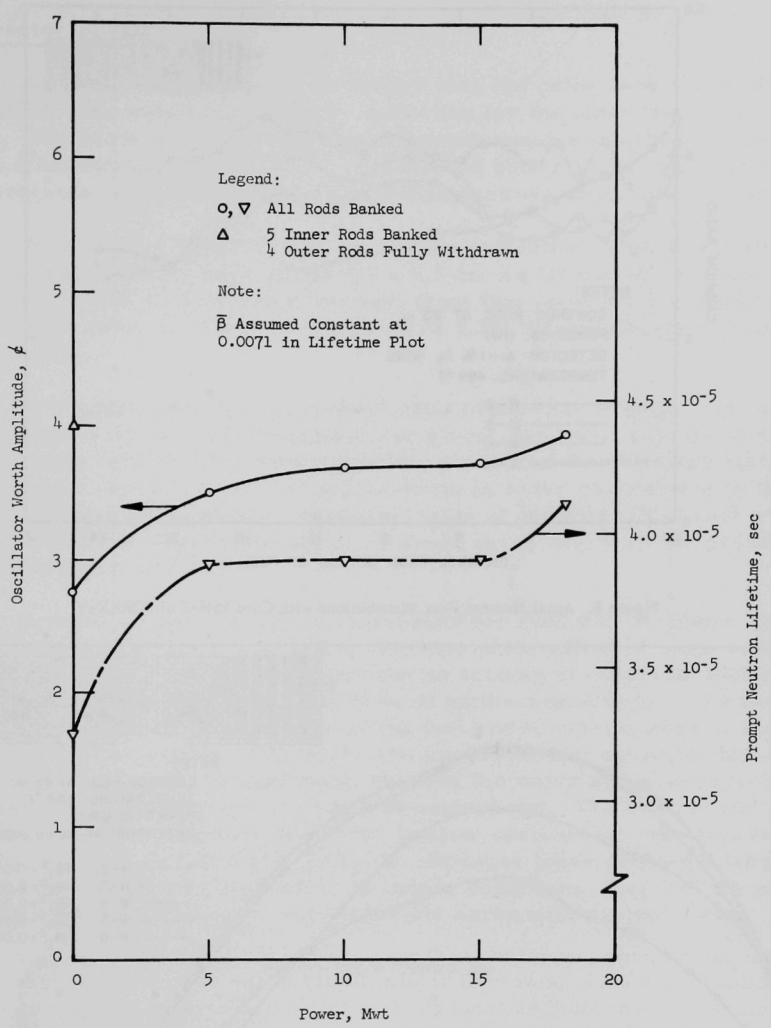

Figure 7. Oscillator Reactivity Worth and Prompt Neutron Lifetime vs. Power with Core PSH-1 of BORAX-V

e. Neutron Flux Distributions. Flux wire irradiations were made at 5, 10, 15, and 19.4 MWt through use of Al - 1% Cu wire. Neutron flux distributions for the 15-MWt irradiation are shown in Figure 8, along with the axial buckling at the flux wire locations. Figure 9 shows the cadmium ratio distributions at 15 MWt. Analysis of the remaining data is continuing.

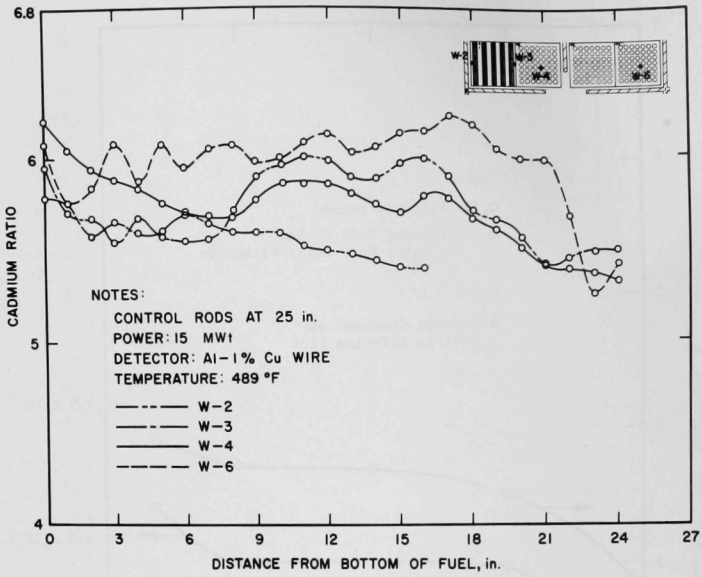

Figure 8. Axial Neutron Flux Distributions with Core PSH-1 of BORAX-V

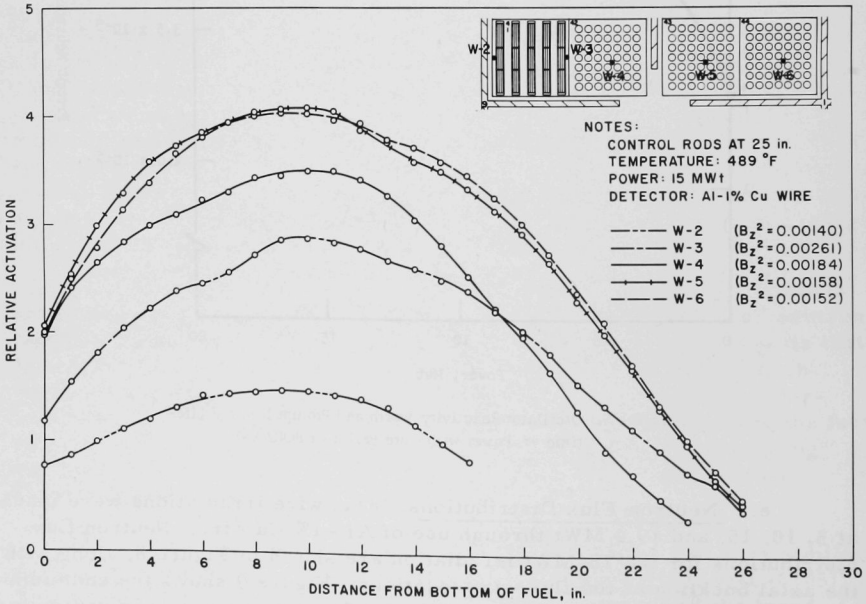

Figure 9. Axial Cadmium Ratio Distributions with Core PSH-1 of BORAX-V

3. Reactor Physics

Several calculations for the boiler fuel rod cells were made with the TOPIC code assuming isotropic reflection for the outer boundary condition. Problems were run with various water annulus thicknesses (to obtain disadvantage factors over a 12-flow-rod boiler assembly), various temperatures, and various boric acid concentrations at room temperature.

Preliminary inspection of the results indicates a significant difference in the disadvantage factor for a 0.5-in.-sq lattice cell at room temperature (the 49-fuel-rod assembly) from that reported previously.[1] The present value of $\overline{\phi}(H_2O)/\overline{\phi}$ (fuel rod) is 1.25; the previously reported value is 1.18.

The experimentally measured[2] ratio of average-to-edge flux in the fuel rod was 0.91 (no experimental error given); the value calculated in the present work is 0.90. The experimentally measured disadvantage factor was 1.18 (not corrected for flux perturbation in water channel due to flux wires). If the experimentally measured value of $\overline{\phi}(H_2O)/\overline{\phi}$ (fuel rod) were corrected for the wire perturbation, it would agree well with the present calculated value of 1.25.

Several simple one-group, one-assembly PDQ cell problems have also been run to obtain a qualitative estimate of the effect of boric acid on control rod worth. These problems take no account of change in fuel rod disadvantage factor due to boric acid or of epithermal effects. The fuel region extended from outside edge of the fuel rod to outside edge of fuel rod - a 3.375-in. square. The water and aluminum fuel assembly box between assemblies was homogenized, as were the water and aluminum box and control rod shroud between fuel and control rod. The control rod region, including the stainless steel clad (poison section in), was treated with the logarithmic boundary condition. Because these problems treated only one assembly with symmetric boundary conditions, they had the effect of completely surrounding a four-assembly array with control rods.

The control rod worth can be defined as

$$\frac{\Delta k}{k}\,(\text{rods}) = \frac{\Delta f}{f},$$

where f is the thermal utilization in the fuel region and

$$\Delta f = [f(\text{rod follower in}) - f(\text{rod absorber in})];$$

$$f = f(\text{rod follower in}).$$

---

[1] Design and Hazards Summary Report, BORAX-V, ANL-6302, p. 68.
[2] Kirn, F. S., and Hagen, J. I., BORAX-V Exponential Experiment, ANL-6707.

Since only ratios of thermal utilization are involved, f can be redefined to be the fraction of all neutrons absorbed in the fuel region. Table IIIA shows the pertinent results of these calculations, and Table IIIB gives the values of control rod worth for this simplified model. These results indicate that with 5 g H_3BO_3 per gallon of water, the fractional change in total control rod worth is about -5%, and with 10 g/gal H_3BO_3 the fractional change is about -10%.

Table IIIA. Absorption Fractions

Boric Acid Concentration, $g(H_3BO_3)/gal(H_2O)$	Control Rod Follower In			Control Rod Absorber In		
	Control Rod Region	Fuel Region	Water-Al Regions	Control Rod Region	Fuel Region	Water-Al Regions
0	0.0062	0.9284	0.0654	0.1921	0.7757	0.0323
5	0.0058	0.9120	0.0822	0.1883	0.7700	0.0417
10	0.0055	0.8971	0.0973	0.1846	0.7647	0.0506

Table IIIB. Calculated Control Rod Worths

Boric Acid Concentration, $g(H_3BO_3)/gal(H_2O)$	Control Rod Worth = $\frac{f(\text{rods out}) - f(\text{rods in})}{f(\text{rods out})} = \frac{\Delta k}{k}$	Percentage Change in Control Rod Worth
0	0.1645	0
5	0.1557	5.35
10	0.1476	10.27

Several one-dimensional one-group calculations had been run previously on this same problem, and their results were almost identical to the two-dimensional work reported here.

4. Maintenance

Maintenance has been mainly for conventional power plant equipment. Steam-line valve packings and flange gaskets have developed leaks and have been replaced. A control rod drive motor control overload heater failed and was replaced. The reactor water level recorder pen drive motor stuck and caused a reactor scram (see Sect. 2c above). The recorder motor was replaced. Four superheater fuel thermocouples failed. One of the failures caused a reactor scram. Various adjustments and tests have been made on automatic control for reactor pressure, reactor water level, and desuperheater temperature control. Three sections of reactor water level gauge glass have been replaced.

5. Water Chemistry

Routine monitoring during operation of pH, resistivity, oxygen concentration, chloride concentration, fission products, and gross specific activity was continued for this period with core PSH-1. Table IV summarizes the range of the values observed for these parameters.

Table IV. Values of Water Parameters

Parameter	Reactor Water	Saturated Steam Condensate	Superheated Steam Condensate	Condenser Condensate	Feedwater
pH	6.0-6.7	5.6-6.15	5.3-6.15	-	-
Resistivity (megohm-cm)	1.2-5.0	0.74-3.3	0.60-3.2	0.3-2.5	4.3-12.7
Chloride Conc (ppm)	-	0.0-0.02	-	0.06	-
Oxygen Conc (ppm)	0.2-0.5	25-28	24-27	-	5.0-7.0
Gross Specific Gamma Activity (counts/min/ml)	91,000 to 382,000	3,300 to 7,500	4,700 to 23,000	-	-
Fission Product Monitor (c/min)	-	0-1800	0-3000	-	-

The resistivity and pH of the reactor water tended to drift down during power operation if the reactor water demineralizer was off. With the demineralizer on, this trend was reversed, with the pH approaching 7 and the resistivity becoming higher. The highest resistivities were generally attained after several hours of operation of the demineralizer with the reactor at zero power.

The chloride concentration remained low in the saturated steam during the entire period and was not power-dependent. On one occasion, shortly after noting a sudden decrease in the resistivity of the condenser condensate, a check of chloride concentration in the condensate gave 0.06 ppm.

The fission product monitor count on saturated steam was generally 400-500 c/min during steady operation at any power and seemed to be independent of power level. The maximum count (1800 c/min) was observed just after achieving power and always decayed down to 400-500 c/min after about an hour of steady operation.

The fission product count on the superheated steam behaved similarly, with a maximum of 3000 c/min observed. At steady operation, the observed maximum was ~1700 c/min. The count rate on the steam was observed to be power-dependent to a slight extent.

The data of an aluminum nitrate addition test to study the increase of Na^{24} in the reactor water, by the (n,α) reaction, are being analyzed. During this test, increased rates of gas production, crud concentration, conductivity, and pH changes were observed. By using the presence of the Na^{24} formed, a steam quality measurement in the reactor vessel steam dome was also carried out with the movable steam probe. The axial traverse shown in Figure 10 indicates that steam quality at the height of the superheater inlets was close to 100%.

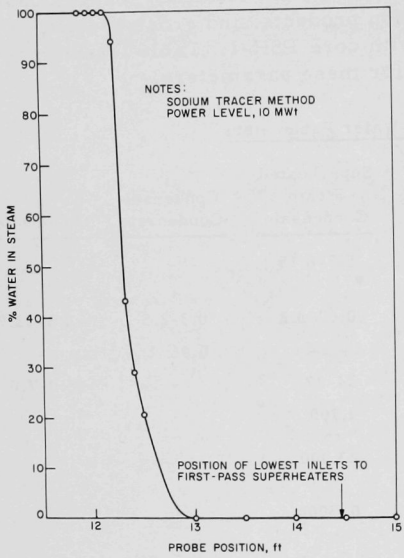

Figure 10. Steam Quality Profile in Steam Dome with Core PSH-1 of BORAX-V

Deposition samples mounted in the steam line about 50 ft from the reactor were removed and scanned for deposited radioisotopes. Initially, only Na^{24} was observed; as this decayed out, detectable amounts of Co^{60}, Co^{58}, and Cr^{51} were identified. No differences in deposited isotopes on the samples of Type 304 stainless steel, Cr-Mo steel, and carbon steel were found.

B. Experimental Boiling Water Reactor (EBWR)

1. Examination of a Fuel Element

The initial phase of the postirradiation examination of fuel element ET-11 after 100-MW operation of EBWR has been completed. The element contained "thin" fuel plates, 5.38 mm thick, and was irradiated to approximately 0.5 a/o burnup.

Visual examination of the element before disassembly indicated a generally good condition. No cracks or preferential corrosion were noted at riveted areas. Scale buildup was noticeable, and buckling of the Zircaloy-2 side plates had occurred to some extent. The individual fuel plates were not warped and did not appear to have external defects. The scale deposit was generally adherent but had undergone flaking on the lower half of the element. A localized area of scale buildup was noted on one plate.

Measurements of the channel gaps (the spaces between the fuel plates) were inconclusive in determining fuel plate swelling. Apparent removal of the scale deposit during measurement contributed

to the scatter of the results. Fuel plate thicknesses were measured prior to descaling. The largest increase, based on an initial thickness of 5.38 mm, was 0.76 mm and was due to localized scale buildup. The average increases in individual plate thickness ranged from 0.18 to 0.33 mm.

Descaling operations were unsuccessful since the bottom layer or layers of scale were extremely tenacious. The maximum amount of scale removed was 0.13 mm. This probably represents the total thickness of nonadherent scale, since portions of scale removed during disassembly operations measured 0.05 mm in thickness. The measured lengths of the plates were within dimensional tolerances.

Four 1.6-mm-thick specimens were removed from the hottest area of the hottest fuel plate, as determined by gamma scanning, to note any distortion caused by the relief of internal stresses. Severe distortion of test pieces had been observed in an element previously examined that had a burnup of 0.39 a/o. However, no warpage or cracking of the thin sections from the present element was observed. Polishing and etching of the present specimens revealed that several cracks occurred near the edge of the specimen corresponding to the area of highest burnup. A void in the fuel core was noted in this area, but it is not presently known whether it existed prior to the examination.

Postirradiation examination yet to be completed includes fuel burnup analyses, hydrogen analysis of the Zircaloy-2 cladding, chemical analysis of the scale, and metallographic examination of the fuel and cladding.

II. LIQUID-METAL-COOLED REACTORS

A. General Fast Reactor Physics

1. ZPR-III

a. Assembly 45. Upon termination of the RAPSODIE critical assembly experiments, work was begun on Assembly 45, which will be principally used for Doppler effect and sodium void measurements.

Zoned loading methods will be used to make such measurements in a central zone which represents a large plutonium/uranium monocarbide fast power breeder reactor. Refinements in the technique of designing zoned loading allow use of a thinner, more transparent filter or buffer zone between the central zone and driver zones. An inner radial reflector preserves neutrons in the energy region of interest to Doppler measurements. Figure 11 shows a cross-sectional representation of the assembly loading; Figure 12 shows the quality of the radial preservation of the spectrum in the energy range of interest to Doppler measurements.

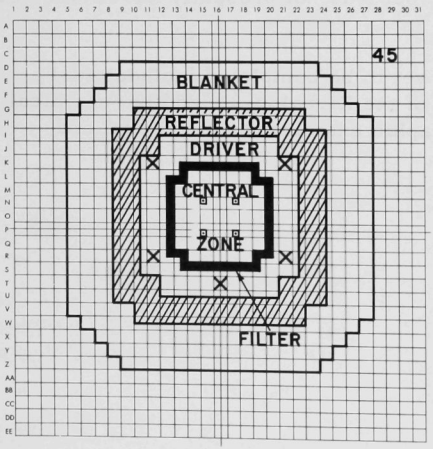

Figure 11. Cross Section of Assembly 45 of ZPR-III

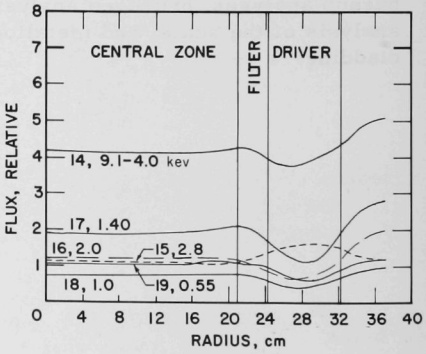

Figure 12. Energy Spectrum for Assembly 45

The Doppler measurements will again be made by the auto-rod procedure which was used to make U^{238} Doppler measurements with Assembly 43.[2] The equipment, however, has been considerably refined. Several Doppler elements will be used rather than a single element; each of

[2] Fischer, G. J., Hummel, H. H., Folkrod, J. R., and Meneley, D. A.; Nuclear Sci. Eng., 18, 290 (1963).

these elements will contain approximately 137 g of fissile or fertile material, rather than approximately 2 kg. U^{238}, Pu^{239}, and U^{235} elements will be used to measure individual isotope effects, and Pu^{239}/U^{238} and U^{235}/U^{238} mixtures will test the Codd-Collins resonance self-shielding effect.

b. Instrumentation. During the month, some of the ZPR-III operating instrumentation was checked.

Work continued on the fast neutron spectrometer experiments. Some success has been achieved with regard to machine calculations for "unfolding" the experimental data. It has been found that a significant number of low-energy neutrons are returned from the concrete shield to the area near the center of the grazing hole. Because of the "1/v" nature of the Li^6 cross section, this gives a large number of low-energy events in the spectrometer data which complicate the "unfolding" of the data. A depleted uranium plug is being fabricated which will be used to block the path through which these low-energy neutrons are returned.

The thermal calibrations of ZPR-III fission foils have been extended to include relative comparisons of the thick-wall Kirn-type fission chambers. The reported electroplated fissile masses have generally been verified.

A comparison between the ZPR-III U^{235} fission chambers and a miniature fission chamber supplied by the French fast reactor group has been completed. Although initial discrepancies existed, the chambers were brought into general agreement after the French group rechecked their mass values.

A comparison has also been made between the ZPR-III fission counters and a counter used by General Electric Company at the Low Power Test Facility.

2. ZPR-VI

a. Assembly No. 3. Experimental measurements with Assembly No. 2 were concluded, and work has started on putting Assembly No. 3 together. Assembly No. 3 (see Table V) will be a carbide core of the same composition as Assembly No. 2, but with length-to-diameter ratio (L/D) of 1:3 instead of 1:1 as in Assembly No. 2. The cylindrical core will be 51 cm in length and have a critical radius of about 77 cm. With this "pancake" core the effect of the increased importance of the neutron leakage on the sodium void coefficient can be measured.

In order to achieve sufficient shutdown reactivity, each dual-purpose control/safety rod will contain five $\frac{1}{16}$-in. fuel columns instead of

two $\frac{1}{16}$-in. columns in the drawers. Three drawers adjoining each control/safety rod position will contain only one $\frac{1}{16}$-in. fuel column to reduce the spectral distortion due to the overloading.

Table V. Composition of Assembly No. 3 of ZPR-VI

	Core		Number and Width of Columns in Drawer, in.	Blanket	
	Atom Density, Atoms/ $cm^3 \times 10^{-24}$	YOM* Volume Fraction		Atom Density, Atoms/ $cm^3 \times 10^{-24}$	YOM* Volume Fraction
U^{235}	0.002285	0.0476	2 x 1/16	8.104×10^{-5}	0.001688
U^{238}	0.009853	0.2052	4 x 1/8	0.03993	0.8318
SS-304**	0.01475	0.1751	-	0.006003	0.07122
Carbon	0.01290	0.1540	3 x 1/8	-	-
Sodium	0.007910	0.3595	4 x 1/4 (cans)	-	-

*Yiftah-Okrent-Moldauer Cross Section. Volume fractions for calculations with YOM cross section sets given in macroscopic units.

**Stainless steel contained in matrix tubes, drawers, and sodium cans. For the calculations the cross sections for iron were used.

Calculated values for Assembly No. 3 are given in Table VI. A value of k_{eff} for a single half was also calculated as part of the safety evaluation during the loading process. Code RE 122, though only one-dimensional, gives the more accurate results because it is used with 16 energy groups, whereas the two-dimensional PDQ code allows calculations with only four energy groups. The calculations tend to overestimate the critical mass because they do not account for the heterogeneity effect which tends to increase the reactivity. It is anticipated that the critical mass will be about 850 ± 50 kg.

Table VI. Calculations for Assembly No. 3 of ZPR-VI

		Critical Parameters						
Code	Cross Section Set	Radius (cm)	Volume (ℓ)	Mass (kg)	No. of Core Drawers	Dual-purpose Rod Worth (%) Δk/k	k_{eff}, Single Half	Poison Rods, (%) Δk/k
RE 122	635	77.55	960.1	858.2	1241	0.184	0.65	0.04 → 0.05
PDQ	149	84.3	1134.4	1010.0	1460	0.164	0.64	(estimated from Assembly No. 2)

b. Sodium Versus Void Coefficients - Modified Drawer Loadings. The drawer-loading pattern of Assembly No. 2 was modified to obtain experimental information about the dependence of the sodium-void coefficients with the sodium distribution. Alternate drawers were filled with sodium-containing cans and the intermediary drawers were filled with fuel, depleted uranium, and graphite. Mating drawers from opposite halves of the reactor were opposite, i.e., a sodium-filled drawer on the stationary half of the reactor was opposite a drawer on the movable half containing fuel, depleted uranium, and carbon. Because of the symmetry of the halves, each radial location in this bunched sodium arrangement still contained on the average

the same quantity of the same core materials as the typical core drawers. Figure 13 shows the modified drawer-loading patterns. Figure 14 shows the portion of the core loaded with these modified drawer loadings. Table VII identifies the drawers contained in each set which make up the experimental region for a typical core loading and for the equivalent bunched loading.

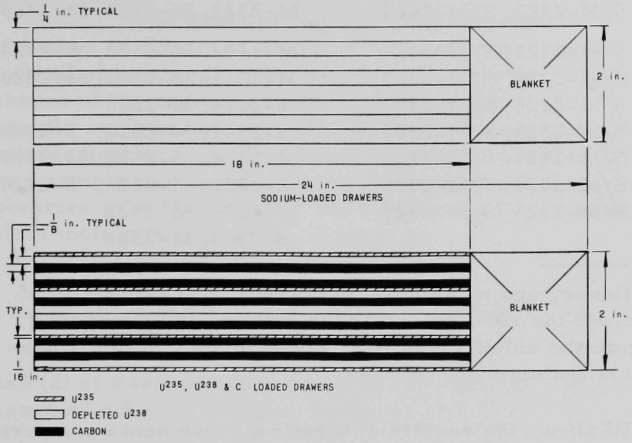

Figure 13

Modified Drawer Loadings

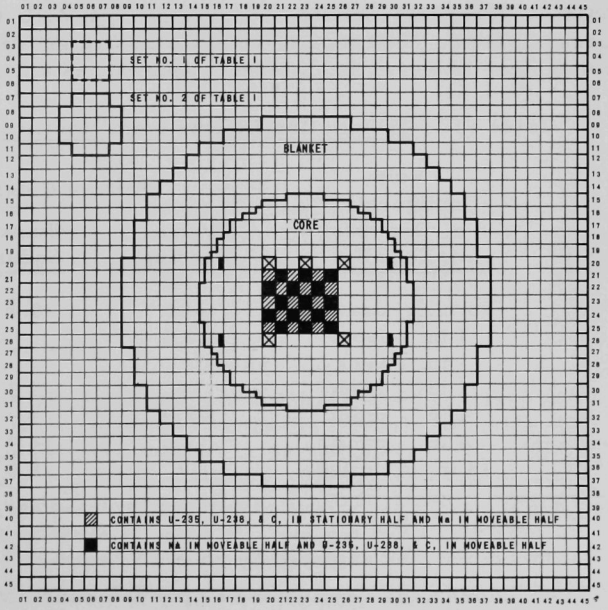

Figure 14

Portion of Core with Modified Drawer Loading

Table VII. Sodium-loaded Drawers

Set	Typical Core Drawers*	Equivalent Bunched Pattern
1	S/M-2222, S/M-2223, S/M-2224	S-2222, S-2224, S-2323
	S/M-2323, S/M-2323, S/M-2324	S-2422, S-2424, M-2223
	S/M-2422, S/M-2423, S/M-2424	M-2322, M-2324, M-2423
2	S/M-2122, S/M-2123, S/M-2124	M-2122, S-2123, M-2124
	S/M-2221, S/M-2222, S/M-2223	M-2221, S-2222, M-2223
	S/M-2224, S/M-2225, S/M-2321	S-2224, M-2225
	S/M-2322, S/M-2323, S/M-2324	S-2321, M-2322, S-2323
	S/M-2325, S/M-2421, S/M-2422	M-2324, S-2325, M-2421
	S/M-2423, S/M-2424, S/M-2425	S-2422, M-2423, S-2424
	S/M-2522, S/M-2523, S/M-2524	M-2425, M-2522
		S-2523, M-2524

*S/M means stationary and movable drawers; the first two digits of the number indicate the row number in the matrix, and the second two digits indicate the column number. Together they define a particular location in the matrix.

Table VIII shows the results of these measurements compared with the measurements obtained for the equivalent typical core drawer loadings (see Progress Report for May 1964, ANL-6904, pp. 15-21). In general, the bunched sodium-void worths are greater than those obtained for typical drawers; the difference approaches a factor of two. This is

Table VIII. Sodium Coefficients from Modified Drawer Loadings

Set	Void Configuration of Drawers in Each Set	Sodium Coefficient, Ih/kg[1]*		
		Typical Loading	Bunched Sodium**	Bunched Sodium†
1	18 in. of drawer	-4.5	-9.1 ± 0.4	-
1	3 in. - front	-1.6	-	-3.0 ± 0.4
1	3 in. - back	-	-	-10.3 ± 0.4
2	7 in. - front	-	-4.3 ± 0.4	-4.3 ± 0.1
2	4 in. - front	-1.9	-4.9 ± 0.6	-4.2 ± 0.2
2	4 in. - back	-7.5	-14.9 ± 0.3	-10.7 ± 0.2
2	18 in. of drawer	-	-8.9 ± 0.1	-

*451 Ih ≡ 1% ρ.

**Sodium cans replaced by void.

†Sodium cans replaced by empty SST cans. Measurements corrected for SST void worth.

probably due mainly to streaming, and raises the question as to the magnitude of the correction necessary to correct the results obtained with the $\frac{1}{4}$-in. sodium cans, used in a typical drawer, as compared with the voiding of a homogeneous mixture as postulated in most calculations.

c. Doppler Effect Measurements

The effect of rapid physical movement of a sample of resonance absorber on the absorption of the sample was investigated as an alternative method of making Doppler effect measurements in critical assemblies. The shapes of the resonance lines can be altered by physical motion of the sample so as to cause an effective broadening analogous to that caused by sample heating. The line shape of a single isolated Breit-Wigner resonance in a sample moving through an isotropic neutron distribution: (1) at a temperature such that Doppler broadening due to temperature-induced target atom motion is negligible, is given by

$$\psi = \frac{\Gamma}{4v_t\sqrt{2m_nE_n}}\left\{\tan^{-1}\left[\frac{(E_n - E_k) + v_t\sqrt{2m_nE_n}}{\Gamma/2}\right] - \tan^{-1}\left[\frac{(E_n - E_k) - v_t\sqrt{2m_nE_n}}{\Gamma/2}\right]\right\}, \quad (1)$$

and (2) at a temperature such that the line, for the stationary sample, has assumed a "pure" Doppler shape, is given by

$$\psi = \frac{\pi}{8}\frac{\Gamma}{v_t\sqrt{2m_nE_n}}\left\{\operatorname{erf}\left[\frac{(E_n - E_k) + v_t\sqrt{2m_nE_n}}{\Delta}\right] - \operatorname{erf}\left[\frac{(E_n - E_k) - v_t\sqrt{2m_nE_n}}{\Delta}\right]\right\}, \quad (2)$$

where

v_t = the sample speed,

m_n = the neutron mass,

E_n = the neutron energy,

E_k = the energy of the center line of the resonance,

Γ = the total width,

Δ = the Doppler width.

A characteristic half-width for the line shape broadened by sample movement that is analogous to $\Gamma/2$ for the natural line shape and to Δ for the temperature broadened case can be defined as $\delta = v_t\sqrt{2m_nE_n}$. An effective temperature T_{eff}, equivalent to a given sample speed, can also be defined as that temperature necessary to give the same lowering of the cross section at the resonance peak. For sample speeds up to those given by the criterion δ comparable to the larger of $\Gamma/2$ or Δ, the resonance line shapes broadened by sample movement are almost identical with

those for a stationary sample at temperature T_{eff}. For the case (2) above, for example, the effective temperature of a sample of atomic mass M_t at temperature T_0 moving with speed v_t is given by

$$\frac{T_{eff}}{T_0} = \frac{\frac{1}{\pi}\left(\frac{2M_t}{kT_0}\right) v_t^2}{\left[\operatorname{erf}\left(\frac{v_t}{2}\sqrt{\frac{2M_t}{kT_0}}\right)\right]^2}. \qquad (3)$$

The criterion for the highest sample speed at which the motion-broadened line shape is still sufficiently similar to the temperature-broadened line shape so that an "effective" temperature is clearly definable is just

$$v_t \sim \sqrt{2kT_0/M_t}\,. \qquad (4)$$

As the sample speed is increased to values significantly higher than that given by Eq. (4), the line shape deviates increasingly from that given by temperature increase until at exceedingly high speeds the characteristic half-width δ completely dominates and the line shape becomes a rectangular step function of width 2δ.

As shown by Eq. (3), the relationship between effective temperature and sample speed is not linear: as v_t is increased, T_{eff} at first increases very slowly, then becomes approximately linear in v_t, and finally increases as the square of v_t.

Preparations are underway to perform experiments using rotating samples in support of the theory thus far developed.

3. ZPR-IX

Experimental studies with Assembly No. 3 were concluded in May. Since then, the facility and the cell have been extensively modified. The changes are as follows:

a. Cell No. 4 "A" and "B" personnel door hinges, supports, and drives were modified and adjusted to correct for difficulties of operation. The main hinge shaft, a number of hinge flap studs, closure damping device, thrust bearing, pressure gauges, and the interlock switch were repaired or modified. The keeper pins, actuating linkage, hydraulic operator system, chain sprocket bracket, and hinge flaps were pinned to both the door and the shaft to prevent further misalignments caused by normal usage.

b. The $7\frac{1}{2}$-cm movable block and support bracket assembly were replaced by a sturdier unit, and the monthly check procedures for this block were changed.

c. A number of drawer tabs were replaced because the aluminum rivets securing them to the drawers were shearing. Several drawers bent or damaged during handling were straightened and returned to service.

d. Double knuckle couplings were installed on all the dual-purpose rods in order to alleviate any difficulty that might be encountered because of poor alignment between rod drive and direction of drawer motion. As a result, the scram times of the rods were reduced, on the average, by 84 ms from those using the arrangement of single knuckle couplings.

e. The matrix tubes were cleaned out by reclamation personnel.

f. Wiring errors in the emergency exhaust alarm system were corrected.

g. A number of modifications were made in the control system:

(i) Corner separation indicators were installed and calibrated.

(ii) The stationary half of the matrix was unloaded and its deflections were measured. The matrix deformation is completely elastic since no significant dimensional changes were observed relative to similar measurements made prior to the initial loading of the reactor last February.

(iii) All the rigid cables connecting the dual-purpose drives to the terminal board were replaced by flexible cables. Similar provisions were made for the safety rods when they are put back into service.

(iv) An interlock test board was installed in the console. All test points needed for the weekly, monthly, semi-annual and annual tests are available at this board. A clear plastic front panel provides visual evidence of interlock jumpering. The lock on the board, when open, activates a red light on the console.

(v) Channels No. 1 and No. 2 have had additional cathode follower output stages added to provide more reliable operation.

B. General Fast Reactor Fuel Development

1. Development of Jacket Materials

a. Vanadium and Vanadium Alloys. Jacket materials for the fuel elements of fast reactors must have suitable high-temperature properties (including strength and integrity), good thermal conductivity, and compatibility with the nuclear fuel and with liquid-metal coolants such as sodium. The jacket materials must also be amenable to fabrication into the desired

shapes. Of the various potential jacketing materials that have been considered, vanadium-base alloys are among the more promising, and titanium is the element favored for use as an alloying element in the vanadium.

Results to date indicate that compositions with about 20 w/o of titanium (TV-20 alloy) are most suitable. Alloys with higher percentages of titanium have been made, but their hardness is greater and they are less easy to fabricate, and alloys with lesser percentages of titanium are not so compatible with the fuel and less resistant to corrosion by oxygen in sodium. The commercial production of TV-20 is therefore being encouraged, and the fabrication development of the alloy is being studied.

(i) Fabrication. Approximately 34 kg of the TV-20 alloy ingots procured from Union Carbide Corp. (Stellite Division), each 10 cm in diameter, have been found acceptable according to ANL specifications. The extrusion characteristics of two of the ingots, extruded at ANL to 4.8- and 3.6-cm-diameter bar stock, were similar to those of ANL-produced arc-cast ingots.

(ii) Young's Modulus of V-20 w/o Ti. The data of Hill and Wilcox,[3] who measured Young's modulus for various compositions from ambient temperature to about 700°C by a dynamic method, have been replotted in Figure 15 as isothermal curves of Young's modulus versus w/o titanium in vanadium. The variation with temperature at the composition

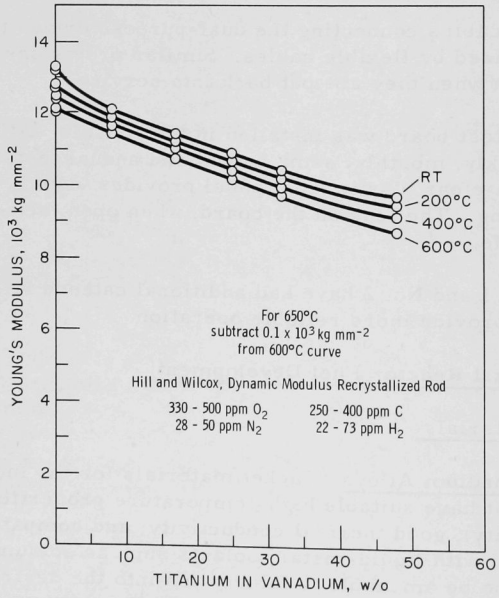

Figure 15

Isothermal Curves of Young's Modulus vs. w/o Titanium in Vanadium

[3]Hill, W. H., and Wilcox, B. A., Elevated Temperature Dynamic Moduli of Vanadium, Titanium and V-Ti Alloys, AD-243479 (May 1960).

V-20 w/o Ti was derived and plotted in Figure 16, along with ANL data[4,5] calculated from static measurements on extruded rod. Although these modulus values appear to be high in comparison with the results of Hill and Wilcox, this difference could be due to difference in material condition. An alternative cause might be the possible malfunction of the extensometer resulting from a damaged flexure plate (this condition was noticed after the data for the extruded rod had been obtained). Additional tests to be run on extruded rod are expected to resolve this possible discrepancy.

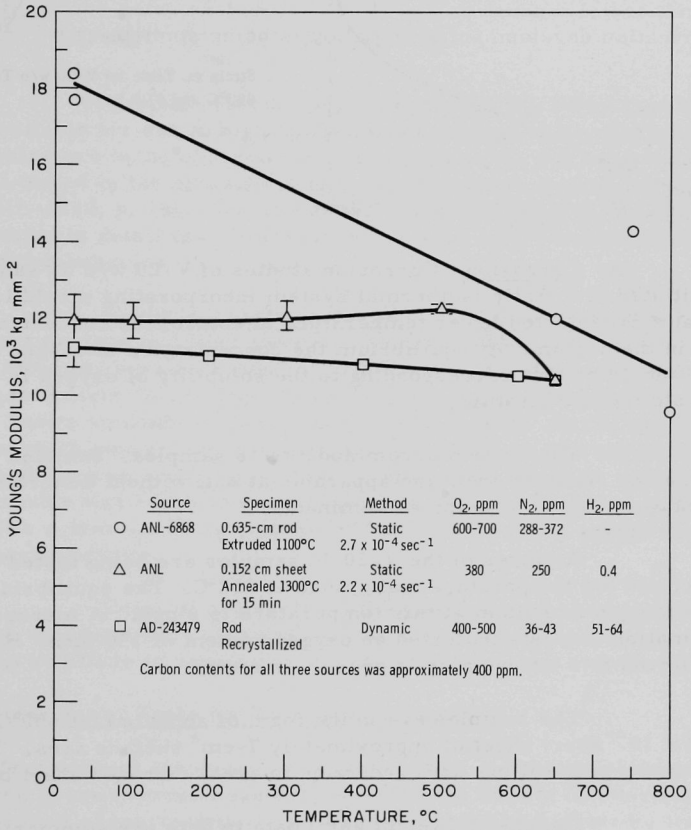

Figure 16. Young's Modulus vs. Temperature for V-20 w/o Ti

Recent measurements with V-20 w/o Ti sheet, shown in Figure 16, are in better agreement with the data of Hill and Wilcox. The specimens of Hill and Wilcox and the ANL sheet specimens were recrystallized, whereas the ANL rod specimens were in the as-extruded condition.

[4] Annual Report for 1963, Metallurgy Division, ANL-6868, p. 131.

[5] Reactor Development Program Progress Report, March, 1964, ANL-6880, p. 20.

(iii) Creep of V-20 w/o Ti. Creep tests are being conducted on V-20 w/o Ti sheet specimens which have a large grain size resulting from a 1300°C anneal for 15 min prior to testing. A creep curve is shown in Figure 17. The creep appears to be primarily second stage. Tests on material with a finer grain size are now in progress.

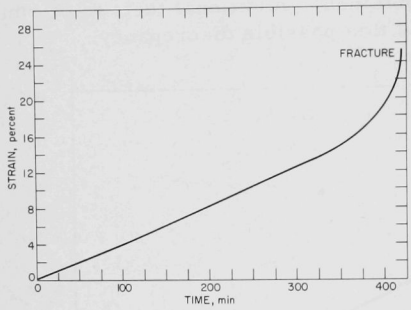

Figure 17

Strain vs. Time for V-20 w/o Ti at 650°C and 37.5 kg mm^{-2}

(iv) Corrosion. Corrosion studies of V-20 w/o Ti samples have been initiated in a static isothermal system incorporating a cold leg maintained at a preselected lower temperature to control the concentration of oxygen in the sodium. At equilibrium the concentration of oxygen in the system should be that corresponding to the solubility of oxygen in sodium at the cold leg temperature.

The system accommodates 16 samples. Samples can be introduced or removed from the apparatus at will without disturbing the test conditions or introducing contaminants.

A series of the V-20 Ti samples are being tested at 650°C with the cold leg temperature maintained at 132°C. The equilibrium solubility of oxygen in sodium at this temperature is 6 ppm. A mercury amalgamation analysis indicated an oxygen content of 150 ppm. However, it is believed this latter value is grossly in error.

The samples are in the form of annealed (at 650°C for 2 hr under 4×10^{-7} torr) sheet of approximately 7-cm^2 surface area. They were fabricated by cold rolling (60% reduction in area) extruded sheet bar.

Corrosion (weight gain) data to date are summarized in Figure 18. Data are included for samples that were in test continuously for the indicated time as well as for samples that were periodically removed, cleaned of sodium, weighed, and returned to test. There is apparently no difference in behavior. To data V-20 Ti is behaving in a manner typical of materials that form protective films.

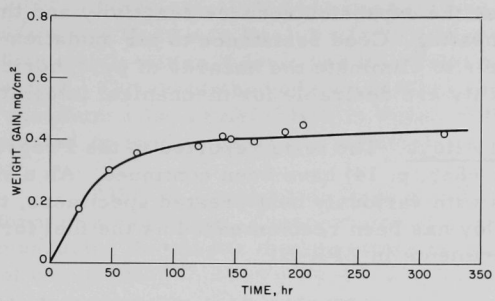

Figure 18

Corrosion of V-20 w/o Ti in Sodium at 650°C

Although results so far encourage the belief that V-20 w/o Ti will be suitable for use in high-temperature sodium, appreciably higher weight gains are being observed in this test than was the case for similar material tested in the circulating loop (see Progress Report for February 1964, ANL-6860, p. 14). The continuing experimental program is designed to determine in detail the effects of variation in environment and material on corrosion behavior.

(v) Screening Tests in Oxygen-contaminated Sodium. A high-pressure autoclave has been used for some screening tests in sodium at 650°C. Attempts have been made to establish a reliable sampling procedure for oxygen content, but to date the analytical results have not been consistent with the known amounts of Na_2O_2 added to the system. In the early experiments in which oxygen was analyzed at about 100 ppm, the attack rate on pure vanadium was much higher than in later tests in which sufficient sodium peroxide was added to bring the oxygen content to the same estimated level. The system is being cleaned and refilled to try to repeat the early experimental results.

Tests of arc-melted alloy buttons in the same experiment with pure vanadium have established that chromium and aluminum are beneficial additions to vanadium-10 w/o titanium.

2. Development of Fuels for Zero-power Reactors

The physical theories used in the design of new reactors are generally tested in zero-power reactors, whereby the effects on reactivity and other physical characteristics may be determined by repeatedly loading and unloading large numbers of small fuel elements in various test configurations. The durability and fire resistance of the elements are important. With plutonium-containing fuel, the possibility of fuel-element rupture is a serious health hazard. A plutonium-fuel-element fire would be disastrous.

A high coefficient of thermal expansion and a high expansion due to allotropic changes on heating are both desirable as safety features in

zero-power reactors because the expansion reduces reactivity and thus tends to prevent excessive heating. Good resistance to air oxidation is important in zero-power fuels to eliminate the hazards of pyrophoricity, and strength and some ductility are desirable for mechanical integrity.

a. U-Pu-base Fuel Alloys. The tests reported in the Progress Report for April 1964 (ANL-6885, p. 14) have been continued. As a result of these and additional tests with variously heat-treated specimens, the U-20 w/o Pu-2.5 w/o Mo alloy has been recommended as the fuel for use in the SEFOR Critical Experiments in ZPR-III.

This alloy has good corrosion resistance in air, good expansion characteristics, is extremely strong, and can be fabricated into fuel plates by casting and machining. Average expansion coefficients for ranges of temperatures on heating are given in Table IX. The average coefficient increases from 15.3 x 10^{-6}/°C in the range from 30 to 220°C to 24.8 x 10^{-6}/°C in the range from 380 to 545°C. A transformation occurs between 545 and 617°C, which results in an expansion of 3.95 x 10^{-3} cm/cm. Below this transformation the average expansion coefficient between 30 and 545°C is 20.4 x 10^{-6}/°C, and above this transformation it is 24.6 x 10^{-6}/°C from 617 to 700°C.

Table IX. Expansion Behavior of a Cast U-20 w/o Pu-2.5 w/o Mo Alloy

Temp Range (°C)	Average Expansion Coef (cm/cm-°C)	Total Expansion (cm/cm)
30-220	15.3 x 10^{-6}	-
220-380	23.7 x 10^{-6}	-
380-545	24.8 x 10^{-6}	-
545-617	Transformation	3.95 x 10^{-3}
617-700	23.4 x 10^{-6}	-

The alloy failed in compression tests at room temperature and at 280°C without yielding. At 480°C it is very ductile in compression. The compressive strength at failure was 134 kg/mm^2 (190,000 psi) at room temperature and 81 kg/mm^2 (115,000 psi) at 280°C. At 480°C the stress at which plastic deformation was first noted was 29 kg/mm^2 (41,000 psi).

A similar alloy of U-25 w/o Pu-2.5 w/o Mo appears to satisfy fuel requirements for ZPPR. We are currently investigating alloying elements other than molybdenum to find, from physics considerations, a more desirable element which will impart the required properties to the U-Pu binary compositions of interest for ZPPR.

Air corrosion tests have been run for 25 days on U-20 w/o Pu-1.3 w/o V and U-20 w/o Pu-1.3 w/o Ti alloys. The titanium alloy gained 0.25% in weight within 3 days, and its weight remained nearly constant thereafter. The specimen had turned black, but still appeared to be sound. The vanadium alloy gained 0.08% in weight within 5 days, 0.25% in 25 days, but started to swell, crack, and disintegrate to powder by the 19th day.

Alloy of composition U-22 w/o Pu-2 w/o Mo was received in the form of a cast plate. Compression specimens and a tensile specimen for measuring the elastic modulus were fabricated from the plate. A cast rod of composition U-20 w/o Pu-2.5 w/o Mo was also used to make compression specimens. The tests were made at ambient and elevated temperatures. The results are shown in Table X. The alloys are strong compared with Type 304 stainless steel, but ductile only above about 400°C.

Table X. Compressive Properties of U-Pu-Mo Alloys

	Nominal Composition (w/o)			Temp	Max Compressive Strength		Compression	Elastic Modulus	
Casting	U	Pu	Mo	(°C)	kg/mm^2	10^3 psi	(%)	10^3 kg/mm^2	10^6 psi
R164	77.5	20	2.5	23	134	190	0	10.5	14.9
R164	77.5	20	2.5	280	81	115	0	-	-
R169	76	22	2	376	49.8	70.8	0	5	7
R169	76	22	2	405	56.2	80.0	5	-	-
R164	77.5	20	2.5	480	28.8	41.0	>50	3	4

The structures as well as compressive properties were studied. Metallography reveals a nearly continuous grain-boundary network and an acicular phase within the decomposed grains. These characteristics do not change significantly after 40 hr at 475°C.

The X-ray powder pattern of the original casting had a few sharp lines only in the forward region. A one-hour anneal at 475°C was sufficient to produce sharp lines throughout the spectrum. By comparison with other patterns, the presence of several phases was indicated. The equilibrium diagram of the U-Pu-Mo system requires the presence of much alpha, with less of the zeta and gamma-prime phases. The lines of the alpha phase appeared to be the strongest, but an unambiguous identification of the other phases was not possible.

C. General Fast Reactor Fuel Reprocessing Development

1. Skull Reclamation Process

a. Demonstration Runs. Demonstrations of the skull reclamation process are continuing on an engineering scale to establish process procedures and mechanical reliability of the equipment. Skull reclamation steps include: noble metal extraction, uranium oxide reduction, precipitation of a uranium-zinc intermetallic compound, decomposition of the

intermetallic compound, dissolution of precipitated uranium metal, and (after removal from a primary vessel to a secondary vessel) retorting of the uranium product solution to concentrate the uranium. Except for the last step, each step is followed by a phase separation in which a molten metal or flux phase that contains impurities is pressure-siphoned out of the process vessel to separate it from a uranium-bearing phase.

Two additional engineering-scale skull reclamation runs have been completed. Process conditions for the second of these were modified in that the reaction temperatures were lowered from 800°C to 700°C for the noble metal extraction, reduction, and intermetallic decomposition steps in an effort to reduce the quantity of metal and salt volatilizing. In these two runs, the waste impurity solutions were all removed with efficiencies of 80 to 96%, which are adequate. Analyses of samples from the waste streams are not yet available.

In two runs on a 100-g-uranium scale, modifications in the flux phase used in the noble metal extraction step and the uranium oxide reduction step of the skull reclamation process were examined. In one run, the quantity of standard flux (47.5 m/o $MgCl_2$-47.5 m/o $CaCl_2$-5 m/o CaF_2) used was reduced by one-half as a possible method of decreasing the volume of salt which would have to be stored as waste. In the other run, the $MgCl_2$ content in a normal amount of flux was decreased from 47.5 m/o to 28.5 m/o with a corresponding increase of the $CaCl_2$ concentration from 47.5 to 66.5 m/o. A flux having a decreased $MgCl_2$ content would have a higher melting point. Such a flux would be desirable since the time necessary to cool the flux to its freezing point would be shortened when it is necessary to freeze the flux and pressure-siphon a liquid metal phase out of a process vessel. Preliminary observations for the two runs indicate that the rapidity and completeness of reduction of uranium oxide were unaffected by either change.

b. Mixing in Liquid Metals and Salts. Additional data have been obtained on the effect of the mixing variables on the extraction of noble metals from uranium-fissium oxides (suspended in flux) by molten zinc. These studies are being carried out in support of the engineering-scale demonstrations of the skull reclamation process.

A noble metal extraction run has been completed with a skull oxide charge to which ruthenium-106 tracer had been added. Wetting of the uranium-fissium oxide was enhanced by dropping the oxide charge through the molten halide flux; the oxide-flux-zinc system was then agitated at 800°C for 160 min. Analysis of zinc samples taken during the run indicated that noble metal extraction into the zinc phase was greater than 95% early in the run and remained at this level throughout the run. In comparison, extraction of less than 50% of the noble metals was indicated in three earlier runs with ruthenium-106 tracer, in which only agitation was used to wet

the skull oxide with flux. Runs are to be performed to determine the effect of stirring the oxide charge in molten flux before the zinc charge is added.

2. Materials and Equipment Evaluation

Corrosion testing has been carried out on four ferrous alloys - Type 1019 carbon steel, Types 304 and 405 stainless steels and Type 2 1/4 Croloy - to obtain a measure of their reliability as container materials for cadmium-magnesium-zinc-uranium/halide flux systems. Eleven 200-hr tests have been conducted at 600 or 650°C under static conditions. The halide flux chosen for this work was 35 m/o NaCl-25 m/o LiCl-40 m/o $MgCl_2$. Seven metal phase compositions were used in the range 0-23 a/o Zn, 31-95 a/o Mg, 5-50 a/o Cd, and 0-1 a/o U. In each test, four corrosion coupons were contained in a single capsule.

Preliminary results are as follows: Attack of Type 304 stainless steel by nickel leaching increased with increasing temperature and with increasing zinc content of the melt. Type 1019 carbon steel exhibited good corrosion resistance at low zinc concentrations. Croloy and Type 405 stainless steel are expected to withstand corrosive attack satisfactorily at zinc concentrations of 10 a/o and less.

A beryllia or beryllia-lined crucible which will not be wetted by molten magnesium-zinc-uranium alloy is required for the retorting step of the EBR-II skull reclamation process. In a preliminary test, a $4\frac{1}{4}$-in.-OD x 6-in.-high nitride-bonded silicon carbide crucible, which had been plasma-sprayed with a 30-mil coating of beryllium oxide, contained a charge of 72 a/o Mg-Zn and flux in an argon atmosphere at 800°C for 1 hr. Visual examination of the crucible after the test showed no evidence of penetration of the wall or base by the melt. Although the BeO coating was darkened, it did not appear to have been wetted by the melt. This is an encouraging result, since crucibles that are large enough for the full-scale skull reclamation equipment can be fabricated from nitride-bonded silicon carbide.

3. Advanced Processes

a. Use of Cd-Zn-Mg Alloy. Cadmium-zinc-magnesium alloys are being investigated as potential liquid metal solvents for separations processes utilizing molten salt extraction of fission products from liquid metal solutions of uranium and plutonium. The stability of plutonium dissolved in liquid cadmium-zinc-magnesium alloy toward various container materials is being studied. Preliminary results indicate that plutonium dissolved in 70 a/o Cd-15 a/o Mg-15 a/o Zn which is contacted with 30 m/o NaCl-20 m/o KCl-50 m/o $MgCl_2$ at 600°C does not interact with Type 304 stainless steel. Within analytical accuracy, the plutonium concentration remained constant throughout a 100-hr period.

b. Properties of Molten Chloride Systems. The LiCl-KCl-$MgCl_2$ system is one of several systems being considered as a flux in liquid metal recovery processes for uranium-plutonium fuel. The flux compositions of greatest interest are those containing more than 50 m/o $MgCl_2$ (to obtain satisfactory distribution coefficients) and having a melting point below about 600°C. Liquidus temperatures for 54 compositions of the LiCl-KCl-$MgCl_2$ system have been measured by thermal analysis. Flux compositions have been found which have sufficiently low melting points for process use and which have distribution coefficients that would allow satisfactory separation of rare earths from plutonium by liquid metal-molten salt extraction. A liquidus minimum of about 336°C exists at approximately 40 m/o LiCl-10 m/o $MgCl_2$-50 m/o KCl.

4. Head-end Treatments for Refractory Fuels

a. Decladding. Refractory metal alloys are currently favored as potential cladding materials for metallic fuels in fast breeder reactor cores. Chemical decladding may be required for such fuels because of a tendency for the fuel and cladding to form a metallurgical bond during irradiation and thermal cycling. The decladding method currently under investigation for advanced core fuel elements clad with vanadium-titanium alloy (10-20 w/o Ti) consists of the reaction of fuel and cladding with chlorine in a molten salt medium. The objective of this procedure is to distill the volatile vanadium and titanium tetrachlorides from the system and to retain the uranium in the salt. However, it is possible that some uranium may also be volatilized as a chloride.

A series of experiments has been performed at 650°C and 700°C, using uranium shot and selected molten salt mixtures and sparging with chlorine, in order to determine some of the factors affecting uranium volatilization. In a run utilizing 65 m/o $CaCl_2$-35 m/o $BaCl_2$, 24% of the uranium was volatilized at 650°C during the time required to convert all of the uranium to UCl_4. However, in other runs, substitution of an alkali metal chloride for one-half of the $CaCl_2$-$BaCl_2$ decreased the uranium loss sharply, presumably as a result of the formation of complexes with UCl_4. With an equimolar quantity of KCl added to the $CaCl_2$-$BaCl_2$ mixture at 650°C, only 0.9% of the uranium volatilized. The order of effectiveness in reducing uranium volatilization is LiCl < NaCl < KCl. In these runs it was also noted that the percentage of uranium that volatilized decreased with decreasing temperature and with decreasing uranium concentration in the salt.

D. Sodium Coolant Chemistry

1. Studies of the Oxygen Content in Sodium

a. Distillation Analyzer. Investigation of various factors having possible influence on the operating characteristics of the distillation analyzer has been continued. Tests in which copper oxide additions were made

to the cooled sodium in the level full distillation cup in an interrupted run before distilling (see Progress Report for May 1964, ANL-6904, p. 42) gave too wide a scatter in titration results to permit proper evaluation of the extent of oxide loss by spattering. This loss could also be caused by the high expansion of sodium metal, which overflows the cup. Believing that the scatter may have resulted from incomplete or erratic reduction of the copper oxide by the sodium at the distillation temperature, 650°F, the tests were repeated with the more easily reduced silver oxide instead of copper oxide. Since the oxide values obtained were all higher than the oxide added rather than less, it is believed that, at the distillation temperature used, loss of oxide by spattering or expansion was practically nil in a partially filled cup. The excess of oxygen found over that added by use of silver oxide is a function of the oxide originally present in the sodium plus that picked up from the atmosphere in the dry box where the silver oxide additions were made, plus that picked up in the transfer between the distillation apparatus and the dry box. Such behavior indicates there is spattering or runover from a distillation cup level full of sodium even at a low distillation temperature of 650°F.

b. Plugging Meter. The sensitivity of the electromagnetic (EM) flowmeter indication on the X-Y plotter has been increased by inserting an amplifier between the two instruments. Possibly as a result of this increased sensitivity, there appears to be some sort of interference in the flowmeter indication when the plugging meter loop EM pump is operating. Evidence of this was the difference in position of the zero flow point on the X-Y plotter with and without the pump operating. When the flow through the plugging meter loop was controlled by the valve in the main loop instead of the plugging meter EM pump, this difference was not observed. The reason for this apparent interference could be magnetic and will be determined.

2. Analysis for Carbon in Sodium

As an auxiliary part of our study of the chemistry of carbon transfer via liquid sodium, attempts to improve the dry oxidation method for the determination of carbon in sodium are being made. In this method, a solid sample of the sodium is oxidized by use of high-purity oxygen. The result of this oxidation is a mixture consisting of sodium oxide and the original carbon as sodium carbonate. The sodium oxide is then neutralized with a strong acid, which also decomposes the sodium carbonate to yield gaseous CO_2. The latter is collected and measured manometrically.

Two procedures have been used in experiments during the past month to neutralize the sodium oxide and liberate the CO_2. The first method involves the use of SiO_2 as the acid. A high-temperature (~1200°C) reaction of the Na_2O-Na_2CO_3 mixture with SiO_2 is carried out. In the second method, the Na_2O-Na_2CO_3 mixture is dissolved in water and neutralized with sulfuric acid. The two methods were compared with sodium samples taken

from the same source. The high-temperature neutralization method gave 76 ± 18 ppm carbon for 6 samples and the low-temperature aqueous neutralization method 71 ± 27 ppm for 5 samples. Sampling techniques are being studied in order to determine the cause of the variations in carbon content of the samples.

E. EBR-II

1. Reactor Plant

Early in June, the low-power experiments were completed. The primary tank sodium was then cooled to about 325°F, and the "dropped" subassembly (see Progress Report for April 1964, ANL-6885, p. 19) was removed from the catch basin. The secondary sodium system was filled, and the "plant standby" condition was achieved with the primary sodium at 600°F. The reactor was then loaded for power operation with the addition of a new source and one enriched subassembly.

Failure tests were then completed. These consisted of a 13.8-kV failure, an instrument (external to reactor building) air failure, and a reactor building instrument air failure. At month's end, the bulk sodium temperature was being raised to the normal operating temperature of 700°F with the secondary sodium and steam systems in operation.

a. Low-power Experiments. The low-power experiments begun on May 22, were completed June 6. The oscillator rod was statically calibrated and the reactivity worth, as a function of stroke, obtained. With the stroke set at $1\frac{3}{4}$ in. "peak to peak," with the center of oscillation about 12 in. above the bottom of the core, the change in worth over the length of the stroke was 16 Ih. Initial difficulties with the null-balance analysis equipment prompted the temporary installation and checkout of analog computer analyses equipment for use in the cross-correlation method of determining transfer function. Both pieces of equipment were made operable and a limited quantity of data obtained. During approach to power, another measurement of the zero power transfer function will be made.

The oscillator rod has operated successfully for more than 12 hr.

The calibration of nuclear instrumentation was done at a reactor power of 100 kW, with a short run at 500 kW. Final instrument positioning will be made when results from absolute fission determination of the calibration foils are obtained.

Measurements of decay of the zero-power reactor coolant were completed.

b. Recovery of "Dropped" Subassembly. On June 10, the dropped natural uranium core-type subassembly (N-14) was removed from the primary tank catch basin. In order to accomplish this, the primary tank bulk sodium was cooled down to 323°F. After removal of the "X" nozzle shield plug, a 7-in.-dia aluminum tube was lowered down over the top end of the subassembly in the catch basin. The tube was pressurized with argon until the top end of the subassembly could be seen through viewing ports in the top end of the tube. A grappling tool was lowered and attached to the top end of the subassembly. The subassembly was removed from the primary tank through the tube and placed in a steel pipe. Later, the sodium was vacuum-distilled from the subassembly and the subassembly shipped to Argonne, Illinois. Examination indicated that the top end of the subassembly was not damaged; however, the subassembly was bent slightly because of impact with the catch basin structure during fall. The "X" nozzle shield plug was replaced after removal of the aluminum tube, and the primary tank bulk sodium was heated to 350°F for filling of the secondary sodium system.

c. Fuel Handling. The newly designed interlocks to assist the transfer arm operator in determining that a valid wiggle test is being performed were installed on the transfer arm.

At a primary tank bulk sodium temperature of 600°F (which is the plant standby condition), the final fuel handling was accomplished for the approach to power. A new antimony source was loaded into an inner blanket beryllium thimble. This source, together with an existing inner blanket source, will be used for the approach to power experiments. The sources were positioned so that they are not immediately adjacent to core-type inner blanket subassemblies. One additional core-type inner blanket subassembly was loaded from the storage basket into the reactor. The outer blanket beryllium thimble was relocated from a 16th row position to an 11th row position. At 700°F, this loading will give approximately 290 Ih of excess reactivity.

d. Fuel-unloading Machine. During the source installation, difficulty was experienced with the fuel-unloading machine gripper and the transfer port tube. When brought back out of the primary tank, the empty gripper was sticking just above the 21 ft elevation. Since the gripper had just been cleaned of sodium and sodium oxide, it appeared that the transfer port tube restricted the gripper movement and may require cleanup of sodium oxide. A scraper is being designed to mechanically remove the sodium oxide from the transfer port tube.

A bevel gear on the fuel-unloading machine was damaged during removal of the gripper from the port tube. The bevel gear was replaced.

Two leaky ball valves in the argon cooling system of the fuel-unloading machine were repaired. The graphite seats were replaced with reinforced Teflon material. In the past, leakage past one of these valves resulted in oxygen and nitrogen contamination of the argon cooling system.

e. Sodium-purification System. Bypass cold trap flow is being maintained at about 58 gpm to permit sodium sampling in the primary system for sodium purification. The cold trap is not in operation, because it imposes an additional heat load upon the primary system under electrical heating conditions. Lead shielding has been installed over the sodium-purification system nozzle on top of the primary tank as well as the nozzle for the fuel-element rupture-detection system.

f. Primary-tank Blanket Argon. Analysis of the primary-tank blanket argon indicated a nitrogen content of about 5%. An argon purge of about 1 cfm was established for 100 hr to reduce the nitrogen content.

g. Failure Tests. During the 13.8-kV "failure" test, the emergency diesels picked up the critical loads in the reactor building. When the instrument air supply in the Power Plant failed, the emergency compressor in the reactor building supplied air to equipment inside the reactor building. Prior to this test, two preliminary tests were conducted in which the 480-V power to critical reactor building loads was interrupted. In each case, the 100-kW diesel generator assumed these loads, which consist chiefly of the shield exhaust fans and instrument thimble turbocompressors.

In a reactor building instrument air failure test, the instrument air isolation valve was closed and the reactor building air compressor deliberately shut off. After about 26 min, the reactor plant instrument air pressure dropped to about 33 lb, whereupon the damper valves started to close and the turbine blowers were automatically shut off. In an additional 10 min, the instrument thimble temperatures had risen about 5°F and the system was then restored to normal operation.

2. Sodium Boiler Plant

Welding of the damaged main secondary sodium pump tube was completed. All welds showed a clear radiograph and passed a helium mass spectrometer leak test.

A strainer was welded into the discharge end of the pump and an auxiliary sodium-leak-detecting device installed in the pump case. The pump was then reassembled, and all piping welds were satisfactorily radiographed and helium mass spectrometer leak-tested. All auxiliaries were reinstalled, piping insulated, and heating wire reinstalled. A vacuum control system was installed to permit running of the pump with reduced pressure in the casing.

The sodium and steam systems were then heated to the filling temperature (350°F) and the system filled with sodium on June 12. The primary and secondary pumps were then started, heaters energized, and combined systems heatup to steam drum operating pressure (1270 psig at 575°F) started. On June 16 the steam bypass system was placed into operation to control drum pressure.

After scheduled electrical failure tests, the secondary sodium flow rate was reduced incrementally, allowing the bulk sodium temperature in the primary tank to rise to 600°F. To raise the system temperature above 580°F, all heat loads were reduced by closing steam traps and manually operating them. The 600°F primary temperature was maintained by adjusting secondary sodium flow, reducing primary tank heat input, and bypassing excess steam to the condenser.

The secondary sodium EM pump was tested. The pump casing pressure was reduced to 6-7 psia and the sodium flow increased to 5500 gpm (greater than 90% flow). Under these conditions, no abnormal noises could be heard in the pump.

As the primary tank temperatures slowly rose to 600°F, the plugging temperature of the sodium in the secondary system slowly rose from 240°F to 315°F. The temporary cold trap was placed in operation, and, although some signs of plugging were indicated, the plugging temperature had been reduced to below 250°F as the period ended.

An electrical failure test, which resulted in automatic startup of the emergency 480-V diesel generator, was conducted to determine if all loads connected to this bus were supplied as required. The test revealed one automatic switching malfunction, which was subsequently corrected. In the Sodium Boiler Plant, all equipment on this bus performed as expected.

A failure test of the 13.8-kV bus was made to determine if emergency procedures for loss of power were adequate and if the safety of the plant was jeopardized in any way. In general, the test was very successful, with only minor difficulties being experienced. All equipment in the Sodium Boiler Plant functioned as expected.

The power was off to this building approximately 2 hr. During this time, there was only a minor cooling of vent lines and drain lines noted, while the main system lost only a few degrees.

A failure test of the instrument air system was conducted to test emergency procedures and to determine if the safety of the plant was compromised. This test was successful, only minor difficulties being noted. All equipment in the Sodium Boiler Plant performed as expected.

The safety valves on the steam drum were tested and set at 1370 psig, and the valve on the steam heater in the Power Plant was tested and set at 1310 psig. These valves are now leaking slightly, but this is not expected to interfere with the approach to power program.

On June 28, heatup of the primary tank to 700°F was started. At the close of the month, the bulk temperature of the primary tank was approximately 650°F, and the plugging temperature of the secondary system was not rising significantly.

3. Power Plant

On June 11 plant heatup began. Failure tests of the 480-V and 13.8-kV electrical systems and of the instrument air system were carried out. Standby status with primary bulk sodium temperature at 600°F was satisfactorily attained.

Because loose flange bolts had previously been found in the Plant, the turbine stop valve and turbine steam lead flange bolts were inspected. Some were, in fact, loose, and all were tightened.

The plant heatup begun on June 11 continued, with interruptions for the electrical failure tests, until drum pressure of 1270 psig was reached, with pressure being controlled by bypassing steam via the automatic bypass valve to the condenser. Feedwater was pumped from the No. 2 heater to the drum by the startup feedwater pump, with flow rate controlled by the manual valve in the motor-driven feedpump warmup line valve.

Three failure tests and testing of the sodium boiler steam drum safety valves were made. The electrical failure tests checked response of the equipment and personnel of the plant to interruption of 480-V and 13.8-kV power. No difficulties were encountered in carrying out the 480-V test, and planned response to this type of failure remains unchanged. This is also essentially true of the 13.8-kV test, except that some minor problems were presented.

It was necessary to secure main steam heater traps; failure to do so results in high pressure in No. 2 heater, which is relieved through safety valves.

The third failure test checked reaction of the plant to interruption of instrument air. Control valves and operators responded to this interruption as predicted. The startup feedwater pump did not unload, however, since it is controlled by plant rather than instrument air supply. This test also was carried out smoothly, and restoration of control air proceeded satisfactorily.

4. Fuel Cycle Facility

a. The Argon Cell. The air in-leakage rate to the Argon Cell, which has been filled with argon since February 27, 1964, continues to remain very low, 0.005 scfm with the cell maintained at a pressure of minus 2 in. of water. The concentrations of impurities (as of June 18, 1964) in the argon were as follows: nitrogen, 5%; oxygen, 8 ppm; and, water, 46 ppm. These impurity levels are considered adequate. (The water concentration is purposely being maintained at this level to minimize wear of the manipulator motor brushes and to improve operating characteristics of the fuel pin decanner and chopper.)

b. Air Cell. Storage racks which have been installed in two floor pits of the Air Cell provide for temporary storage of spent and refabricated subassemblies (see Progress Report for October 1963, ANL-6801, p. 24). Cooling of the storage pits and their contained subassemblies is by means of two lobe-type blowers. One blower will be in continuous operation; the second blower is provided for standby operation and is automatically placed in operation should the other blower fail. Operational testing of the blowers has been completed. The results of these tests showed that each blower is operating at rated capacity and is capable of delivering about 120 scfm of air at a pressure drop of about 1 psi when supplying air to two storage pits. In addition, the test data show that the flow of air and the pressure drop through the storage racks are near the design values.

c. Preparations for Operations

(i) In-cell Manipulators. A continuing program to improve the performance and reliability of the in-cell operating manipulators is being carried out. Based on an evaluation of the field operating experiences of persons using the manipulators along with observations of operating and design engineers, necessary modifications are being made. Consideration is being given to improvements in clutches used for the protection of equipment from mechanical overloads. The design of an improved clutch must take into account the limitations imposed by the extremely dry argon atmosphere, the expected high levels of gamma radiation, and the fitting of any modification into existing equipment.

A disc-pack type of slip clutch has been designed by the Chemical Engineering Division at Argonne for use in the hoist drives of the in-cell operating manipulators. The slip clutch (utilizing a Maxitorq* Disc-Pac No. 22) can be readily installed inside the housing of the drive motor gear reducer. The slip clutch is adjusted to slip at an overload of 50%. After initial slipping, the transmitted torque drops to about one-half

*A product of Carlyle Johnson Machine Corporation, Manchester, Conn.

the break-away torque.* The break-away torque is adequate for all normal operations including acceleration of loads. Work is now underway to install these clutches on the eight operating manipulators and the two spare drive units.

Although conventional friction clutches will be satisfactory for many applications, there is a need for a clutch which would display a steady torque response. The disc-pack type of slip-clutch, for example, which is to be installed in the manipulator hoist drive, has a breakaway torque that is about twice the torque transmitted when slipping.

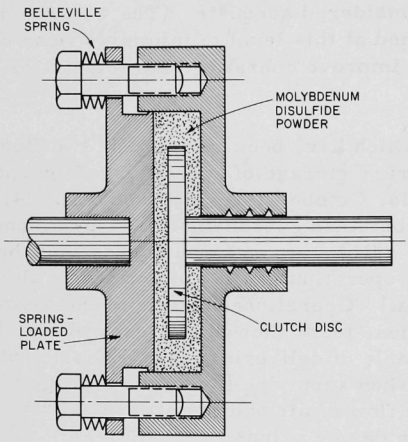

Figure 19. Dry Powder Slip Clutch

A second slip-type clutch has, therefore, been designed by the Chemical Engineering Division at Argonne which will meet the following requirements: (1) a steady slip-torque** nearly equal to break-away torque, (2) high resistance to radiation and heat, and (3) low cost. A prototype slip-clutch (see Figure 19) has been built and tested. This clutch consists of two parts: (1) a cylindrical housing that is filled with molybdenum disulfide powder and is attached to one shaft, and (2) a clutch disc that is enclosed in the housing and is driven by a second shaft. The powder forms a $\frac{1}{4}$-in. blanket around the clutch disc and is compressed by a Belleville spring-loaded plate which forms one end of the housing. Friction between the powder and the disc determines the torque transmitted. No special shaft seals were used and no leakage of powder was observed in the tests. All parts are made from mild steel without surface hardening or special machining, such as grinding. Initial test results show that there was practically no difference between break-away torque and torque transmitted while slipping.

(ii) Core Subassembly Dismantler. A number of improvements and changes have been made to the dismantler. Another natural uranium fuel subassembly was completely dismantled, and all operations were satisfactory. The dismantler is now equipped to handle all six types of core subassemblies.

---

*Break-away torque is the torque at which the components of the clutch first start to slip relative to each other.

**Slip-torque is the torque transmitted between the driver and the driven shaft when the components of the clutch are slipping relative to each other.

The control-panel circuitry has been changed in order to display the assigned number of the fuel element being inspected, as well as the total number of elements accepted or rejected from a given subassembly. Circuitry modifications have also been made to conform with changes in operating procedures, and the circuits connected with the transfer grapple have been added.

Modification of the blanket disassembly unit was completed to enable it to unscrew rather than to shear the nut holding the blanket sections. In addition, modifications were made to the rolling cutter unit used to section the hexagonal sheath on the subassembly. The depth of cut was increased and one of the three rolling cutters was eliminated.

(iii) Tests of Subassembly Grapple. Initial tests have been made on a grapple which is to be used for handling the subassemblies between the interbuilding coffin and dismantling machine and for returning reprocessed subassemblies to the coffin. The mechanical operability of the grapple in withdrawing several types of dummy subassemblies from the cask in position beneath the Air Cell floor plugs was satisfactory, and transfers to the disassembly machine were readily accomplished.

(iv) Injection Casting. Two additional injection casting runs were made with enriched uranium-fissium alloy. With charges of 10.2 and 8.1 kg of all-recycled feed material, the yields of cast metal were 70 and 61%, respectively. A melt refining run will next be made on the heels and unacceptable castings to remove dross.

(v) Pin Processing. One hundred twenty-five castings from the third and fourth injection casting runs on enriched alloy were subjected to comparative measurements on the pin processing machine and in the laboratory. Excellent agreement was noted among the measurements, as summarized in Table XI.

Table XI. Comparison of Machine and Laboratory Data

	Average Data from Pin Processor	Average Data from Laboratory	Average Difference*
Length (in.)	14.212	14.215	0.0035
Weight (g)	68.24	68.17	0.08
Volume (cc)	3.810	3.810	0.006
Density (g/cc)	17.91	17.90	0.06

*These values represent averages of absolute differences between pairs of measurements on the same casting.

(vi) Bonding and Bond Testing. Calibration of the bond testing apparatus has continued. Each of 20 pins was subjected to three tests for sodium bond level: radiography at room temperature, testing at room

temperature by means of an eddy current, and stripping of cladding from the rod to permit visual examination. Comparative data are shown in Table XII. The X-ray data are read as single levels (most probably the lower level of the sodium); the eddy current data partially reflect the angular level, and the stripping data indicate the mean level observed.

Table XII. Comparison of Indicated Sodium Levels

Pin No.	Sodium Level, in. above Top of Fuel, Indicated by		
	X ray	Eddy Current	Stripping
1	0.73	0.71	0.81
2	0.55	0.63	0.61
3	0.80	0.78	0.78
4	0.57	0.51	0.50
5	1.00	1.00	1.06
6	0.80	0.76	0.82
7	0.86	0.89	0.92
8	1.06	1.15	1.07
9	1.13	1.14	1.12
10	0.85	0.91	0.88
11	1.08	1.10	1.12
12	0.87	0.78	0.81
13	0.83	0.83	0.83
14	0.77	0.77	0.81
15	0.82	0.84	0.83
16	0.67	0.70	0.70
17	0.94	0.88	0.95
18	1.15	1.12	1.12
19	1.10	1.12	1.13
20	1.20	1.22	1.20
Average	0.889	0.892	0.904
Standard Deviation (sigma)	0.183	0.204	0.194

The sodium level is too high, for the acceptable level is 0.65 ± 0.15 in. With a correction in the amount of sodium added to reduce the average height from 0.90 to 0.65 in., the standard deviation indicates that over half of the pins would have had acceptable levels. As experience with the remote equipment is gained, the proportion of acceptable elements may increase considerably.

A majority of the stripped pins showed a sodium-void interface that is at an angle to the pin axis. Pins 13, 15, 16, 19, and 20 showed relatively flat sodium levels upon stripping, and the results indicate

a good comparison of values. The average difference between the X-ray and eddy current readings for a pin were 0.035 in., and the average difference between the visually observed level and the eddy current indicated level was 0.030 in.

In addition to the level comparisons, the eddy current indications for peripheral voids were compared with observed voids upon stripping. The results of this comparison were good; a void was observed for each eddy current trace indication, and no observed voids were found that had not been picked up by the eddy current coil.

d. Fuel-recovery Operations

(i) Fate of Iodine in Reprocessing Operations. Additional runs have been made with equipment in the Argon Cell to determine the fate of fission product iodine in discharged reactor fuel. One Curie of I^{131} (as palladium iodide in a glass capsule) was charged with chopped uranium-fissium pins in a melt refining crucible in Furnace B. The crucible was covered with a fume trap (previously coated with sodium), the charge was heated to 1400°C, and then liquated at this temperature for 3 hr prior to pouring the ingot.

The results as follows, are well within the expected error of the analysis of the samples:

Component	% of Charge
Fume Trap	81
Bell Jar and Base Plate	23
Crucible plus Skull	2
Ingot	7×10^{-3}

Most of the iodine was deposited within the fume trap, and substantially all was retained within the furnace bell.

The in-cell filter removed approximately 99.5% of the activity that reached it. This value agrees with the previous test of the filter for melt refining Furnace A, at which time no fume trap was used (see Progress Report for May 1964, ANL-6904, p. 48). About 93% of the iodine that reached the sub-cell vacuum pump was retained in the pump oil. No detectable iodine was discharged to the off-gas delay tank.

As a continuation of this experiment, both the ingot and the skull resulting from this run were processed further. After the skull was oxidized in the skull oxidation furnace, examination indicated that all of the iodine remained in the resultant oxide. Samples from the vacuum pump oil and a solution used to scrub all of the off-gas from the run revealed no detectable amounts of I^{131}.

The pins resulting from an injection casting run on the ingot, as well as the heel, showed substantially the same concentrations of iodine as the charge ingot. About 1.5% of the iodine charged in the ingot was found in the oil from the injection casting furnace vacuum pump. The off-gas from the vacuum pump was not sampled.

(ii) Skull Reclamation Process. The distillation of magnesium-zinc and the consolidation of the uranium product in the skull reclamation process is being demonstrated in engineering-scale retorting runs (being carried out by the Chemical Engineering Division at Argonne). The distillation and consolidation steps are conducted in a modified melt refining furnace which is installed in an argon-atmosphere glovebox (see Progress Report for May 1964, ANL-6904, p. 47). Five additional retorting runs have been completed with the same BeO crucible for all runs. This crucible was also used in a previously reported retorting run (see ANL-6904, p. 47). In four runs conducted to recover uranium from zinc-magnesium-uranium ingots (resulting from the dissolution step of uranium concentrate in demonstration runs of the skull reclamation process), 97% of the total uranium charged to the retorting furnace was recovered in the form of a metallic button which did not adhere to the BeO retorting crucible. However, the rest of the uranium product was in the form of a black powder, which also could be easily removed from the crucible. The major phase in the black powder was identified as uranium hydride.

Since no uranium hydride powder was noted in the previously reported run (see ANL-6904, p. 47) in which the charge (Zn-12 w/o Mg-10 w/o U) to the retorting furnace was prepared by dissolving uranium in a zinc-magnesium solution at 800°C, it was thought that the hydrogen was introduced into the retorting system in the form of moisture present in traces of flux believed to be included in the ingots from the skull reclamation demonstration runs. During a retorting run, the magnesium in the magnesium-zinc vapor could reduce the moisture, liberating hydrogen which, in turn, could react with the uranium product after cooling below the decomposition temperature for uranium hydride.

A run was then made with a similarly prepared ingot (Zn-12 w/o Mg-10 w/o U), in which flux material was not present. At the completion of the run, about 99% of the retorted uranium product was found in the form of a metallic button; the remainder was in the form of a black powder whose major phase was again identified as uranium hydride. These results tend to indicate that the atmosphere of the retorting unit is the source of hydrogen contamination. The Fiberfrax insulation material used in the retorting apparatus may be a source of moisture. If the insulation is not properly degassed, this could result in the presence of residual moisture in the retorting system. The operating procedure for future retorting runs is being modified so as to remove, at the end of a retorting run, any hydrogen

gas that might have formed during the course of the run. This will be accomplished by cooling the retorting system under vacuum, thus removing the hydrogen from the atmosphere in the system.

F. FARET

1. General

The principal activities during this reporting period have been concerned with general Title II engineering, both at the Laboratory and at the Architect's office. A general review of the major portion of the Piping and Instrumentation Diagrams was held at the Laboratory between Architect-Engineer and Laboratory representatives. Detailed comments were prepared and provided to the Architect-Engineer. In addition, Laboratory comments resulting from a review of revised design criteria have been forwarded to Bechtel.

Bechtel has prepared the drawings and specifications for the fixed portion of the reactor vessel. The Laboratory is completing similar work for the core support cylinder, vessel spool, and the cover of the vessel. The design of these vessel internals and associated components is sufficiently complete that a single procurement effort for both the vessel and vessel internals is now anticipated.

Recent coordination and information transmittals to Bechtel have included the furnishing of sodium-systems material, data to aid in the selection of criteria for cell shielding windows, progress on design of reactor vessel components, design considerations for electrical equipment operation in argon, special cell lighting requirements, shielding consultations, calculation reviews, drawing reviews, miscellaneous analytical consultations, reviews and data, and plans for procurement procedures.

The project cost estimate has been updated in accordance with the Commission's request.

A suggested plan for procurement and construction activities has been prepared by United Engineers and Constructors, Inc. This material includes a preliminary PERT network for construction, an equipment procurement schedule and other miscellaneous related documents. Evaluation of these plans is currently in progress particularly in regard to the identification of interface problems which may affect present Title II design plans.

2. Safety Analysis

A general meeting and a number of preparatory and follow-up meetings have been held with the Commission to discuss the FARET Preliminary Safety Analysis Report (ANL-6813, Approval Copy). Suggested changes and/or additional materials are being prepared.

3. Control Rod Drives

The scram latch for the FARET control rod drive is the releasing member which connects the normal speed motor-driven portion of the drive to the pneumatically actuated portion. The latch should operate flawlessly with an acceptable minimum release time. Because of its fail-safe feature and the lack of linkages, an electromagnetic latch (see Figure 20) was chosen for the scram latch in the FARET control drive. A prototype magnet and armature have been designed, fabricated and tested. The lifting force is determined as follows:

$$f = B^2A/7.213 \times 10^7, \quad (1)$$

where

f = Lifting force, lb

A = Effective contact area, sq in.

B = Flux density, lines per sq in.
(16000 G or 1.03×10^5 lines/sq in. for Armco Iron)

$$NI = 0.313B\ell/u = \text{Ampere turns of coil} \quad (2)$$

ℓ = Length of flux path, in.

u = Permeability of magnet material
(unity for air and ~1200 for Armco Iron).

A tentative lifting force of 1100 lb has been selected. This force is significantly in excess of the armature load of 750 lb, consisting of the weight of the actuated parts and the pneumatic force.

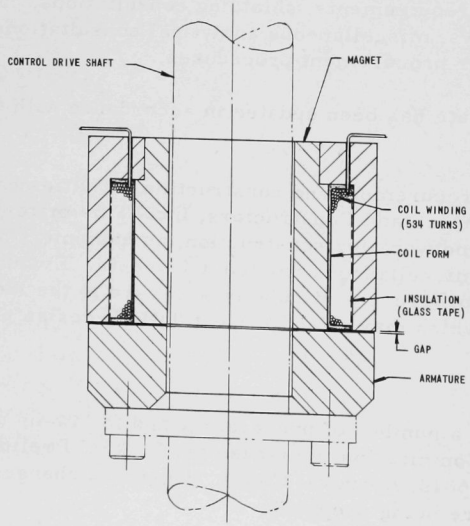

Figure 20

Magnet Armature Assembly

A test setup was assembled to determine performance characteristics of the magnet (see Figures 21 and 22). A dc current was applied to the magnetic latch by a rectifier, and a load was applied to the magnet with a hydraulic jack. An ammeter and voltmeter were used for the electrical measurements. To measure the load release time, a sensitive limit switch (see Figure 22) was attached to the magnet support. The limit switch actuator was adjusted to barely close the switch when the armature was in contact with the magnet. The magnet power circuit was opened by pushbutton switch B. When the magnet circuit was opened by switch B, switch C (in series with switch A) was simultaneously closed, thus closing a timer circuit. As soon as the armature broke away from the magnet, switch A opened, which stopped the timer. The timer indicated the load release time in milliseconds.

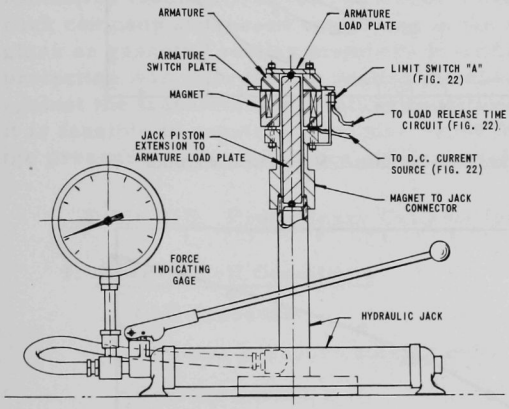

Figure 21

Magnet Lifting Force Test Setup

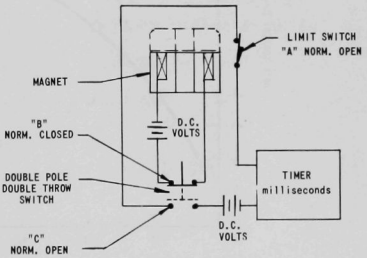

Figure 22

Armature Load Release Time Circuit

The magnet characteristics were measured as a function of the gap thickness between the magnet and the armature, which was varied by means of various thicknesses of brass shim stock. The test results are shown in Figures 23 and 24. From these data it has been concluded that the optimum gap should be approximately 0.003 in. This gap size has resulted satisfactorily in a lifting force of 1100 lb, a load release time of about 17 ms, and a coil temperature rise of 23°F.

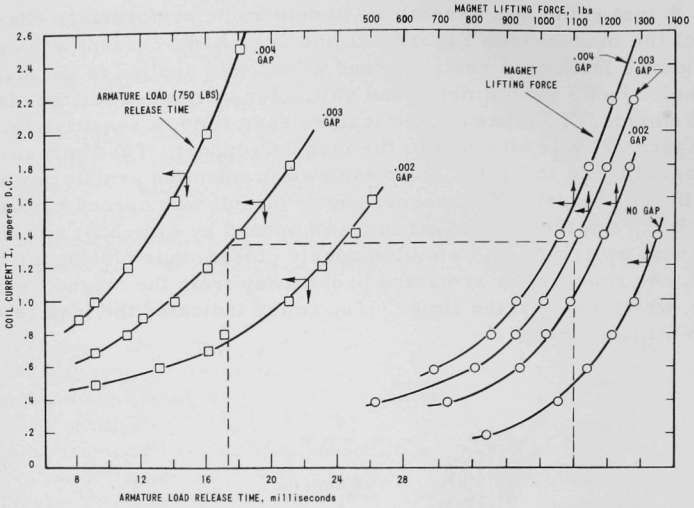

Figure 23. FARET Control Rod Drive Scramlatch Magnet Characteristics

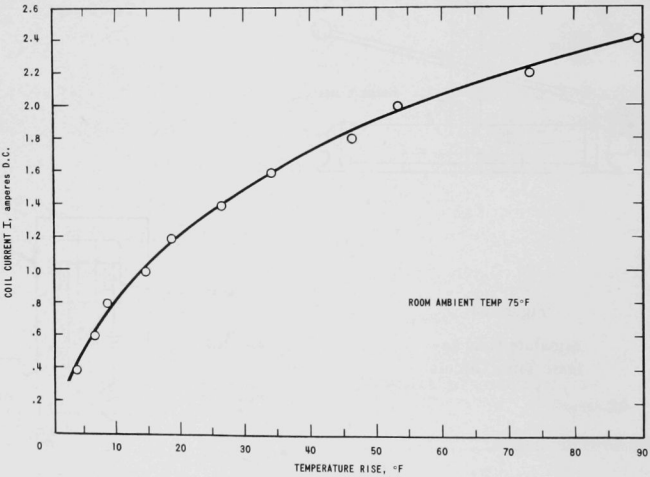

Figure 24. Magnet Temperature Rise (Due to coil current flow)

To produce the 0.003-in. gap it is planned to chrome plate both the armature and the magnet with a 0.0015-in. thickness of chrome plate. Pure chrome has a permeability of unity like that of air or brass. The magnet and armature will be retested when chrome plating has been applied. The operating atmosphere of the magnetic latch will be argon, which should not adversely affect the magnet characteristics.

4. Cell Shielding Windows

The FARET cell shielding windows are to meet rather stringent requirements. In addition to furnishing necessary biological radiation shielding, they form an integral part of the facility containment structure. This requires the windows to withstand (1) a transient pressure rise to 30 psig, (2) a transient temperature excursion of the cell gas to perhaps 1900°F, and (3) possible impact from a variety of missile fragments which may be released in a reactor incident without violation to the containment structure. In addition, normal cell operations require the total window leakage rate to be less than 0.01 cu ft/day at 4 in. w.g.

In separate meetings held at the Laboratory with technical representatives from each of the two major shielding window manufacturers, each company expressed confidence in the use of thick monolithic slabs of glass as gasketed sealing members to withstand 30 psig, provided ample protection was afforded the sealing member against impact breakage and against the transient temperature condition. Each company believed that it is feasible to construct a window to meet the criteria of Table XIII, and the pressure and temperature conditions of Figures 25 and 26.

Table XIII. Preliminary Criteria for FARET Window Design

I. Normal Cell Conditions	
Cell pressure	-2 to +2 inches WG
Ambient pressure outside cell	12.2 psia
Cell temperature	70°F to 100°F
Cell atmosphere	Argon; mixture of argon and air; air
Maximum gamma level	10^6 R/hr
Accumulated yearly exposure	10^8 R
Gamma radiation rate tolerable at operator's side	2.5 mR/hr
II. Maximum Transient Conditions	
Cell pressure	See Figure 25
Cell temperature	See Figure 26
Window design pressure	30 psi
Glass slab pressure capability	60 psig

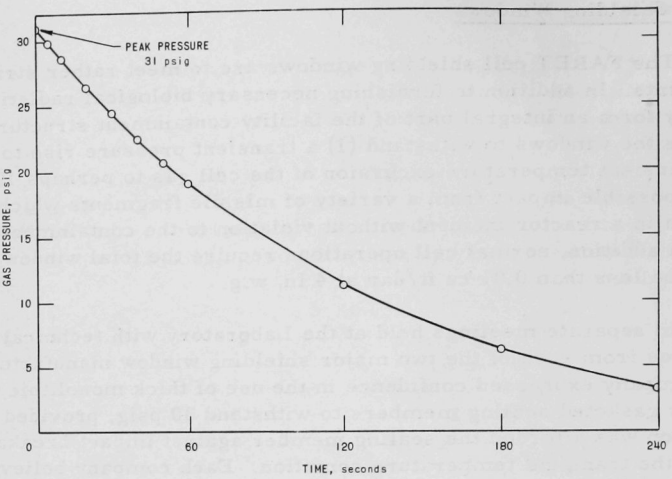

Figure 25. FARET Cell Pressure-Time Profile (0-240 sec) Sodium-Air Reaction

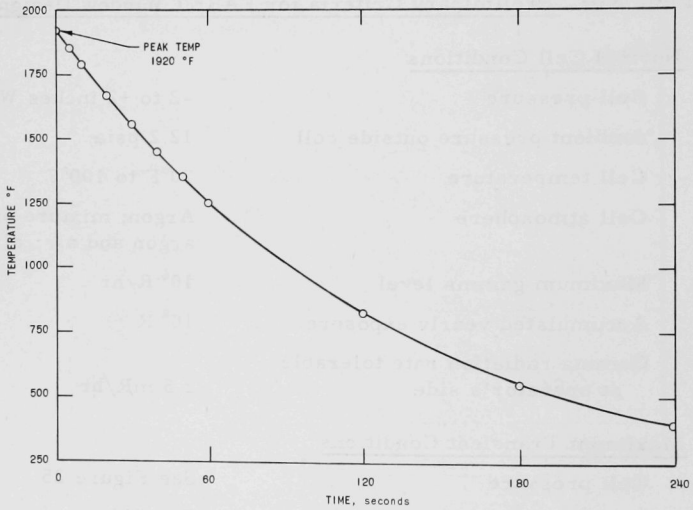

Figure 26. FARET Cell Temperature-Time Profile (0-240 sec) Sodium-Air Reaction

a. Window Testing. Since there is no background of experience for the use of glass slabs of approximately 3 ft sq x 6 to 9 in. thick as pressure members, four glass slabs are being purchased from Pittsburgh Plate Glass Co. in order to test certain design features. The glass slabs are

29 x 44 x 8$\frac{1}{2}$ in. thick. The slabs (polished on the optical faces) were rejected for shielding window use because of optical defects, but are mechanically sound for test purposes. A test fixture has been designed to test the slabs hydraulically (mounted and gasketed vertically in a manner similar to one proposed window design).

Following the hydraulic test, the fixture will be positioned in a horizontal position. A second framed glass slab will be mounted atop the first slab, and the two glass faces will be separated by a $\frac{1}{8}$-in.-thick gasket around the periphery. Impact tests will be conducted in which weights will be dropped from various heights to land on the center of the top slab. While the fate of the top slab will be of interest, the main concern will be the degree of protection the upper slab affords to the lower one.

If the glass passes these tests, window design will proceed on the basis of a single thick slab (~6 in. thick) for sealing, protected by two additional thick slabs (~6 in. and 8 in., respectively).

b. Window Arrangement. A plastic model of the FARET cell has been built, scale 1 in. = 1 ft, with walls and roof of $\frac{1}{4}$-in. plexiglass. One use of the model will be to demonstrate the viewing effectiveness of windows at various locations along the walls. In keeping with operating requirements and acceptable cost limits, the current most acceptable number and placement of windows is as follows:

(1) Total number of windows - 9 or 10 depending on unit cost.

(2) Placement: 3 along east wall and 5 along the west wall, one at a height of ~16 ft above the cell floor in the west wall and one spare liner in the north wall.

Since the equipment and actual tasks to be performed remotely in the cell are still only at a conceptual stage, uniform spacing of windows seems advisable to assure best overall viewing.

5. Component Development

a. In-core Instrumentation

(i) Extension Lead Wire. A typical FARET fuel pin temperature instrument system has been simulated. A tungsten-3% rhenium (W-3% Re)/tungsten-25% rhenium (W-25% Re) thermocouple was attached to a high-temperature connector which had stainless steel (304) and Alumel pins and sockets. Stainless steel and Alumel extension lead wire was attached to the connector and terminated at a reference junction. The thermocouple, connector, and extension lead wire withstood a temperature as high as 656°C in an argon atmosphere.

The total system performance was compared with the original data for the extension lead (see Progress Report for October 1963, ANL-6801, pp. 28 and 29). A slight decrease in the emf output of the system at temperatures above ≈400°C was noted (see Progress Report for January 1964, ANL-6840, p. 50). This effect was attributed to the inadvertent use of 302 instead of 308 stainless steel for the extension lead wire. Chemical analysis showed that the 308 alloy had ≈2% more nickel and chromium and ≈1% more manganese than the previously used 302 alloy.

In order to verify this change in output, the same simulated system was used in a duplicate test except that 308 stainless steel was used as one leg of the extension lead wire. Table XIV gives the data and the calculated errors in the measured temperature due to the entire system when a W-3% Re/W-25% Re thermocouple hot junction is at the temperatures shown. These new data compare favorably with the original. The data obtained from the test using the 302 alloy has, therefore, been discarded.

Table XIV. Thermocouple, Connector, and Leadwire (308 SST/Alumel) Characteristics and Errors

Temp, °C	Output, mV			% Error in T_m Hot Junction Temp of		
	System	W-3% Re W-25% Re	ΔE Error	1000°C	1500°C	2000°C
122	2.15	1.44	+0.71	+3.6	+2.6	+2.4
172	2.94	2.17	+0.77	+3.9	+2.9	+2.7
242	3.91	3.29	+0.62	+3.1	+2.3	+2.1
302	4.72	4.33	+0.39	+2.0	+1.5	+1.3
301	4.73	4.31	+0.42	+2.1	+1.6	+1.4
362	5.72	5.41	+0.31	+1.6	+1.2	+1.1
426	6.78	6.64	+0.14	+0.7	+0.5	+0.5
486	7.86	7.82	+0.04	+0.2	+0.2	+0.1
573	9.44	9.55	-0.11	-0.6	-0.4	-0.4
656	11.25	11.23	-0.02	-0.1	-0.1	-0.1
582	9.77	9.73	+0.04	+0.2	+0.2	+0.1
522	8.65	8.53	+0.12	+0.6	+0.4	+0.4
450	7.30	7.11	+0.19	+1.0	+0.7	+0.7
382	6.10	5.79	+0.31	+1.6	+1.2	+1.1
320	5.10	4.64	+0.46	+2.3	+1.7	+1.6
252	4.05	3.46	+0.49	+2.5	+1.8	+1.7
200	3.30	2.60	+0.70	+3.5	+2.6	+2.4
150	2.56	1.84	+0.72	+3.6	+2.7	+2.5
100	1.66	1.15	+0.51	+2.6	+1.9	+1.8
50	0.89	0.52	+0.37	+1.9	+1.4	+1.3

Note: T_m - Temperature Measured by W-3% Re/W-25% Re Thermocouple

The data obtained from the above test with the 308 stainless steel lead wire, along with the original data, was used to obtain a standard stainless steel/Alumel emf-temperature table. A "least squares" fit to all the data was found by using an equation of the form

$$emf = At + Bt^2 + Ct^3,$$

where emf is in millivolts, A, B, and C are constants, and t is the temperature in C°. The tabulated values are listed in Table XV along with the corresponding W-3% Re/W-25% Re values.

Table XV. Comparison of 308 Stainless Steel/Alumel Lead Wire and W-3% Re/W-25% Re Thermocouple Wire

Temp, °C	STST. Alumel mV	W-3% Re W-25% Re mV	Temp, °C	STST. Alumel mV	W-3% Re W-25% Re mV
0	0	0	330	5.215	4.821
10	0.179	0.096	340	5.370	5.002
20	0.355	0.197	350	5.525	5.186
30	0.529	0.302	360	5.681	5.372
40	0.702	0.411	370	5.838	5.558
50	0.872	0.525	380	5.997	5.747
60	1.040	0.642	390	6.157	5.937
70	1.206	0.763	400	6.318	6.128
80	1.371	0.888	410	6.481	6.322
90	1.534	1.015	420	6.645	6.518
100	1.696	1.145	430	6.811	6.714
110	1.856	1.278	440	6.979	6.911
120	2.015	1.414	450	7.149	7.108
130	2.172	1.553	460	7.321	7.305
140	2.328	1.695	470	7.495	7.503
150	2.484	1.840	480	7.671	7.701
160	2.638	1.989	490	7.849	7.899
170	2.792	2.138	500	8.030	8.097
180	2.945	2.290	510	8.213	8.294
190	3.097	2.445	520	8.399	8.492
200	3.249	2.602	530	8.588	8.689
210	3.400	2.764	540	8.779	8.887
220	3.551	2.928	550	8.973	9.088
230	3.701	3.093	560	9.170	9.290
240	3.852	3.258	570	9.370	9.490
250	4.002	3.426	580	9.574	9.691
260	4.153	3.596	590	9.780	9.890
270	4.303	3.767	600	9.990	10.092
280	4.454	3.940	610	10.204	10.294
290	4.605	4.114	620	10.421	10.496
300	4.757	4.290	630	10.642	10.699
310	4.909	4.465	640	10.866	10.903
320	5.062	4.642	650	11.094	11.107

The stainless steel (308)-Alumel extension lead wire combination still appears to be the best base metal combination known for use at high temperatures (above 300°C) with W-3% Re/W-25% Re thermocouples. Other lead wire combinations which might better match the above-mentioned tungsten-rhenium alloy over a wider temperature range and matches for the other tungsten-rhenium alloy combinations are still being sought.

(ii) Flowmeters. Three types of instruments are currently being considered to measure the coolant flow rates through the FARET fuel assemblies.

The first consists of an electrical heater element and two or more thermocouples placed in the flow stream. A small amount of the total fuel assembly flow is directed past the special heater assembly and the measured temperature rise between the inlet and outlet of the heater assembly at a constant heater power is an indication of the flow rate. The second instrument is a commercially available turbine flowmeter, and the last is a specially designed permanent-magnet electromagnetic flowmeter. All three devices are being evaluated for performance characteristics and feasibility of construction.

b. Plenum Plates. Preliminary stress analysis of the FARET plenum plates showed that the middle plate, being unsupported in the center, was a source of great concern. However, if the pressure is assumed to be acting on the net area of the plate (total plate area minus the area of the holes), then the magnitude of the load reduces by a half. In place of the expected pressure of 75 psi in the high-pressure plenum, only 36.5 psi would have to be resisted by the middle plate. Under this assumption, a 6-in.-thick plate appears to be adequate.

6. Fuel Assembly Sodium Flow Test Facility

The preparation of the deep pit in Building 308 for this test facility is in progress. The base plate for the dump tank, the pressure vessel support stand, and the pressure vessel upper guide assembly are completed and ready for welding in position. Fabrication of piping spools will be started soon. The modifications of the interim pump should be completed shortly. The thermal insulation is expected about the middle of July. The major portion of the heaters should be delivered by July 15. The only major components not yet on order are the pipe hangers.

Detailed stress analyses of vessels and piping for the above loop have revealed the fallacies of blindly following the ASME and ASA Codes. Analysis in progress shows the necessity for eliminating standard radius weld elbows in favor of pipe bent to large radii.

7. Subassembly Water Flow Test

An existing EBR-II water loop has been adapted for measuring the pressure drop versus flow rate characteristics of the FARET subassemblies. The lower grid plate section of the loop is designed so that changes in grid plate thickness or spacing, in subassembly seating arrangement, or in clearances between grid plates and subassembly lower adaptors may be made readily. Enough test components are on hand to permit checking flow control between high and low pressure plenums, leakage through clearances, subassembly holddown characteristics, and reactor bypass flow control. Complete subassemblies for test are on order.

III. GENERAL REACTOR TECHNOLOGY

A. Experimental Reactor and Nuclear Physics

1. High-conversion Critical Experiment

Much of the data obtained during the course of the High-conversion Critical Experiment (Hi-C) is presented in the accompanying plots. As indicated in the plots, some data were obtained with stainless steel and others were with aluminum-clad fuel. Some cores were uniformly loaded in square or triangular pitch lattices, but intermediate fuel-loading densities were obtained by removing fuel pins in patterns of one from each group of nine, or one from each group of six, etc., leaving a somewhat nonuniform distribution of fuel and moderator.

Figure 27 shows the amount of U^{235} required to achieve criticality in fully reflected cylindrical cores fueled with 3.04 w/o (Hi-C) and 5.04 w/o (BORAX-V) enriched UO_2, with H_2O used for both moderator and reflector. The data are plotted in terms of kilograms of U^{235} versus the atom ratio of H/U^{238}. The volume ratios (H_2O/UO_2) are one-third the magnitude of the atom ratios H/U^{238}.

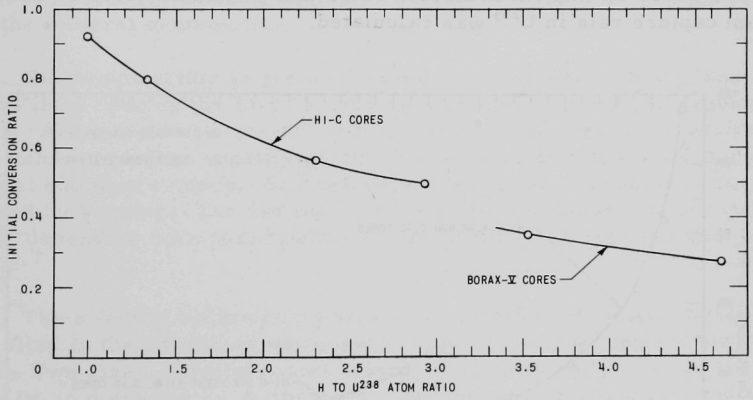

Figure 27. Critical Masses for Cylindrical Hi-C and BORAX-V Cores

Critical buckling values, obtained from fitted activation plots, are shown in Figure 28. Each point was obtained from foil traverse activation measurements and was fitted by using either the Bessel or cosine functions to yield the extrapolated dimensions of the reactor. Great care was exercised in determining the radii, and data obtained from peripheral activations which were affected by reflected neutrons were eliminated.

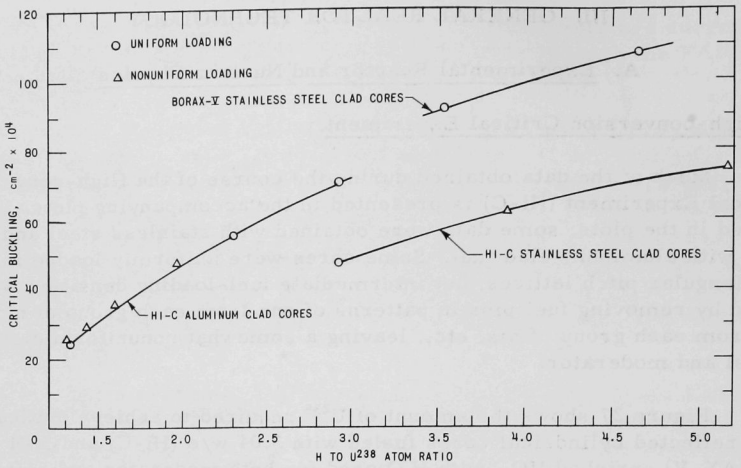

Figure 28. Critical Bucklings for Hi-C and BORAX-V Cores

Initial conversion ratios ranging from 0.3 to 0.9 were obtained during the course of the experiments, with the results shown in Figure 29. The data are based on measured fission rates and plutonium yields. The nonfission capture rate in U^{235} was calculated.

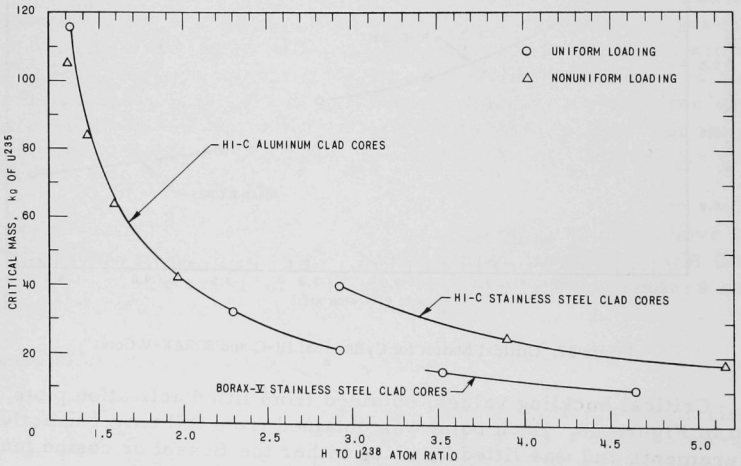

Figure 29. Initial Conversion Ratios in Hi-C and BORAX-V Cores

In future experiments, a more densely loaded fuel zone will permit additional buckling and conversion ratio measurements. It was originally expected that a plot of the initial conversion ratio values would indicate a maximum in the curve as the fuel density was increased. A maximum, however, is not indicated in Figure 29. Nominally, epithermal systems fueled with U^{235} have relatively poor conversion ratios, since the epithermal capture rate in U^{235} increases with fuel density. It was expected that this factor would limit the conversion ratio.

Various techniques for measuring the nonfission capture rate in U^{235} are also being studied. Since fission rates are measurable, the rate of nonfission captures of neutrons in U^{235} may be obtained by measuring the net reactivity worth of a sample of U^{235} and then determining the reactivity worths caused separately by the fission energy and by the thermal energy neutrons. This measurement will be investigated in a proposed method in which a spontaneous fission source is inserted into the reactor to establish the separate reactivity worth of fission neutrons on the U^{235}.

2. Absolute Measurement of P^{32} Activity Produced by $S^{32}(n,p)P^{32}$

S^{32} is one of the most widely used threshold neutron detectors. Upon exposure to a fast neutron flux, the S^{32} undergoes an n,p reaction to produce P^{32}. It is necessary to determine the absolute P^{32} activity in order to estimate the integral neutron flux.

Elemental sulfur is generally used for exposure in low intensities of neutron flux. The sulfur may be used as a powder or it can be processed into pellets. After exposure, the P^{32} activity in the target can be counted directly or, to achieve greater sensitivity, the P^{32} can be separated from the target material and then counted. In these experiments the elemental sulfur was removed by burning. The portion of P^{32} activity left behind varies from 90 to 93%; depending upon test conditions, the results are reproducible within $\pm 1.5\%$.[6,7]

The effect of sulfur pellet size was investigated, since the sample sizes cited in the literature were much larger than those used in this investigation. Two sizes of pellets were tested: $\frac{3}{4}$ in. in diameter by $\frac{1}{4}$ in. thick, and $\frac{3}{16}$ in. in diameter by $\frac{1}{16}$ in. thick. The results obtained with the smaller pellets agreed with the results reported in the literature, whereas the variation in results obtained with the larger pellets was considerably greater than expected.

---

6 Parker, B. H., The Measurement of Fast Neutron Flux Using the $S^{32}(n,p)P^{32}$ Reaction, AERE-R-3443 (1960).

7 Reinhardt, P. W., and David, F. J., Health Physics 1, 169 (1958).

The variation in reproducibility obtained in testing the larger pellets is attributed to a geometry effect. Since there are situations in which flux levels require the use of large pellets to obtain countable activities, the investigation to develop a reproducible geometry for large pellets will be continued.

B. Theoretical Reactor Physics

1. Numerical Analysis

The linear fractional transformations of the independent variable discussed in the Progress Reports for April 1964 and May 1964 (ANL-6885, p. 40, and ANL-6904, p. 71, respectively) have been applied to the Fourier-Chebyshev expansions of the error function, of Dawson's integral (the error function of a pure imaginary argument), and of the exponential integral. Expansions of the following forms were investigated:

$$\frac{\mathrm{erf}(x)}{x} = \frac{2}{\sqrt{\pi}}\, x^{-1} \int_0^x e^{-t^2}\, dt = {\sum_{q=0}^{\infty}}' c_q T_q^* \left\{ \frac{\beta x^2}{1 + [\beta - (1/16)]\, x^2} \right\}; \qquad (1)$$

$$\frac{e^{-x^2}}{x} \int_0^x e^{t^2}\, dt = {\sum_{q=0}^{\infty}}' c_q T_q^* \left\{ \frac{\beta x^2}{1 + [\beta^2 - (1/25)]\, x^2} \right\}; \qquad (2)$$

$$E_1(x) + \ln(|x|) = \int_x^{\infty} \frac{e^{-t}}{t}\, dt + \ln(|x|) = -{\sum_{q=0}^{\infty}}' c_q T_q^* \left\{ \frac{\beta x}{1 + [\beta - (1/4)]\, x} \right\} \qquad (3)$$

(the prime on the sums indicates that the first term is to be multiplied by 0.5).

Results are summarized in Table XVI, where the number of terms in the series required for 10, 15, 20, and 24 decimal accuracy are given for the value of β which causes the denominator to be independent of x, and for one close to the optimum value. In all cases, a dramatic improvement is apparent.

Unlike the Fourier-Chebyshev expansion in the original variable, the coefficients in these expansions do not tend to decrease in a regular manner. This is because the coefficients change sign as β varies. By a judicious choice of β, it is possible to construct an expansion in which the first neglected term is far smaller than would normally be expected, and thus to increase the efficiency of the approximation for a particular desired accuracy. The alteration of sign of the coefficients also indicates that the parameter space is <u>not</u> convex with respect to β. This means that conventional descent methods will not be applicable for producing true minimum-error approximations with a rational transformation of the independent variable.

Table XVI. Transformation of Independent Variable in Fourier-Chebyshev Series

Function:	Error Function		Dawson's Integral		Exponential Integral	
Range:	$-4 \leq x \leq 4$		$-5 \leq x \leq 5$		$0 \leq x \leq 4$	
β =	0.0625*	0.0865	0.040*†	0.0613	0.2500*	0.2915
Terms for 10 D	20	15	26	18	13	10
Terms for 15 D	26	20	34	23	17	13
Terms for 20 D	32	24	-	27	21	17
Terms for 24 D	36	27	-	31	24	19

* This β corresponds to a linear transformation of the original variable.

† The series rearrangement lost all significance. Values taken from D. G. Hummer, Expansion of Dawson's Integral in a Series of Chebyshev Polynomials, Math. Computation, 18, 317-319 (1964). Value for 15 D is actually for 14 D, his maximum.

C. High-temperature Materials Development

1. Ceramics

Among the fertile and fissile materials being studied or developed for reactor use at a maximum temperature in the range from 750 to 2000°C are the ceramic compounds of uranium, plutonium, and thorium, and of various mixtures of solid solutions of these compounds. Some of the binary compounds have melting temperatures of about 3000°C. Although most of the work on ceramic fuels has been on the oxides and the carbides, the sulfides, phosphides, and such combinations as UP-US, UC-US, PuS-US, and PuP-UP are receiving considerable attention; the arsenides, selenides, antimonides, and tellurides will eventually be investigated.

Some of the more important considerations, besides melting point, are thermochemical and irradiative stability, fabricatability, composition control, the effects of impurities, compatibility with cladding materials, mechanical properties, volatility, thermal conductivity, and thermal expansion. No one of the binary compounds has all the desired characteristics in sufficient degree, but no one of the compounds is beyond the possibility of improvement through certain modifications and combinations of the compounds. Considerable emphasis is therefore being given to preparing these ceramics and studying their properties.

a. Plutonium and Plutonium-Uranium Carbides. The sintering of (U,20Pu)C has been investigated in an effort to characterize the sintering process so that the best method of sintering can be used for production of fuel pellets. Material for this study was prepared by melting pieces of plutonium, uranium, and carbon in an arc-furnace. This starting material usually contained <0.01 w/o of both oxygen and nitrogen. Powder was handled in a nitrogen atmosphere with oxygen impurities of about 0.005 a/o and water-vapor content of <0.01 w/o. Preliminary work showed that solid-solution material lost plutonium when fired under vacuum to temperatures of 1600°C for 2 hr. The plutonium content decreased from 19.1 w/o in the arc-melted buttons to about 16.5 w/o in pellets made from powder with a particle size of $<15\ \mu$. Pellets prepared from <44-μ powder fired in vacuum for 4 hr at 1850°C changed in plutonium content from 19.1 w/o to about 14 w/o.

To reduce plutonium vaporization, the pellets were fired in flowing high-purity argon. Pellets of (U,20Pu)C prepared from powder with a particle size of $<8\ \mu$ sintered in argon for 2 hr at 1600°C acquired densities of 80 to 85% of theoretical. Sintering at 2000°C for 2 hr increased the density of the pellets to 90% of theoretical. There was no loss of plutonium when the pellets were sintered in flowing argon. Pellets made from fine-particle-size powders had about 1 w/o of oxygen, and the sesquicarbide phase was present in X-ray photograms of the pellet material. In comparison, pellets prepared from <44-μ powder and sintered at 1600°C had densities of about 76% of theoretical, but the oxygen content was usually <0.3 w/o and X-ray photograms showed only lines from the (U,Pu)C solid solution. Blended powders of <15-μ UC with 20 w/o of <44-μ PuC behaved about the same as the arc-melted solid-solution material. Densities of pellets made from the blended powders and sintered at 1600°C for 2 hr were about 80% of theoretical. These pellets will be chemically analyzed to determine the amount of plutonium loss, if any, that can be expected from blended powders. Sintering at temperatures above the melting point of PuC (1660°C) will also be investigated.

Because of the problems of high oxygen content and control of the phases in fine-particle-size powders, further work was directed toward understanding the sintering characteristics of <44-μ powder. This powder was coated with 0.5 w/o Carbowax binder and pressed into pellets at about 2.1 metric tons/cm^2. Pellets were sintered at increasing temperatures 2 hr. The change in density with sintering temperature is shown in Table XVII. Pellets of 90% theoretical density were obtained by sintering at 2100°C. Chemical analysis shows no detectable loss of plutonium from sintering at this temperature. This procedure is now being used to make pellets 0.634 cm in diameter by 1.2 to 1.5 cm long for instrumented irradiation studies in MTR and for test fuel elements for EBR-II. To date all of the arc-melted material for the work has been made, and 40 cm of fuel pellets have been fabricated; 10 cm of these pellets have axial holes. Future work will be devoted to production of pellets.

Table XVII. Density of (U,20Pu)C Pellets with Sintering Temperature

Sintering Temperature (°C)	Percent of Theoretical Density
1600	73.8-76.8
1950	84.9
2000	87.6
2100	89.9

b. Uranium and Plutonium Monosulfides.

(i) Preparation of Uranium Monosulfide. The investigation of the preparation of uranium monosulfide by a fused-salt process was resumed. This process consists of the reaction of UF_4 with H_2 and H_2S gases in a fused, NaCl-KCl salt bath. Previous work showed that the product was highly contaminated with oxygen. The best product obtained contained approximately 51% US and 49% UOS.

The reaction apparatus has been put back into operation. Attempts will be made to carry out the reaction in a LiCl-KCl eutectic salt bath whose melting point of 360°C should permit lower operating temperatures than were possible with the NaCl-KCl mixture, which melts at 660°C. A LiCl-KCl mixture was prepared and heated to 400°C. The resultant melt showed considerable fluidity and no excessive evaporation.

The apparatus is being modified for electrolysis experiments. This modification should permit the removal of dissolved water by electrolytic decomposition, thus eliminating a major source of oxygen contamination. In addition, attempts will be made to prepare US by the electrolytic reduction of UCl_4 followed by reaction with an alkali sulfide present in the salt bath.

(ii) Fabrication of Uranium Monosulfide-Tungsten Composites. Previous attempts at preparing uranium monosulfide-tungsten cermets by the sintering of powder mixtures were unsuccessful because of segregation of the components during sintering. However, it has been reported that US can be contained in a sufficiently dense tungsten crucible. In addition, high-density UO_2-W composites have been successfully prepared by co-deposition from solution of uranium and tungsten compounds followed by heat treatment to yield UO_2-W mixtures.

The above facts suggest that similar, intimate mixing of US with a thermally unstable tungsten compound might lead to US-W bodies with more desirable properties. A literature survey of data on tungsten compounds led to the choice of the hexachloride and hexacarbonyl as possible additives. Supplies of these compounds have been ordered for preliminary experiments.

c. Preparation and Properties of Plutonium Sulfide. Over the past few months various Pu-S compositions have been synthesized by the reaction of hydrogen sulfide gas with partially dehydrided plutonium. Present work is now being directed toward sintering studies and property measurements on this material.

Pieces of plutonium metal were reacted with hydrogen at 200°C to form $PuH_{2.0}$-$PuH_{2.7}$, and then alternately dehydrided at 400°C and hydrided at 200°C until the reaction was complete. The plutonium hydride was then crushed to a particle size of <44 μ, dehydrided at 400°C, and reacted with H_2S gas at temperatures from 400 to 600°C. The amount of sulfur in the plutonium was accurately controlled by careful monitoring of the quantity of H_2S gas used in the reaction. The product, consisting of a mixture of PuH_x and Pu_2S_3, was homogenized under vacuum at 1700°C for 4 hr. The homogenized material usually contained about 0.05 w/o oxygen. The ANL Chemsitry Division is presently testing apparatus to measure the sulfur content. X-ray diffraction patterns showed sharp doublets for the PuS and Pu_2S_3 phases.

Preliminary work to determine the melting point of PuS gave a value above 2200°C, the temperature limit of the heating element in the furnace used for this measurement. Work is in progress to change the heating element so that higher temperatures can be achieved.

The sintering characteristics of two compositions were investigated: one contained the PuS phase only, and the other contained both the PuS and Pu_2S_3 phases. Powder was crushed to a particle size of <44 μ, coated with 0.5 w/o Carbowax binder, and pressed at 2.11 metric tons/cm^2. The resulting pellets were sintered in a flowing high-purity argon at atmospheric pressure for 2 hr at increasing temperatures. Table XVIII shows the change in density of the pellets with sintering temperature. A density of about 90% of theoretical was obtained with a sintering temperature of 1700°C. Higher temperatures did not improve densification. These pellets contained <0.050 w/o oxygen after sintering.

Table XVIII. Density of Pu-S Pellets as a Function of Sintering Temperature

	% Theoretical Density			
Composition	1600°C	1700°C	1800°C	1900°C
PuS	85.8	91.6	91.6	90.2
PuS + Pu_2S_3	85.4	89.3	89.3	87.7

d. Properties of (Th,U) Phosphides. The relative stability of UP and the fact that thorium phosphide exhibits a melting point of about 3000°C arouse interest in the possibility of using actinide phosphides as fuel and/or breeding materials in reactors at very high temperatures. Before the phosphides of uranium and thorium can be evaluated for reactor use a great deal of information on the characteristics of uranium phosphide, thorium phosphide, and thorium-uranium phosphide must be obtained. A program has therefore been initiated to supplement the little data now available. The high-temperature stability, stoichiometry, and fabricating characteristics are being investigated. Besides giving basic data, the results of this month's research show that decomposition of UP accelerates above 2300°C in vacuum. In addition, large samples of UP, suitable for thermal conductivity measurements, were fabricated by hot pressing.

Heating of UP in vacuum above 1400°C invariably causes a decrease in its lattice constant of 5.589 Å, which value appears to correspond to that for stoichiometric material. The contraction of the lattice is attributed to preferential loss of phosphorus. On heating UP in vacuum at 2000°C the lattice constant showed a value of 5.583 Å, which did not change with prolonged heating at this temperature. The lattice constant increased slightly to 5.584 Å with heating at 2200°C, and showed a substantial further increase to about 5.588 Å with heating at 2300°C. These results appear to indicate that above 2000°C (in vacuum) the UP lattice begins to lose uranium preferentially, and that above 2200°C the preferential loss of uranium accelerates. Support for this conclusion is given by the observation of moderate amounts of free uranium as an intergranular liquid phase in samples heated to 2300°C. X-ray diffraction confirmed the microscopic observations. These samples also bonded to the tungsten sheet upon which they rested, most probably as a result of the reaction between tungsten and uranium. Tungsten and UP show no sign of reaction in the absence of free uranium in the latter. In vacuum, "UP" appears to melt at a temperature considerably lower than its melting point of 2540°C, owing to the presence of large amounts of liquid phase. In this respect its behavior is similar to that of UN.

Large specimens of UP, for use in thermal conductivity measurements, were successfully fabricated by hot pressing. The fineness of the UP powder (2.5 μ) necessitated special treatment to achieve optimum results. A large number of hot-pressing runs were required to establish the best firing parameters (pressure, time, and temperature). A sample, 7.6 cm long and 2.0 cm in diameter, with a density of 82.6% of theoretical, was produced by using a pressure of 2000 psi and a temperature of 1640°C. Raising the pressure to 8500 psi resulted in a sample of equivalent size, but with a density of 92.4% of theoretical.

Uranium phosphide and thorium phosphide appear to form a complete series of solid solution after heating at 2000°C for 8 hr. However, the X-ray powder photographs indicate that the lattice is very highly strained.

The back reflections are very diffuse, which will make accurate determinations of the lattice parameter virtually impossible. The intermediate compositions are all blue in color, although less so as the UP content decreases.

e. Thermal Property Measurements of Ceramic Materials

Measurements of specific heats and thermal diffusivities of ceramics and ceramic reactor materials are being carried out on available specimens. A standard sample of Armco iron is being run concurrently with the unknowns to prevent equipment variations from affecting the results. Table XIX gives data obtained with sintered uranium dioxide and high-purity alumina.

Table XIX. Thermal Properties

Material	Percent of Theoretical Density	Thermal Diffusivity $\alpha(cm^2\ sec^{-1})$	Specific Heat C_p $(cal\ gm^{-1}\ °C^{-1})$	Thermal Conductivity K_p $(cal\ gm^{-1}\ cm^{-1}\ sec^{-1})$
Aluminum Oxide	88	0.075	0.18	0.047
Uranium Dioxide	91	0.023	0.063	0.014

The specific heat values agree very well with literature values. Calculated thermal conductivities appear to be reasonable. A numerical comparison with published data is unrealistic because of the absence of room-temperature measurements of well-characterized oxides. Also, a much larger decrease in conductivity of porous alumina and urania, compared with dense material, than would be proportional to the ratio of densities is reported in the literature, so that a simple correction to zero porosity cannot be carried out.

2. Corrosion by Liquid Metals

a. Lithium. Molybdenum, tantalum, niobium, tungsten, and their alloys are generally considered as potential containment materials for lithium at high temperatures. However, very few data pertinent to corrosion and solubility of these materials above 1000°C are available. Accordingly, a program is being conducted to gain basic knowledge of the behavior of these materials on exposure to the liquid and vapor phases of lithium.

High-temperature liquid-metal testing techniques have been developed, and capsules for the study of the corrosion and solubility of molybdenum, tantalum and niobium have been prepared from high-purity arc-melted rod stock. The capsules are loaded with lithium in an inert atmosphere and are vacuum-sealed by electron-beam welding.

The molybdenum capsule assembly described in the April report (ANL-6885, p. 41) consisted of a capsule and a small molybdenum rod sample. The material was fabricated from wrought bar stock of 99.95+% purity. Oxygen and nitrogen contents were 20 and 10 ppm, respectively. Reagent-grade lithium was used in this test. The capsule was exposed at 1000°C for 100 hr.

The area above the level of liquid lithium showed a smooth surface with a recrystallized structure, revealing no corrosion attack. However, random penetration occurred below the liquid level, particularly on the bottom portion of the capsule, to a depth of about 1.5 mils. There was no measurable weight change nor apparent corrosion attack of the rod sample except for some discoloration on the area where the end rested on the bottom of the capsule. Chemical analysis of lithium awaits completion of suitable facilities for sample transfer.

The results with molybdenum indicate that attack by lithium vapor is negligible. The resistance of molybdenum to attack by liquid lithium has not been completely evaluated. A study of various environmental and material factors will continue. Additional tests, and tests of tantalum samples are in progress.

b. Studies with Sodium. A variety of materials have been tested briefly in highly oxygenated sodium at up to 650°C in a search for materials appropriate for electrodes therein. Unalloyed vanadium lost weight rapidly in 18 hr and was embrittled; tantalum and Nb-5V formed voluminous reaction products and lost weight; platinum dissolved rapidly, as expected; stainless steel exhibited noticeable attack but may be useful; nickel was relatively resistant.

All of the foregoing (excepting stainless steel and nickel) and zirconium and its alloys displayed a low, positive emf of from 9 to 13 mV with respect to a cool extension of the nickel chamber. This potential is interpreted as a thermocouple emf primarily, and the behavior was in keeping with this interpretation over the range from near room temperature to 650°C.

The most appropriate sample materials appear to be zirconium and zirconium alloys such as Zr-3 w/o Ni-0.5 w/o Fe and Zr-1 w/o Cu-1 w/o Fe, which form dark, adherent corrosion-product films that are insulators at room temperature. These materials have exhibited net weight gains after 540°C exposure and net losses at 650°C, apparently reflecting a film-deterioration process that is more prominent at the higher temperature.

The weight-change behavior may explain difficulties, due to electrical shorts through corrosion films, encountered when polarization currents have been imposed at 650°C, in contrast with a degree of protection

afforded by films at 540°C. Tests with sample surfaces prefilmed in steam gave similar results. At 540°C apparently valid anodic polarization curves have been obtained and anodic currents have been maintained for experimentally useful times, i.e., days, with resistive surface films preformed either in steam or in the cell sodium.

An attempt at cathodic polarization across such a surface film at 540°C was aborted when the cell resistance decreased rapidly as current flow was begun. Tests afterward in mercury at room temperature revealed only one small shorted region at the sites of surface roughness near the electrode tip, in spite of an effort to avoid film cracks by rounding the electrode tip prior to exposure. That difficulties at 650°C have been promoted by a similar cause has not been ruled out. Electrodes having smooth, polished surfaces as well as hemispherical tips are in preparation.

3. Elastic Moduli in High-temperature Materials by Ultrasonics

To measure the temperature dependence of the elastic moduli of materials that show promise in high-temperature reactor applications, a vacuum furnace has been constructed in which solid bar-shaped samples will be mounted. Pulsed ultrasonic waves will be propagated along the length of these samples, and the transit times of pulses passing a heated, indexed region in each bar will be measured. The indexing is done by machining one end to a smaller diameter than the rest of the bar (see Progress Report for April 1964, ANL-6885, p. 45).

Construction of a secondary heater winding is not yet complete. It is hoped that the thermal gradient along the specimen will be reduced when this auxiliary winding is used.

Measurements of both longitudinal wave and shear wave velocities, and of attenuations of both longitudinal and shear waves propagating in vanadium-titanium alloys were made at room temperature. The data have not yet been reduced, so no values of moduli can be reported at this time.

D. Other Reactor Fuels and Materials Development

1. Corrosion in Superheated Steam

a. Zirconium Alloys. Study of the influence of alloy microstructure on corrosion behavior is continuing. Sections of ring samples have been examined metallographically. The as-cast microstructure was substantially retained through the moderate reduction achieved in the rapid-forming process. Comparable sections are being corrosion tested in superheated steam at 540°C and 42.2 kg/cm^2. Smooth, dark, adherent corrosion films free of blister attack have developed, typical of the behavior of the better steam-resistant alloys.

Efforts toward microstructural stabilization of steam-resistant materials by means of additional alloying have been continued. Alloys based on Zr-1 w/o Cu-1 w/o Fe and modified by beryllium in smaller percentages than previously used have been prepared. Alloys containing 0, 1, 2, and 4 w/o Be are currently in corrosion test with steam at 650°C and 42.2 kg/cm^2.

Further study (see Progress Report for April 1964, ANL-6885, p. 47) is being made of the effect of surface electrical phenomena on hydrogen absorption by zirconium alloys during corrosion in steam. Samples of Zr-1 w/o Cu-1 w/o Fe and Zr-3 w/o Ni-0.5 w/o Fe have been pre-corroded in 540°C, 42.2 kg/cm^2 steam in preparation for coating with a BaO layer by plasma-jet spraying. It is believed that some free barium may be produced by reduction by hypostoichiometric zirconium alloy corrosion product during subsequent corrosion, and that electron-emission characteristics may be improved in spite of a contrary poisoning influence by steam.

b. Ferrous and Nickel Alloys. The 18 percent chromiun, 8 percent nickel types of austenitic stainless steels do not resist corrosion by superheated steam as well as do some of the higher-nickel alloys, such as some of the Inconel alloys or as Incoloy 800, especially those containing small additions of aluminum or of aluminum plus titanium. The corrosion behavior in superheated steam of the relatively corrosion-resistant ferrous alloys is therefore being studied in detail.

The initial test of promising materials for 750°C oxygenated (30 ppm) steam at a pressure of 42 kg/cm^2 has been completed. Defilmed metal losses are being obtained for the corroded specimens. Those values available to date are shown in Table XX.

Table XX. Corrosion in Steam at 750°C and 42 kg/cm^2

	Metal Loss, mg/cm^2, Days				
Alloy	7.0	14.0	21.0	28.0	35.0
Type 304	8.3	10.9	14.3	23.0	29.5
316	12.2	17.8	17.7		
321	12.9	17.5	25.2		
347	11.9	16.7	24.8		
406	0.4	0.2	0.4	0.4	0.6
Inconel 600	9.4	13.5	17.9	12.4	13.8
625	0.4	0.6	0.6	0.7	0.7
X750	2.9	2.4	2.4	2.6	3.3
Incoloy 800	6.7	7.2	6.8	6.8	7.2

The Inconel 625, which had the lowest metal-loss rate, differed from the other high-nickel alloys principally in that it contained less iron (1.86 w/o), more molybdenum (8.75 w/o), more niobium plus tantalum (4.24 w/o), and a little more chromium (22.0 w/o).

Incoloy 800 (modified by aluminum to improve the corrosion resistance) is being corrosion tested in flowing steam (at 650°C, 42 kg/cm^2, and 61 m/sec). The data available to date are shown in Table XXI. These data indicate that the modified alloys are only slightly superior in corrosion resistance to the standard Incoloy in flowing steam; earlier tests had indicated that the modified alloys are markedly superior under static conditions (see Progress Report for January 1964, ANL-6840, p. 65).

Table XXI. Corrosion in Flowing Steam at 650°C

Time, days	Metal Loss, mg/cm^2		
	Incoloy 800 + 3.90% Al	Incoloy 800 + 3.70% Al and 0.3 Ti	Incoloy 800
14.0	0.53	0.33	1.10
28.0	0.72	0.38	1.74
42.0	0.66	0.71	1.16
56.0	0.94	0.78	1.21
71.6	1.02	0.78	-

2. Nondestructive Testing

a. Correlation of Heat Transfer and Bond Quality. The ultrasonic tests on the copper braze-bonded specimens have been completed. The through-transmission method at a frequency of 2.25 Mc was used; both the sender and receiver transducers were collimated to a 0.159-cm beam. The system was calibrated so that a point-by-point scan could be made of the specimen.

Results on the solid, i.e., perfect-bond, copper specimen indicated that the scattered ultrasound from the edge of the specimen interfered with the transmitted pulse in all but the central 0.5-cm^2 area. Consequently, a comparison of the ultrasonic and heat-transmission properties were made only in this area. The complete analysis showed that a close correlation exists between the drop in ultrasonic transmission and the drop in thermal diffusivity for less than perfect bonds.

b. Infrared Imaging. Present data on the infrared sensitive Vidicon system indicates that the television system can detect an object temperature 155°C above ambient. Useful object temperatures for testing purposes,

however, appear to be in the 250°C or higher range. Efforts are now under way to determine temperature differences detectable for a variety of object temperatures in order to determine an optimum area for testing applications.

c. Development of a Neutron-image-intensification System. Presently available data on the capability of a neutron-image intensifier, in which a neutron scintillator and a photoemissive layer would be used to convert the neutron image into an electron image, indicate that such a tube would respond to thermal-neutron intensities of 10^5 n/cm^2-sec or higher. Such an intensifier would be expected to provide a very useful image with the neutron intensities available from Juggernaut.

E. Remote Control Engineering Development

1. Electric Master-Slave Manipulator Mark E4

Design studies have been made of two slightly different variations of the master-slave manipulator configuration discussed last month (see Progress Report for May 1964, ANL-6904, p. 81). In both of these variations, a pair of manipulator arms can be moved as a unit to enable them to work over a table, toward a wall, or toward a ceiling. Of course, each arm of the pair retains its seven independent master-slave motions.

In one of the variations studied, a single member is used in conjunction with both arms and the servo drive package. In the other configuration, separate members are used. The counterweighting problems are somewhat simpler with the single-member variation; however, the mechanical cabling is simplest with the two-member variation.

Both variations show promise, and several layouts were made of each to study them in further detail. From these studies, it seems that the two-member variation provides the best all-around solution. Consequently, additional detail layouts are being made of this configuration. The two members can be either independently driven or attached to each other and driven together. Studies are being made to determine the most useful of these two approaches.

Enough servo drive gearboxes have been fabricated for a pair of master-slave arms plus some spares. The gears, shafts, motors, synchros, and tachometers for the servo drive units are already on hand.

Fabrication has been started on 16 servo amplifiers (14 for one master-slave arm plus 2 spares). About 70% of the electrical parts are on

hand and the rest are on order. A prototype amplifier was fabricated and tested to check out placement of components and the operation with this placement. This prototype works satisfactorily.

2. Special Motors for Master-Slave Manipulators

Preliminary tests have been made with the recently constructed very-low-inertia servo motor (two-phase, 60-cycle) having a cup rotor. The motor was specially designed to enable the rotor to be cooled by low-pressure air, and the desired flow-pressure characteristics were achieved. There are deep slots in the stator to increase the room for windings and to thus reduce the power loss in the windings. Preliminary static torque measurements, at the maximum design torque of 150 oz-in., indicated that the total power input is about equal to the original design value of 300 W. An extensive program of testing is planned including speed-torque and temperature-torque measurements.

3. Viewing Systems

Electron irradiations of small samples of shielding window glasses have been continued to determine the effect of changes in glass composition on the susceptibility of the glass to fracture by electrical discharge. In preliminary tests, cerium, which is used to control radiation-induced coloration, was found to be a factor in decreasing the rate of dissipation of the injected electrons. This effect will be studied further since it is another aspect of the role of cerium in altering the irradiation properties of glass.

As part of the program to develop better radiation-resistant glasses, a study was started on the existing data on radiation-induced color centers in the fused boric oxide, alkali borate, and alkali alumino-borate glasses. By correlating the experimental information on the borate glasses, it is expected that useful information will be learned concerning the nature of the induced centers and the effect of glass modifiers on these centers.

F. Heat Engineering

1. Two-phase Flow Studies

a. Void Fraction - Pressure-drop Facility. This experimental facility is designed to investigate the two-phase flow characteristics of boiling sodium; in particular, it is desired to obtain experimental information pertinent to the vapor volume fraction and two-phase frictional losses in an adiabatic test section. The loop is constructed of Type 316 stainless steel and is limited to short-term operation at approximately atmospheric pressure and about 1630°F.

During the procedure for filling the facility with sodium, several anomalies were apparent in the various level readings obtained from the eddy-current liquid-level probes. After a series of secondary checks by means of the gamma-attenuation void detector, two minor calibrations errors were noted and have been corrected. All readings now appear to correlate within ±0.25 in.

The approach to medium-temperature (1200°F) operation is proceeding well, although a series of power trip-outs has delayed calibration of the electromagnetic flowmeter. A series of power failures in the building supply lines caused the sodium to freeze at several points. The reheating required approximately 12 hr and has caused some delay. This situation has been corrected, and the medium-temperature calibration runs will be completed in the near future.

2. Boiling Liquid Metal Technology

a. Niobium-1% Zirconium Loop Construction. Preliminary specifications for the sodium pump and its auxiliary equipment have been prepared for supplier bids. Detailed design of the vacuum chamber walkway was completed and forwarded to the shops for fabrication. The original conceptual layout of the chamber electrical power and control wiring was completely revised. The reworked design and specifications were submitted to the servicing group for review and possible further detailing. The vacuum chamber lifting fixture has been completed and most of the hardware for the various coolant circuits has been obtained or is being fabricated.

A number of alternatives to the original vacuum chamber bell jar cooling concept were reviewed. A welded coil design which appears to satisfy both heat transer and fabrication requirements was selected and is now in the process of being applied to the vessel. Fabrication and assembly of the chamber base and pumping system has been completed, and this portion of the equipment has been evacuated to the 10^{-8}-torr region with use of a rough unbaked steel plate as a cover.

b. Heater Experiments. Initial operation of the thermal radiation-heated loop began June 1. The thermal-radiation heater has been operated for 30 hr during June. During this period, NaK temperatures ranging up to 700°F and flow rates ranging up to 1 gpm were obtained. The thermal-radiation heater has been used only in the lower power range and has supplied heat fluxes to the flowing liquid metal up to 10,000 Btu/hr-ft^2. Future testing is planned with higher temperatures and larger heat fluxes.

The thermal radiation-heated loop was filled with sodium prior to operation by evacuating the loop and supply tank, filling the supply tank with the liquid metal, and filling the loop by pressurizing the liquid metal

surface inside the supply tank with an argon gas blanket. Pressure control of the system was obtained by control of the pressure of the argon gas blanket. Both the fill technique and the method for controlling the system pressure have been been found quite satisfactory.

3. General Heat Transfer - Analysis of a Double-pipe Liquid Metal Heat Exchanger

A study of the plug flow solutions for the wide annular formulation of a double-pipe heat exchanger with fluids of low Prandtl number in parallel flow has begun. The fully developed heat transfer coefficient may be expressed in terms of four basic parameters, H, K, K_w, and R:

$$H = C_2W_2/C_1W_1;$$

$$K = k_1\sigma/k_2R;$$

$$K_w = \frac{k_1}{k_w}\ln\left(1 = \frac{b}{a_1}\right);$$

R = inner diameter of annulus/outer diameter of annulus,

where

$\sigma = 1 - R$

C_i = specific heat of fluid in channel "i"

W_i = mass flow rate of fluid in channel "i"

k_i = thermal conductivity of fluid in channel "i"

k_w = thermal conductivity of wall

b = thickness of tube wall

a_i = width of channel "i"

i = 1, for tube side

i = 2, for annulus side.

As reported in the Progress Report for April, 1963 (ANL-6717, p. 49), a plug flow solution exists for the case of a double-pipe heat exchanger configuration consisting of a circular tube surrounded by a thin annular space. The narrow-annulus solution results from assuming an annular ratio of unity in the differential equations for the double-pipe exchanger.

For annular ratios close to unity, the narrow annular-space approximation may be applied in double-pipe heat exchanger calculation. As the annular ratio decreases, the approximation becomes less accurate. Figures 30 and 31 illustrate the differences in the fully developed Nusselt numbers obtained by the narrow-annulus approximation and the wide-annulus solution for the tube side and annulus side, respectively, at an annular ratio of 0.5 and equivalent values of the parameters K and K_w for the two formulations. In both figures, the Nusselt number has been normalized to the plug flow solutions corresponding to the boundary conditions of uniform wall heat flux. It is apparent that the greatest difference between the values predicted by the two formulations lies in the annulus-side Nusselt number. In comparison with the results reported for slug flow in adjacent parallel planes (see Progress Report for October 1962, ANL-6635, p. 41), the heat transfer coefficients can be significantly lower than those predicted for boundary conditions of constant heat flux.

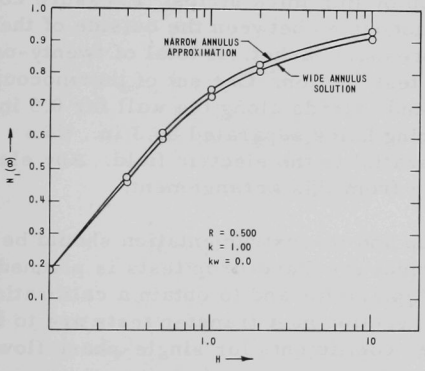

Figure 30. Fully Developed Tube Side Nusselt Number Normalized to Plug Flow Solution for Constant Heat Flux Boundary Conditions

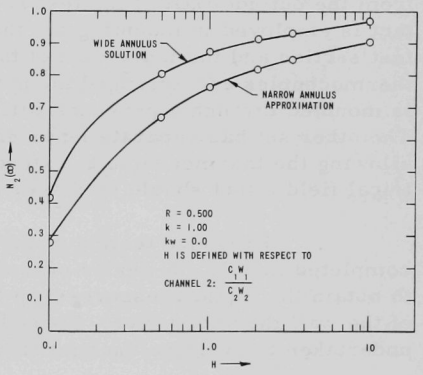

Figure 31. Fully Developed Annulus Side Nusselt Number Normalized to Plug Flow Solution for Constant Heat Flux Boundary Conditions

Other quantities are also being investigated. Among these is the "fully developed heat exchanger effectiveness coefficient."[8] Preliminary results show that this quantity can be significantly less than unity and varies as a function of the operating conditions of the exchanger.

4. ANL-AMU Program

Other heat engineering experiments, performed as part of a joint program (not supported by the Division of Reactor Development) between the Laboratory and the Associated Midwest Universities (AMU), are described below:

[8]Stein, R. P., The Graetz Problem in Co-current Flow Double Pipe Heat Exchangers, AIChE Preprint 64H11, to be presented at Seventh National Heat Transfer Conference, Cleveland, Ohio, August 1964.

a. Two-phase Flow Characteristics during the Complete Vaporization of a Fluid. Assembly of the heated test section and pressure jacket with attached power lugs is near completion. A pressure check of the test section unit will be made prior to installation in the forced-circulation loop. The flow loop will soon be completely fixed and insulated. Several minor welding operations are still required for completion of the piping network. Several fittings on order are required for the conclusion of this phase.

The inlet and exit sections remain incomplete since the test sections are being fabricated in England. It is expected that these units will be available early in July. Meanwhile, the flow loop will be pressure tested by insertion of a straight run of pipe.

Two methods of mounting the thermocouples for wall-temperature measurements have been employed. All thermocouples have been insulated from the outside wall of the test section by thin mica strips. Pressure contact is employed in mounting the thermocouples between the outside of the test section and the inner wall of the pressure jacket. A total of twenty-one thermocouples are arranged along the test section. One set of thermocouples is mounted through a pressure fitting and extends along the wall for 0.5 in. The other set has separate leads entering holes separated by 3 in., thus allowing the thermocouple to extend parallel to the electric field. Any electrical field effect should be discernable from this arrangement.

Pressure testing of the loop and its instrumentation should be completed in July. A series of isothermal pressure-drop tests is planned to obtain the liquid pressure-drop friction factor and to obtain a calibration of the wall thermocouples. Forced-convection heat transfer tests are to be undertaken to evaluate the heat transfer coefficients for single-phase flow.

b. Inception of Hydrodynamic Instability in a Natural-circulation Loop. Equipment checks and calibration in preparation for loop operation started. A defective relay on the control circuit of the Ignition power supply and some bad connections in the Ignition control circuit were overhauled. Two 15-psig strain-gauge differential pressure transducers were calibrated and installed across the test section and riser.

The loop was pressurized for checking the newly welded pressure taps on the test section and steam separator. A pressure leak was found through the dump valve, which was replaced. The loop was then heated with 10-kW power across the test section at 200 psig for a preliminary check and found to be operating satisfactorily. The instability tests will be started soon.

c. Power-to-void Transfer Functions. The experimental investigation of power-to-void transfer functions has been delayed by a rupture in the test section while operating at 600 psia. A new power oscillator control unit and enlarged power shunt have been designed and constructed.

The enlarged power shunt now consists of fifteen fixed resistors consisting of 34 Ga., $\frac{3}{16}$-in.-wide nichrome ribbon, 12 ft in length, which are mounted vertically immediately behind the Small Scale Loop. Each ribbon is individually spring loaded to maintain a constant tension when the shunt is in operation, and a movable bus bar contacts the strips to allow resistance settings from 2.5 to 0.25 ohms. The ribbons are cooled by forced-air convection, and the entire shunt will be able to dissipate 20 kW of power. The redesigned power control unit has also been completed and rock mounted with its own power supply. Figure 32 illustrates one subunit in which silicon-controlled rectifiers in a fuel wave arrangement control the current through the resistance ribbon. The firing of the rectifiers is controlled by a magnetic trigger which supplies trigger pulses to the gate electrode. The control current for the trigger is supplied from a triode circuit which has the cathode biased at 4-V intervals. By applying a sinusoidal control signal to all fifteen grids of the control system, the power regulator reproduces a sinusoidal power modulation.

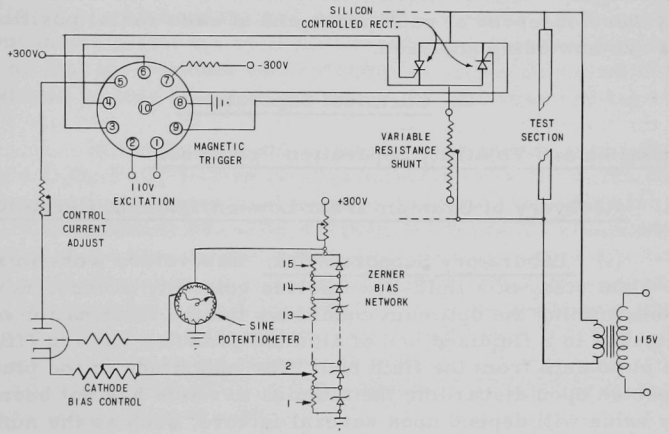

Figure 32. Power Oscillator Control Subunit

The new thin-wall ($\frac{1}{64}$-in.) test section assembly is nearing completion. The mica mat insulation is the only part of the assembly not yet received.

The analysis of the data at 400 psia has been made and no "null" or "notch" in the amplitude versus frequency (Bode diagram) plot has been found. The phase log shows a gradual increase with frequency beginning at zero log at zero frequency (0.01 cps). The amplitude of the zero-frequency void response was 4% peak to peak for a 10% power modulation peak to peak. When the new test section is installed, a low-pressure test will be run where

the theoretical analysis predicts a notch in the low-frequency range (<1 cps). Then the experimental results will be directly compared with the theoretical predictions to test the validity of the model.

d. Propagation of Void Waves in an Air-Water System. Two runs with a square-wave air input have been made, and the signals from the five probes have been recorded on magnetic tape and sampled by an analog-to-digital converter. The playback speed of the probe signals was varied, but due to faulty digital tapes all files were not accepted by the computer. One run, however, was analyzed manually as well as by the computer. On the basis of these results, it appears that the computer program is satisfactory.

Since the reliability of the experimental procedure was verified, a few test runs were made. Five probes were inserted at five different vertical positions, but at a constant radial position. Without changing the operating conditions, records of the probe signals were made at radial positions of r/R = 0.0, 0.14, 0.27, 0.46, 0.64, and 0.82. Four different values of quality were observed at each probe and at each radial position. These test runs are now being analyzed.

G. Chemical Separations

1. Fluidization and Volatility Separation Processes

a. Recovery of Uranium from Low-enrichment Ceramic Fuels.

(i) Laboratory Support Work. Laboratory work in support of the pilot-plant study of a fluid-bed fluoride volatility process is directed toward determining the optimum conditions for the fluorination of U_3O_8-PuO_2 mixtures in a fluidized bed of alumina granules and for efficient removal of plutonium from the fluid bed. The magnitude of the plutonium loss to be expected upon discarding the alumina to waste has not been established, since the value will depend upon several factors, such as the number of times that the alumina bed can be re-used. Current experiments are intended to determine the amount of plutonium retained by the alumina after successive re-use of the bed.

In the preceding report (see Progress Report for May 1964, ANL-6904, pp. 88-89), partial results were given for an experiment which continued the study of the effect of the re-use of the alumina bed material on plutonium retention after multiple additions of feed material, each addition followed by a period of recycle-fluorination. In this experiment, eight additions of a U_3O_8-PuO_2-fission product mixture were made. However, only the quantity of plutonium which had volatilized, >99%, after the first seven additions of feed material was reported. Data on the eighth addition of feed material are now available.

For the first 7 additions of feed material, the concentration of plutonium in the feed was about 0.4 w/o (~1.2 g), and the concentration of a mixture of ten fission product oxides (La_2O_3, CeO_2, Pr_6O_{11}, Nd_2O_3, Sm_2O_3, Eu_2O_3, Gd_2O_3, Y_2O_3, BaO, and ZrO_2) was about 0.85 w/o (~2.6 g). For the eighth addition, the concentrations of plutonium and of the mixture of fission product oxides were increased to about 3 w/o and about 5.3 w/o, respectively. For each addition, the fluorination reaction sequence consisted of a feeding-fluorination period at 450°C, using 20 v/o fluorine in nitrogen; after this period three successive recycle-fluorination periods were carried out with 100% fluorine: a 5-hr period at 450°C, a 5-hr period at 500°C, and a 10-hr period at 550°C. After the recycle-fluorination of the first addition, the alumina bed contained 0.0046 w/o plutonium, whereas after the seventh addition, the bed contained 0.0088 w/o plutonium, which corresponded to a volatilization of 99.4% of the total plutonium (8.13 g) charged in the seven feeding-fluorination periods. Even after the fluorination of the much larger eighth addition of plutonium (8.65 g), the residual plutonium concentration of the bed remained small, 0.018 w/o, and the percentage of the total plutonium charged (16.78 g) which volatilized remained at 99.4%. The results of this experiment indicate that the multiple re-use of an alumina bed appears feasible and that the residual concentration of plutonium retained by the alumina should be less than one percent of the plutonium charged.

In the fluid-bed fluorination experiment in which eight batches of a U_3O_8-PuO_2-fission product mixture were fed to the reactor, the fluoride content (conversion of alumina to aluminum fluoride) and the surface area of the alumina bed after recycle-fluorination of each addition of feed material were also determined in order to correlate these factors with the retention of plutonium on alumina. The conversion of alumina to aluminum fluoride amounted to 1.2% after the recycle-fluorination of the first addition, and showed a moderate increase to 1.8% after the fifth addition. After the sixth and seventh additions, it rose to 2.8% and 3.3%, respectively. However, after the eighth addition, the conversion of alumina to aluminum fluoride was largest, being 7.9%.

The surface area of the alumina changed in a manner parallel to that observed for the fluoride content of the alumina. The surface area of unused 120-mesh alumina is 0.011 m^2/g. The surface area of the alumina was 0.017 m^2/g after the first addition and increased to 0.037 m^2/g after the fifth addition. Corresponding to the abrupt increase in the aluminum fluoride content of the alumina, the surface area of the alumina increased to 0.11, 0.13, and 0.19 m^2/g after the sixth, seventh, and eighth additions, respectively.

(ii) Alpha Decomposition of Plutonium Hexafluoride. The effect of alpha-induced decomposition of plutonium hexafluoride is being investigated as a part of a fundamental study of the radiation behavior of plutonium hexafluoride. Additional data have been obtained on the rate of alpha decomposition

of gaseous plutonium hexafluoride to plutonium tetrafluoride and fluorine (see Progress Report for January 1964, ANL-6840, p. 75). Short-duration experiments were carried out to determine whether a surface-dependent chemical reaction of the PuF_6 with pre-fluorinated, nickel storage vessels would account for the deviation in PuF_6 decomposition rates previously noted in replicate experiments. The extent of such a chemical "corrosion" reaction should be more easily observed in runs of short duration, in which alpha decomposition is expected to be small. In addition, the PuF_6 decomposition data obtained thus far were examined to correlate the effects of this decomposition with plant process operations.

The decomposition rates of samples of plutonium hexafluoride at 100 mm Hg, stored in prefluorinated, nickel spheres (127 ± 2 cc) at 26 ± 2°C, were determined in runs which varied in duration from $\frac{1}{2}$ to 16 days. For each run, the decomposition rate for PuF_6 was calculated from data obtained by two different analytical methods. One method involved determining the weight of PuF_4 formed. The second involved the radiochemical determination of the plutonium content (PuF_4 formed) of an aliquot of a solution resulting from the dissolution of the storage sphere (valve previously removed) and the leaching of the internal surfaces of the removed valve. (However, in one run, the leach solution from the valve was not combined with the dissolved sphere solution, but was analyzed separately.) There is reasonably good agreement in the values for the decomposition rate obtained by these two methods. The results of the runs are summarized in Table XXII. The data show that the PuF_6 decomposition rate is high in the runs of short duration, 0.5, 1, and 2 days, but decreases rapidly in the runs with increasing storage times, 5, 8, 12, and 16 days. In the one run (2-day duration) in which the leach solution for the valve was analyzed separately, about 31% of the total amount of decomposed PuF_6 was found on the internal surfaces of the valve. This decomposition is believed to be due to a corrosion reaction between PuF_6 and the phosphor-bronze bellows in the valve. The bellows were only exposed to PuF_6 during the filling and emptying of the spheres, a period ranging from fifteen minutes to two hours.

The data from these runs, together with previously noted effects of surfaces on the rate of PuF_6 decomposition, indicate that the PuF_6 reacts with the prefluorinated surfaces of the nickel vessel. Very little reaction with nickel is required to account for the observed decomposition. The rate of chemical reaction decreases with time and proceeds at a very low rate after 12 to 16 days. However, the available data are not sufficient to determine the relative contribution of the chemical reaction mentioned above and the influence of the back reaction between PuF_4 and F_2, which is minimal in short-term experiments.

Table XXII. Summary of Data on Alpha-induced Decomposition of Plutonium Hexafluoride

Sample storage vessels: Prefluorinated, nickel spheres of 127 ± 2 cc volume

Storage temperature: 26 ± 2°C

Initial pressure of plutonium hexafluoride: 100 mm Hg

Decomposition Time (days)	Number of Experiments	Average PuF_6 Decomposition Rate (%/day) From Weight of PuF_4 Formed	From Radiochemical Analysis[a]
0.5	5	4.51 ± 1.05	4.16 ± 0.63
1.0	4	1.99 ± 0.25	2.07 ± 0.32
2.0	5	1.22 ± 0.14	1.40 ± 0.26
5.0	5	0.388 ± 0.126	0.690 ± 0.130
8.0	5	0.441 ± 0.039	0.464 ± 0.058
12.0	5	0.480 ± 0.118	0.376 ± 0.032
16.0	2	0.254 ± 0.156	0.328 ± 0.103

[a] The plutonium (from the PuF_4 formed) was determined by alpha-counting methods. The storage vessel (its valve previously removed) was dissolved in a 6 N HNO_3-0.1 M $Al(NO_3)_3$ solution. The interior surfaces of the removed valve were leached with a similar acid solution, and the wash solution was added (except for one experiment) to the solution containing the dissolved sphere. This resulting combined solution was then used for the radiochemical analysis of plutonium.

All data obtained thus far in the study of PuF_6 decomposition have indicated that less gaseous PuF_6 will be lost (i.e., decompose to PuF_4) by reusing a storage vessel. These data also indicate that there will be a decomposition of small amounts of PuF_4 in equipment and lines used to handle PuF_6. The PuF_4 can be recovered without difficulty by refluorination.

(iii) Plutonium Pilot Plant Facility. In the processing of spent oxide fuels by the fluid-bed fluoride volatility process, uranium and plutonium are recovered in the form of volatile hexafluorides. In one process concept, separation of the uranium and plutonium will be accomplished by thermal decomposition of the PuF_6 to the nonvolatile PuF_4. In another, more advanced concept, separation will be done by fractional distillation; then, the PuF_6 product stream, still mixed with some UF_6, will be converted

to mixed PuO_2-UO_2. A 2-in.-dia fluid-bed reactor is being installed in the pilot plant to convert the mixed hexafluorides to oxides by reaction with hydrogen and steam.

In preparation for tests involving plutonium hexafluoride, engineering studies are being made of the conversion of UF_6 to UO_2 particles in a 3-in.-dia Monel fluid-bed reactor. The conversion of UF_6 to UO_2 proceeds by a vapor deposition process in which the newly formed solid products coat the UO_2 particles of the bed. Current work involves the demonstration of an oxidation-reduction method as a replacement for mechanical grinding previously employed to control the particle size of the fluid-bed material (see Progress Report for July 1963, ANL-6764, p. 56). The method consists of effecting particle breakup by oxidizing the UO_2 partially to U_3O_8 and then reducing the oxidized material with hydrogen back to UO_2. The use of the oxidation-reduction method for in-place particle size reduction of an entire bed was evaluated in three complete cycles of particle size reduction (oxidation-reduction) and particle growth (hexafluoride-to-oxide conversion). The oxidation-reduction periods effected a decrease in the average particle size of the uranium oxide bed from 350 μ to about 154 μ, while during hexafluoride conversion periods of 10 to 17 hr the average particle size was increased by nearly a factor of two.

The oxidation-reduction technique, successfully demonstrated in this test, appears useful as an in-column method for resizing a fluid-bed of UO_2 (or UO_2-PuO_2) and thus avoiding extensive handling of the material. No further work is planned.

b. Recovery of Uranium from Highly Enriched Uranium-alloy Fuels by Chlorination and Fluorination Steps.

(i) Bench-scale Studies. Development studies on the chlorination and fluorination steps of a fluid-bed volatility process for recovering uranium from uranium-alloy fuels were continued. Currently, tests are being carried out with uranium-aluminum and uranium-Zircaloy fuels in a $1\frac{1}{2}$-in.-dia fluid-bed reactor. An additional test was made with uranium alloyed with Zircaloy-2 and added selected fission product (FP) elements* to determine the disposition and distribution of fission products and to compare the results with those obtained previously from tests in which simulated fission products were added separately to the fluid-bed material (see Progress Report for February 1964, ANL-6860, pp. 76-77). In the current tests, a modified fluorination technique was employed to obtain data on the effects of time and temperature on the uranium retention by the sintered alumina in the fluid-bed reactor and packed-bed filter.

Two subassemblies of the uranium-Zircaloy-FP alloy were charged to the fluid-bed reactor. Each subassembly weighed 205.5 g and

*The fission product elements were cerium, niobium, ruthenium, molybdenum, barium, and tellurium.

contained 4.0 w/o uranium. The hydrochlorination was carried out for 11 hr at a fluid-bed temperature of 400°C and a packed-bed filter temperature of 350°C. The hydrofluorination step was conducted at 350°C.

The modified fluorination procedure involved four separate steps: (1) heating the fluid bed from 250°C to 400°C in a period of $1\frac{1}{2}$ hr, while the alumina bed material was fluidized with 5 v/o fluorine in nitrogen; (2) reducing, during the next $\frac{1}{2}$ hr, the nitrogen concentration in the reacting gas to nearly zero (~95 v/o fluorine), thereby producing a static-bed condition within the reactor; (3) maintaining the static bed at 400°C for 2 hr; (4) concluding the fluorination at 500°C for 11 hr under static-bed conditions. The fluorine feed rate was 0.4 liter/min (at 70°F and 1 atm) throughout the entire fluorination procedure.

On the basis of uranium analyses of samples periodically withdrawn from the fluid-bed reactor, it appears that a two-temperature fluorination scheme in which initial fluorination at 250°C is followed by fluorination at 500°C is superior to one in which the initial fluorination at 250°C is followed by a final fluorination period at 400°C. In the current test, the uranium concentration of the sintered alumina fluid-bed material at the end of the 400°C fluorination period was 0.066 w/o, whereas in a test in which the final step of the fluorination was conducted at 500°C, the uranium concentration in the alumina was 0.005 w/o (see Progress Report for January 1964, ANL-6840, pp. 73-74). Subsequent fluorination of the alumina bed at 500°C resulted in additional recovery of uranium and the concentration of uranium decreased to 0.009 w/o in 5 hr. Prolonged fluorination of the alumina for an additional 6 hr did not reduce the uranium concentration. Uranium material balances indicated that the uranium recovered amounted to 99.7% of the uranium charged. The two modes of uranium losses were the uranium associated with the sintered alumina bed material (0.3%) and the uranium which passed through the packed-bed filter during hydrochlorination (0.02%).

The distribution of fission product elements alloyed with Zircaloy-2 was similar to that reported previously (see ANL-6860, pp. 76-77). In addition, the fluorination procedure employing static-bed conditions has definite economic merit, since the quantity of fluorine fed to the reactor during the current test was an order of magnitude less than that used in the previous test.

2. Chemical-Metallurgical Process Studies

a. Chemistry of Liquid Metals. In the systematic study of the thermodynamics of a rare earth-cadmium intermetallic system, it is necessary to know the temperature of the eutectic between MCd and M (M = rare earth). These temperatures are being determined by differential thermal

analysis. The following are the provisional values which have been obtained for the eutectic temperatures: 476°C for La-Cd, 417°C for Ce-Cd, 435°C for Pr-Cd, 486°C for Nd-Cd, and 554°C for Sm-Cd.

H. Plutonium Recycle Program

1. Data Analysis

Thermal parameters were calculated for the Hi-C 1.166-cm Δ lattice, with both aluminum and stainless steel clad, by means of multigroup THERMOS, one-group THERMOS, and B692/RP collision probability codes. As expected, the results of the three methods were in close agreement.

A reactivity calculation for the Hi-C 1.166-cm Δ lattice with aluminum clad with the use of constants derived from the original GAM-I library for three fast groups and thermal constants from the THERMOS code yielded a reactivity value about 7-$\frac{1}{2}$% higher than the experimentally determined value. Again, calculated values show increasingly higher reactivity values with decreases in the ratio of water to fuel volumes in the assembly. As noted in previous reports, the major reason for the disagreement appears to be due to the use of the GAM-I cross-section library. The calculations will be repeated with new U^{235} and U^{238} cross sections obtained from Hanford for the GAM-I library. It was previously reported that use of the Hanford values reduced reactivity by about 3% for the Hi-C 1.24-cm square lattice with aluminum clad.

As part of the Plutonium Recycle Experiment, it is planned to irradiate foils to yield meaningful information on the effect of voids, temperature, and, possibly, burnup on the neutron spectrum. THERMOS calculations are being performed to determine whether the ratios of the activation of certain foils (of Eu^{151}, Lu^{176}, Ir^{191}, Ir^{193}, U^{235}, and Pu^{239}) are sensitive to these effects. To facilitate the use of THERMOS, a program has been written to compute Doppler-broadened line shapes from resonance parameters and to punch the resulting cross sections on cards with a format suitable for input to the THERMOS library program.

2. Plutonium Recycle Fuel

Fabrication of the fuel loading for the Plutonium Recycle Experiment is a joint Argonne-Hanford program. The fuel loading is a three-zone loading with plutonium in the central zone, partly enriched uranium in the intermediate shim zone, and natural uranium in the outer blanket zone (see Progress Report for May 1964, ANL-6904, pp. 91-92).

Some of the original plutonium supplied for the Plutonium Recycle loading was found to be contaminated with halides, which had to be removed.

Additional plutonium has been supplied for replacement of the contaminated material. Facilities for converting this additional material to the oxide are being made ready.

A total of 75% of all PuO_2-UO_2 oxide fuel required for the Plutonium Recycle loading has been processed through the Nupac step.

A total of 800 central-type Plutonium Recycle fuel rods acceptable for reactor service have been loaded. 450 rods not acceptable for service will be used in approach to critical and other physics tests at Hanford.

Testing and acceptance of all necessary hardware for loading all PuO_2-UO_2 fuel rods has been completed at Hanford.

All of the components and hardware needed by United Nuclear Corporation for the enriched and natural fuel element loadings have been ordered. All of the Zircaloy-2 strip stock has been delivered and accepted. Approximately 1,000 Zircaloy-2 fuel-jacket tubes have been accepted for loading. Evaluation lots of natural UO_2 pellets, enriched UO_2 pellets containing burnable poison, Zircaloy-2 plug stock, Zircaloy-2 jacket tubing, finish-machined end plugs, stainless steel retainer springs, and stainless steel lower end fittings have been delivered to, inspected, and accepted by ANL.

United Nuclear has begun production of the 144 evaluation rods containing natural UO_2 pellets. All these pellets have been assembled into weighed stack-heights ready for loading into fuel jacket tubing.

All 6% enriched UF_6 has been converted to oxide, and a master blend of enriched high-fired UO_2 with the required concentration of rare earth oxides has been prepared. The first lot of ceramic-grade enriched UO_2 containing the correct proportion of master blend UO_2-rare earth oxide is being processed to finished pellets.

An automated end-plug-to-tube welding process for the fuel rods has been developed to produce consistently sound welds meeting the ANL specification requirements. All forming dies, tooling, and welding facilities are available for the fabrication of fuel element cans and spacer grids. Welding procedures are being developed at United Nuclear for the first group of evaluation fuel cans.

3. Plutonium Recycle Control Rods

The boron-stainless steel for the control rods (see Progress Report for May 1964, ANL-6904, p. 93) was fabricated by Carpenter Steel Co. A total of 34 pieces of strip stock were finished to 0.33 x 28 x 152 cm (0.130 x 11 x 60 in.). The total boron content was specified at 1.75 w/o min. and

2.13 w/o max. A check analysis for boron content in finished strip representing the top, middle, and bottom of each of two separate ingots gave the following results:

Strip from Heat No. V-91077	Boron (w/o)
Top	1.92 - 1.93
Middle	1.93
Bottom	1.93 - 1.94

Strip from Heat No. V-91084	Boron (w/o)
Top	1.86 - 1.87
Middle	1.86 - 1.87
Bottom	1.86 - 1.87

Certified ladle and check analyses for all other alloying additions and impurities, and isotopic analyses for B^{10} content were all within the specified tolerances per Met. Spec. Pu Recycle B-SS-63.

Samples from finished strip representing the top, middle, and bottom of each cast ingot were subjected to a room-temperature bend test. All material withstood a 90° bend around a 1.3-cm ($\frac{1}{2}$-in.) radius for the full thickness of the strip bent parallel to the rolling direction without rupture or without cracking the surface.

All hafnium for the oscillator rod was converted to plate stock by Wah Chang Corporation from material furnished by ANL.

Completed control rods and oscillator rod will be fabricated from boron-stainless steel and hafnium in accordance with Met. Spec. Pu Recycle CR-64. Materials have been furnished to Dresser Products, Inc., Great Barrington, Mass., for the fabrication of the control rods.

4. Pressure Vessel Steel

The 4-in.-thick EBWR pressure vessel steel has been examined to identify final rolling directions prior to cutting up the extremely limited supply of this steel into standard Charpy vee-notch specimens for irradiation in the EBWR when loaded with plutonium fuel.

To accomplish the irradiation surveillance, new irradiation containers and container sealing fixtures will have to be designed and built. The new design will utilize stocks of end closures prepared for the shorter irradiation capsules used previously.

The stainless steel-boron plates have been purchased for the EBWR plutonium fuel storage racks. The alloy is in ingot form at present and will be rolled out into sheets for delivery in 4 to 5 weeks.

IV. ADVANCED SYSTEMS RESEARCH AND DEVELOPMENT

A. Argonne Advanced Research Reactor (AARR)

1. Core Physics

The AARR CYCLE 2 Code (RP 282) with special dimensions[9] is being used to determine burnup. Initially, test calculations were carried out with an 18-group cross-section set with upscattering. However, since these calculations require a long computing time, the 16-group set with no upscattering was used in survey problems to reduce the amount of time required.

In the first problem, the burnup with Sm^{149} added as a burnable poison was computed. Sm^{149} was added in each region in constant ratio to the U^{235}. The clean k_{eff} with additional Sm^{149} present was 1.04 as compared to 1.18 with only equilibrium poison in place. Thus, the initial reactivity worth of the Sm^{149} was about 14%. This problem was run in 8 intervals with

$$\frac{\text{Total fissions over all intervals}}{\text{Total atoms of } U^{235} \text{ initially present}} = 0.2.$$

At the end of the first interval, k_{eff} was up to 1.11, indicating that more than one-half of the Sm^{149} initially present had burned out. The k_{eff} increased slowly at the end of the second and third intervals, and then went into a straight-line decrease to a k_{eff} of 1.06 at the end of the 8th interval.

This corresponds to more than 60 days of operation at 240 MW. Thus an economic and operational gain may be realized by maximizing the fuel content of the core. The reactivity life may be nearly doubled through the increase in fuel inventory obtained by decreasing dead space at the sides and interbox tolerances.

The maximum power in the innermost, high-power region went from a normalized initial value of 3.6 to a final value of 0.3 at the end of the burnup period.

Calculations will next be made with boron in place of samarium in an attempt to obtain a more flattened curve of k_{eff} versus operating time. Europium will also be investigated.

It is planned to investigate the use of various burnable poisons for power depression as well as control utilizing the added flexibility provided by the increased reactivity of the core.

---

[9] Toppel, B., Avery, R., and Fischer, G., Cycle Cost Codes for Fast Reactor Fuel Analysis and Related Costs and Evaluation, Am. Nuclear Society, 5(1), 92.

2. Preliminary Safety Analysis

The outline of the physics work for the preliminary safety analysis is complete. A large portion of the first draft of the physics analysis is written.

The external whole-body doses plus the internal whole-body, bone, and thyroid doses (from inhalation) have been calculated for a ground-level leak at the rate of 0.1 volume % per day from the 1.25×10^6 cu ft AARR containment building (see Progress Report for April 1964, ANL-6885, p. 66 for source of fission products released from core). The direct gamma-ray dose was calculated for an 18-in. ordinary concrete shielding wall and added to the above doses. This case represents the failure of the stack ventilation.

The exclusion-area and the low-population-zone radii are determined by the thyroid dose, and are 420 and 1950 m. The infinite-period bone dose would cause the extension of the low-population radius to beyond 5 km assuming no deposition and a single wind direction. The thyroid dose will be controlling if the bone dose due to the strontium inhaled after 30 days is reduced by more than a factor of 8, assuming the bone dose limit is 25 rads. This factor is probably realized for weather conditions averaged over a few months. In any event the time period is sufficiently long to permit adequate remedial action.

3. Heat Transfer

A comparison was made of the predicted conditions for flow instability by the STDY-3[10] code and the HFIR (High Flux Isotope Reactor) heat transfer tests.[11] The latter were conducted with rectangular flow channels, reduced heat generation rates in the corners, and L/D ratios similar to those planned for AARR. Reported data covered power increases only.

Although this study would not definitely establish the existence of flow instability in the HFIR tests, the experimental procedure did not conclusively establish that flow instability was not a limiting factor. Hence, the resulting study was considered well justified, as shown by the results of Table XXIII.

---

[10] Pyle, R. S., STDY-3, A Program for the Thermal Analysis of a Pressurized Water Nuclear Reactor During Steady State Operation, WAPD-TM-213 (June 1960).

[11] Gambill, W. R., and Bundy, R. D., HFIR Heat-Transfer Studies of Turbulent Water Flow in Thin Rectangular Channels, ORNL-3079 (June 19, 1961).

Table XXIII. Comparison of STDY-3 Flow Instability Calculations with HFIR Critical Heat Flux Test Data

HFIR DATA							STDY-3	
					Channel Test			
Test No.	Inlet Temp, °F	Pressure, psia	Mass Velocity, lb/hr/ft² x 10⁶	Subcooling, °F	Space, in.	Average Heat Flux, BTU/hr/ft²	Average Heat Flux, BTU/hr/ft²	Deviation of STDY-3 from Data, %
1	123.8	560	5.87	26	0.043	3.55	3.25	-8.5
2	123.8	465	6.85	46	0.045	3.84	3.50	-8.8
3	129	535	7.0	90	0.049	3.74	4.00	+7
4	124.2	550	8.5	36	0.053	3.64	3.80	+4.4
5	96.5	566	5.75	54	0.054	2.62	3.00	+14.4
6	91.6	160	11.1	46.5	0.054	3.42	3.82	+11.7
7	120.2	355	17.0	74.9	0.057	6.15	6.75	+9.8
8	112.4	521	7.3	49.3	0.064	3.26	3.80	+16.5
9	113.4	465	8.8	47.1	0.054	3.21	3.90	+21.5
10	116.4	505	8.2	64	0.056	3.01	3.85	+28
11	109.2	462	6.42	4.8% (steam)	0.054	3.19	2.93	-8.2

Table XXIII indicates good agreement for tests 1-7. A channel spacer which did not have a good thermal bond to the test section was used in tests 8-11. Heat was generated in the material covered by the spacer, and perhaps in the spacer, increasing the probability of a heat flux peak or "hot streak" along the spacer. This effect was not estimated by STDY-3, and its neglect leads to the prediction of a more optimistic power as indicated in tests 8-10. Test 11 had net steam generation and was not expected to fit STDY-3 calculations.

This study is being continued with the use of ATR (Advanced Test Reactor) burnout heat transfer data.[12] These tests are believed to be limited by flow instability and will provide a better check of STDY-3. Preliminary results indicate excellent agreement with consistently conservative estimates.

B. Magnetohydrodynamics (MHD)

1. Electromagnetic Condenser

An analytical study of the effects of an electromagnetic field on the film condensation of metal vapors (see Progress Report for April 1964, ANL-6885, p. 68) has been completed. It was concluded that the proposed technique is still practical in both space and terrestrial applications after including energy dissipation (Joule heating). Condensation rates for sodium were shown to increase by factors of two to ten over gravitational condensation by use of an electromagnetic field. However, experimental confirmation is still not available.

[12] Croft, M. W., Advanced Test Reactor Burnout Heat Transfer Tests, ATR-FE-102 (Jan 1964).

The efficiency of the process was shown to depend strongly upon a new parameter which indicates the amount of electrical energy dissipated relative to the amount of thermal energy liberated by condensation.

2. MHD Power Generation - Jet Pump Studies

A design layout is being prepared for the fabrication of a converted jet pump, based upon the features studied in the steam models used in current experiments. The essential difference between the standard and converted jet pump lies in the change in the injector cross section. Predominantly, this change consists of converting the standard circular cross section to a rectangular configuration. In this way the flattened structure of the high-velocity section will be adaptable to the insertion of the modified unit between the poles of a magnet during the studies performed with liquid metal. Appropriate arrangements are also being made to allow flexibility in the positioning of the combiner section relative to the motivating nozzle.

The 5-kW magnet and associated power supply have been received. Flux and power measurements have shown that the unit adequately meets all of the specification requirements.

A throttling calorimeter is being constructed to determine the quality of the steam supplied to the operating experimental jet pump. This is necessary since some question exists with respect to the thermodynamic energy state of the inlet steam. Determination of this parameter will allow a more accurate assessment of the operating efficiency of the rectangular nozzle.

3. MHD ac Generator Flashing Cycle

An MHD generator (see Figure 33) which produces dc pulses has been completed and operated. Slugs of NaK are introduced into a duct, followed by nitrogen gas. The gas pressure drives the slug through the magnetic field where it contacts electrodes and produces a dc pulse of power. An oscillograph tracing of typical data is shown in Figure 34.

The formation, integrity, conductivity, and reaction to magnetic field and gas pressure are being studied. When the dc pulses are adjusted to the proper width and shape, they will be combined and used to feed a transformer to generate ac electrical power. Present frequency of pulses is 30/sec. The data indicate that higher frequencies are possible. Present drive gas pressures as measured with the transducer in the pulsator are 30-40 psi. Drive gas pressures up to 150 psi in the pulser will be used.

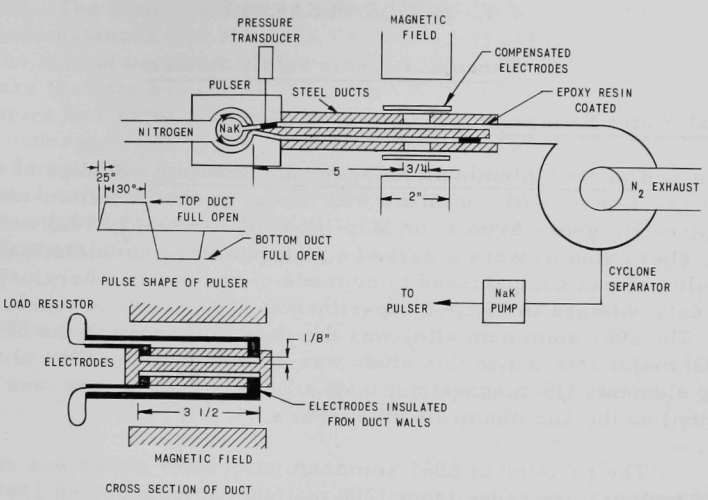

Figure 33. Schematic Diagram of an MHD Generator

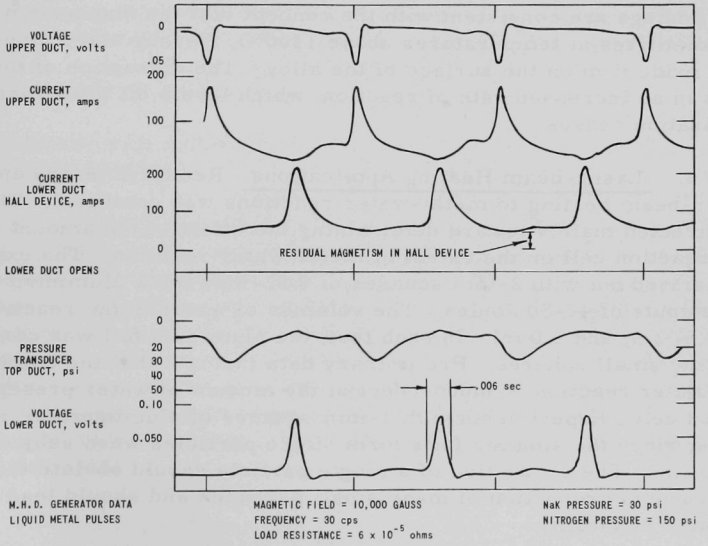

Figure 34. Pulses Observed from an MHD Generator

V. NUCLEAR SAFETY

A. Thermal Reactor Safety Studies

1. Metal-Water Reactions

a. The 6061 Aluminum Alloy-Water Reaction. Studies of the isothermal reaction of 6061 aluminum with steam by the levitation-melting method (see Progress Report for May 1964, ANL-6904, p. 102) were completed. These studies were a part of a program to accumulate data that would allow direct comparisons to be made of results of laboratory experiments, data obtained in TREAT experiments, and results of reactor meltdowns. The 6061 aluminum alloy was the base alloy used in the SPERT-ID core. Of major interest in this study was the effect of the 6061 aluminum alloying elements (1% magnesium, 0.6% silicon, 0.25% copper, and 0.25% chromium) on the aluminum-steam reaction.

The reaction of 6061 aluminum alloy with steam was studied over the temperature range from 1200 to 1600°C. At 1200 and 1300°C, the reaction followed a cubic rate law. At 1400°C, the reaction rate increased rapidly after 10 min. At 1500 and 1600°C, the extent of reaction achieved in about 10 min was 15 mg of aluminum reacted per sq cm, and the rates appeared to be independent of temperature and nearly independent of time. These findings are consistent with the concept that the magnesium in the alloy volatilizes at temperatures above 1400°C, thereby disrupting the protective oxide film on the surface of the alloy. The disruption of the film results in an increased rate of reaction, which levels off after magnesium volatilization ceases.

b. Laser-beam Heating Applications. Research on the application of laser-beam heating to metal-water reactions was continued. The studies were directed mainly toward determining the effect of the amount of water in the reaction cell on the extent of metal-water reaction. The experiments were carried out with 2-mm squares of 0.02-mm-thick aluminum foil, using laser outputs of 44-50 Joules. The volumes of water in the reaction cell were 0.5, 2.5, and 5.0 ml. In each test, the aluminum foil was converted into many small spheres. Preliminary data indicate that the extent of metal-water reaction is independent of the amount of water present in the reaction cell. Experiments with 1-mm squares of aluminum foil are being planned, since the smaller foils form single particles when subjected to a laser beam. The production of a single particle should obviate the effect of the random production of many small particles and should lead to data of greater reliability.

c. Studies in TREAT of Oxide-core, Zircaloy-2-clad Fuel Pins. Studies were continued of the reaction of water with UO_2-core, Zircaloy-2-clad fuel pins when the pins, immersed in water, are exposed to TREAT

transients. The main purpose of these studies is to obtain kinetic data under circumstances that simulate a power excursion or a runaway incident. The data of particular importance to the analysis of reactor safeguards are the rate and extent of reaction between molten metals at high temperature and water. Information on the degree of subdivision that a fuel pin undergoes during the course of a transient is important to the understanding of the metal-water reaction. In current work, emphasis has been placed on the reaction of water with UO_2-core, Zircaloy-2-clad fuel, since this type of fuel is of interest to the technology of water-cooled power reactors.

In the experiments, a single fuel pin is submerged in water contained in a stainless steel capsule or autoclave. The autoclave, with a graphite crucible as its primary container, is capable of withstanding the high temperatures and pressures generated during the meltdown that is initiated by fission heating resulting from the TREAT neutron pulse. During the power excursion, the pressure in the autoclave is measured by means of a strain gauge transducer. Since radiation can also cause the transducer to produce an output signal, the transducer is located outside of the reactor core to reduce the effect of radiation. After the irradiation has been completed, a sample of the gas phase in the autoclave is taken, and the hydrogen content of the gas is determined by means of a mass spectrometer. From the amount of hydrogen present in the gas phase and the known weight of zirconium in the fuel pin, the amount of zirconium that reacted with water is computed from the following stoichiometry:

$$Zr + 2H_2O \rightarrow ZrO_2 + 2H_2.$$

Finally, particle size determinations of the fragmented fuel are made by a sieve-screen analysis.

The results of the experiments are given in Figure 35 and in Table XXIV. In Figure 35, each datum is located by its extent of reaction (%) and by its fission energy input (cal/g of core). Figure 35 also gives the data obtained in previous experiments with mixed oxide* core, Zircaloy-2-clad fuel pins. To place the two sets of data on the same basis, two energy scales and one temperature scale are used in the figure. It should be noted that the two energy scales have been placed so as to give correspondence with the single temperature scale by choosing a melting point of 2700°C as the fixed point of comparison. Table XXIV gives the data on pressures and particle sizes.

*Mixed oxide is 81.5 w/o ZrO_2-9.06 w/o CaO-0.74 w/o Al_2O_3-8.69 w/o uranium oxide (93% enriched).

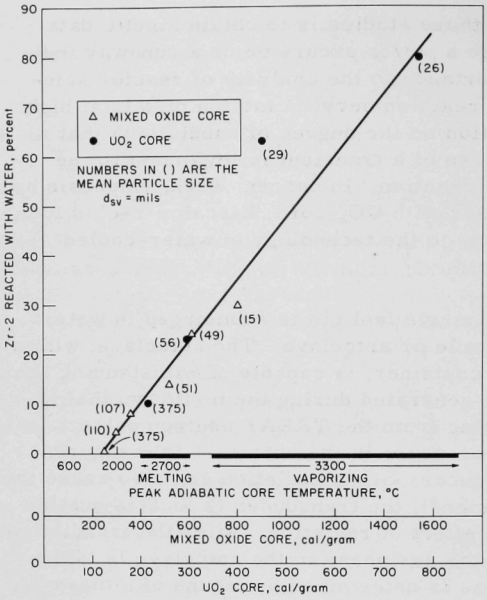

Figure 35

Results of Meltdown Experiments in TREAT on UO_2-core and Mixed Oxide-core, Zircaloy-2-clad Fuel Pins Submerged in Water

Table XXIV. TREAT Metal-Water Meltdown Experiments with UO_2 Core-Zr-2 Clad Fuel Pins

Conditions: The fuel pins were submerged in room-temperature water with a total pressure of 20 psia initially in the autoclave. Each fuel pin was a single pellet of 11.2% enriched UO_2, clad with 20-mil-thick Zircaloy-2. The UO_2 pellet was of 80% theoretical density. The overall dimensions of the fuel pin were 375-mil dia x 0.535-in. length.

	CEN Transient Number		
	181	175	173
Reactor Characteristics			
Integrated Power, MW-sec	323	505	867
period, ms	72	52	39
Results			
1. Reaction of metal, % of Zircaloy-2 reacted with water	23	63	80
2. Pressure in autoclave			
peak pressure, psi	61	180	480
max rate of rise, psi/ms	0.025	0.6	1.5
3. Temperature of UO_2 core of fuel pin, temperature peak, adiabatic, °C	2800 (melted)	3300 (part vapor.)	3300 (part vapor.)
4. Energy release			
nuclear, cal/g UO_2 core	287	450	771
chemical, cal/g of Zircaloy-2 cladding	360	983	1250
portion of total energy release of chemical origin, %	27	40	32
5. Particle size of fragmented fuel pin			
d_{sv}, mean particle size of core and clad, mils	56	29	26
d_{sv}, of clad, mils	70	34	45

These data plus those accumulated from previous TREAT experiments have been utilized to draw the following conclusions concerning the UO_2-core, Zircaloy-2-clad fuel pins:

(1) The behavior of UO_2-core fuel pins is similar to that of mixed-core fuel pins from the standpoint of the chemical or metal-water hazards problem.

(2) In reactor transients in which the oxide core is heated to the melting temperature (about 2700°C), from 10 to 20% of the Zircaloy-2 reacts with water. In reactor transients in which the oxide core is heated to the vaporization temperature (about 3300°C), from 60 to 80% of the Zircaloy-2 reacts with water.

(3) Comparison of the results of experiments with Zircaloy-2-clad fuel pins with the results of previous experiments with Type 304 stainless steel-clad pins (see Progress Reports, ANL-6880, p. 73; ANL-6840, p. 93) indicates that, for a given peak adiabatic core temperature, Zircaloy-2 reacts to a greater extent with water than does Type 304 stainless steel. Moreover, the dependence of the extent of the metal-water reaction on the energy input is greater in the case of Zircaloy-2 than it is in the case of stainless steel. The much larger extent of the zirconium-water reaction at high temperatures, as compared with the extent of the stainless steel-water reaction, may result from the loss of protectiveness of the ZrO_2 film on the cladding when the temperature of the cladding reaches 2700°C, the melting point of ZrO_2.

(4) Both the peak pressure in the autoclave and the rate of the pressure rise increase as the energy of the reactor pulse is increased. No explosive pressure increases were observed in tests with oxide-core, Zircaloy-2-clad fuel pins; the most rapid increase in pressure was 1.5 psi/ms. This rate is low compared with rates in steam explosions. In the case of the SPERT-1, plate-type core (U-Al alloy) meltdown, the rate of pressure rise was about 20 psi/μsec.

(5) The cylindrical UO_2 core and the Zircaloy-2 cladding are converted into small fragments and particles in destructive meltdown experiments. When the energy input is only sufficient to heat the UO_2 core to its melting temperature (about 2700°C), the Sauter mean diameter, d_{sv},*

---

* $d_{sv} = \dfrac{1}{\sum_{i=1}^{N} w_i/d_i}$, where d_i = average diameter of the i^{th} size group, w_i = fraction by weight of particles in the i^{th} group, and N is the number of size groups.

of the resulting particles is 56 mils. When the pulse is sufficiently energetic to cause particle vaporization of the UO_2, the mean diameter of the particles ranges between 26 and 29 mils. The particles resulting from the UO_2 core are smaller than those resulting from the cladding. Since the diameter of the original fuel pin is 375 mils, it is evident that the specific surface area undergoes a considerable increase as a result of a meltdown; for example, a 14-fold increase in surface area occurs when a mean diameter of the particles formed is 26 mils.

(6) For a nuclear power excursion having an energy release of 287 cal/g of UO_2 core (on a 72-ms period), the extent of the Zircaloy-2-water reaction is 23% and the chemical energy released is 360 cal/g zirconium. For this case, the chemical energy released is 27% of the total energy released during the transient. For a transient in which the energy imparted is 450 cal/g of UO_2 core (on a 52-ms period), the extent of the Zircaloy-2-water reaction is 63%. For this case, the chemical energy released is 40% of the total energy. It is evident, therefore, that the energy released in the exothermic zirconium-water reaction is a substantial percentage of the initiating fission energy.

(7) In general, as the energy of a nuclear power transient increases, each of the following also increases: the extent of metal-water reaction, the final total pressure, the rate of pressure rise, the chemical energy release, the surface area of the fragmented fuel, and the peak fuel temperature.

d. Studies of Preirradiated Fuels in TREAT. A second TREAT experiment was completed with an aluminum-17 w/o uranium alloy fuel plate (SL-1 composition) to determine the effect of preirradiation on the extent of the metal-water reaction. The conditions and results of this test (CEN-182) and of a previous test (CEN-180) with aluminum-uranium fuel are summarized in Table XXV. In both runs, the fuel was preirradiated to a 2.2% burnup of the heavy atoms. The results of these tests and of previous tests (see Progress Report for March 1964, ANL-6880, p. 73) indicate that preirradiation does not influence the extent of metal-water reaction.

Table XXV. Metal-Water Meltdown Experiments in TREAT with Preirradiated SL-1 Fuel Plate Samples[a]

	CEN Transient Number	
	180	182
Reactor Characteristics		
Integrated Power, MW-sec	691	985
Period, ms	43	39
Results		
Calculated Energy Input, cal/g	520	745
Appearance of Metal after Transient	globule and some fines	globule and some fines
Metal Reacted with Water, %	10.0	23.8

[a]Composition of fuel samples was 81 w/o Al, 17 w/o U, and 2 w/o Ni. The samples, which had been preirradiated to a 2.2% burnup of the heavy atoms, were submerged in water at 22°C.

2. Metal Oxidation-Ignition Studies

a. Uranium-Plutonium Alloys. Studies of the ignition temperatures of uranium-plutonium ternary alloys are being continued. These studies are being carried out to find an alloy of suitable composition for zero power critical experiments.

The results of the studies may be summarized as follows: Although ternary alloys of 6 a/o titanium or vanadium with uranium-20 a/o plutonium and alloys of 6 a/o of aluminum, carbon, copper, iron, or zirconium with uranium-30 a/o plutonium have improved ignition resistance, as compared with the appropriate binary uranium-plutonium alloys, ternary alloys containing 6 a/o of iron or molybdenum show the greatest resistance to ignition. However, the ignition behavior of the 6 a/o Fe-30 a/o Pu-U alloy was considerably affected by its method of fabrication, and a 6 a/o Fe-18 a/o Pu-U alloy showed no improvement in ignition behavior as compared with a 18 a/o Pu-U alloy. On the other hand, ternary alloys containing 6 a/o molybdenum and either 20 a/o or 30 a/o plutonium were nearly as resistant to ignition as is uranium. Ternary alloys with smaller concentrations of molybdenum were also tested. Uranium alloys containing 20 a/o plutonium with either 3 or 4.5 a/o molybdenum showed somewhat less resistance to ignition than that obtained with the 6 a/o molybdenum alloys, but a greater resistance than that obtained with a binary uranium-20 a/o plutonium alloy.

b. Aluminum-U_3O_8 Reaction. Additional studies were made of the aluminum-U_3O_8 thermite reaction (see Progress Report for March 1964, ANL-6880, p. 74). A report[13] of a very violent thermite reaction in aluminum-U_3O_8 cermets led to the re-examination of this reaction. The violent reaction was reported to occur in pressed compacts containing 74.5 to 89.8 w/o U_3O_8. The violent reaction was initiated at temperatures in the range from 800 to 1000°C and was characterized by spontaneous self-heating to a temperature of about 2200°C at rates of several thousands of degrees per second.

The violent reaction was recently reproduced at Argonne with pressed compacts of aluminum-83 w/o U_3O_8 when the compacts were inserted into a furnace at 1250°C. The violent reaction was observed as a second exothermic pulse and was observed only with compacts that had been previously sintered at 600°C. Rapid heating of unsintered compacts did not result in a violent reaction, although a moderate second exothermic pulse did occur. A sintered compact of aluminum-75 w/o U_3O_8 also showed a substantial increase in its self-heating rate and reached a somewhat higher temperature during a single pulse as compared with unsintered compacts of the same composition.

---

[13] Fleming, J. D., and Johnson, J. W., Nucleonics, 21(5), 84 (1963).

B. Fast Reactor Safety Studies

Two of the most important factors influencing the safety characteristics of fast power reactors are the large quantity of fuel and the short prompt-neutron lifetime. Therefore, it is possible to postulate a class of "meltdown" accidents, consisting of multistage incidents proceeding as follows: (1) some operating abnormality occurs in which the fuel undergoes failure; (2) material movements occur, which produce a more reactive configuration; and (3) a destructive burst of nuclear energy terminates the accident. The mechanisms involved in fuel failure and the material movement are complex. They are being studied experimentally in a program centering on tests being performed in the TREAT reactor.

1. Experiments in the Integral TREAT Loop

The first transient experiments were performed in the Mark-I integral TREAT loop, designed to fit into the 10-cm-square by 240-cm-long space of one TREAT fuel element, and to permit exposure of 1-7 EBR-II-type pins in a flowing sodium environment. For the initial tests, one loop was used, loaded with a single 4.1% enriched U^{235} EBR-II pin surrounded by six dummy pins on an EBR-II pitch. The loop was instrumented with: (1) stainless steel-sheathed chromel-alumel thermocouples placed in the sodium at the inlet and outlet of the loop test section; (2) a tantalum-sheathed tantalum-molybdenum thermocouple cast into the sample pin; and (3) pressure transducers located at the inlet and outlet of the test section. Transient records from the tests are being analyzed. Maximum recorded sample temperatures and reactor energy releases for the initial series of tests are given in Table XXVI.

Table XXVI. Results of Tests in the Integral TREAT Loop

Test	Sodium Flow, m/sec	Maximum Sample Temp, °C	TREAT Energy, MW-sec
1	0	650	47.8
2	1.8	610	45.9
3	0	1030	90
4	1.8	1200	105
5	1.8	1270	143
6	0	1280	144

The fabrication of the loop shipping container has been completed and is being shipped to Idaho. The container will be used to return the loop to Du Page site for post-mortem inspection.

2. Large TREAT Loop

The insulation specification and installation instruction for the large TREAT loop has been prepared. This text includes a set of equipment arrangement, heater-location, and piping drawings, including the gas system.

Currently, the gas system is being modified to include the addition of two vent lines connecting the header with the dump and the storage vessels. There is also an inert-gas pressurizing line which will serve to break any "siphon action" that may develop in the test section. Each of the three lines will include a pneumatic-operated, bellows-sealed valve located near the header. Air, for the pneumatic valves, and the inert gas to break the siphon action will be piped up the side and across the top of the reactor to this equipment.

At a meeting between Reactor Engineering and Idaho, it was decided that Idaho would be responsible for:

(1) insulation of the loop and components under the above specifications and instructions as supplied by Reactor Engineering;

(2) radiography of all field welds which will be made in the course of the construction;

(3) on-site fabrication of the shielding blocks for the isolation wall.

3. Small TREAT Loop

The checkout of the remote disassembly equipment has continued. It is expected that the recently irradiated loop will be available on site for operational manipulation in mid-July, although it will not be necessary to use remote equipment on the first fuel capsule.

VI. PUBLICATIONS

Papers

THE ROLE OF COPRECIPITATION IN ALLOY PARTITION DURING THE CRYSTALLIZATION OF TERNARY SYSTEMS

J. L. Moriarty, Irving Johnson, and H. M. Feder
Trans. Met. Soc. AIME 230, 777-780 (June 1964)

LATERAL SOLIDS MIXING IN FLUIDIZED-PACKED BEDS

J. D. Gabor
AIChE Journal 10(3), 345-350 (May 1964)

HEAT TRANSFER IN FLUIDIZED-PACKED BEDS AS APPLIED TO THE FLUORINATION OF URANIUM DIOXIDE PELLETS

J. D. Gabor, W. J. Mecham, and A. A. Jonke
Nuclear Engineering, Part X. Chem. Eng. Progr. Symp. Ser. 60(47), 96-104 (1964)

HALOGENATION STUDIES ON NUCLEAR-FUEL-ELEMENT MATERIALS IN A TWO-ZONE FLUID-BED REACTOR

N. M. Levitz, J. J. Barghusen, J. T. Holmes, and A. A. Jonke
Nuclear Engineering, Part X. Chem. Eng. Progr. Symp. Ser. 60(47), 84-85 (1964)

PILOT PLANT STUDIES OF A DIRECT FLUORINATION PROCESS APPLIED TO URANIUM DIOXIDE REACTOR FUELS

W. J. Mecham, J. D. Gabor, and A. A. Jonke
Nuclear Engineering, Part X. Chem. Eng. Progr. Symp. Ser. 60(47), 76-83 (1964)

HEAT CAPACITY OF PLUTONIUM MONOCARBIDE FROM 400° TO 1300°K

O. L. Kruger and H. Savage
J. Chem. Phys. 40(11), 3324-3328 (June 1, 1964)

A SIMULATION OF A GENERALIZED THERMAL RADIATING FIN

Marion J. Janicke and L. C. Just
Simulation 2(6), 19-22 (June 1964)

ANALYSIS OF A NUCLEAR REACTOR SUPPORT STRUCTURE

A. H. Marchertas and G. M. Smith
Journal of Spacecraft and Rockets 1(3), 247-252 (May-June 1964)

ERRORS IN NOISE MEASUREMENTS DUE TO THE FINITE AMPLITUDE RANGE OF THE MEASURING INSTRUMENT
C. E. Cohn
Rev. Sci. Instr. 35, 701-703 (June 1964)

COLLISION PROBABILITIES IN CYLINDRICAL LATTICES
E. M. Pennington
Nucl. Sci. Eng. 19, 215-220 (June 1964)

"ON-LINE" OPERATION OF A DIGITAL COMPUTER IN NUCLEAR PHYSICS EXPERIMENTS
J. F. Whalen, J. W. Meadows, and R. N. Larsen
Rev. Sci. Instr. 35, 682-690 (June 1964)

The following papers were presented at "A Symposium on High Temperature Conversion - Heat to Electricity," sponsored by The University of Arizona in cooperation with Argonne National Laboratory, at Tucson, Arizona, February 26-March 2, 1964, and appear in the Proceedings, TID-7687:

SYMPOSIUM INTRODUCTION
B. I. Spinrad
pp. 1-9

THE DEVELOPMENT OF NUCLEAR THERMIONIC MATERIALS
James F. Schumar
pp. 27-44

HIGH TEMPERATURE CONVERSION HEAT TO ELECTRICITY
H. K. Richards
pp. 161-199

Transactions of the American Nuclear Society, 7(1) (June 1964):

DIMENSIONS OF PLUTONIUM CORES BY EXTRAPOLATION OF PERTURBED URANIUM CORES
David Meneghetti and Hiroshi Ishikawa
p. 37

AN ADAPTIVE AUTOMATIC CONTROL OF A NUCLEAR REACTOR FOR A MINIMAL TIME RESPONSE
Isaac Kliger
pp. 59-60

THE FAST REACTOR TEST FACILITY
N. J. Swanson, O. S. Seim, and J. D. Geier
pp. 175-176

SOME METALLURGICAL CONSIDERATIONS IN THE DESIGN AND OPERATION OF LIQUID-METAL SEALS
B. Blumenthal, L. R. Kelman, and H. V. Rhude
p. 190

REPLACEMENT OF MAJOR COMPONENTS IN SODIUM-COOLED REACTOR SYSTEMS
Ernest Hutter
pp. 190.191

THE DESIGN OF A 1000-MWe FAST-BREEDER REACTOR
C. E. Klotz, R. S. Miller, E. A. Fischer, J. B. Nims, R. G. Palmer, and G. R. Winders
p. 196

USE OF DEPLETED URANIUM IN THERMAL REACTORS WITH SLIGHTLY ENRICHED FUEL TO ACHIEVE HIGH NEUTRON ECONOMY AND BURNUP
H. P. Iskenderian
pp. 197-198

ANL Reports

ANL-6728 A PULSED ELECTROMAGNETIC TEST SYSTEM APPLIED TO THE INSPECTION OF THIN-WALLED TUBING
C. J. Renken

ANL-6733 A TWO-ZONE FAST CRITICAL EXPERIMENT (ZPR-III ASSEMBLY 42)
P. I. Amundson, R. L. McVean, and J. K. Long

ANL-6743 SOME APPLICATIONS OF SCINTILLATION SPECTROMETRY TO NONDESTRUCTIVE TESTING
Ronald B. Perry

ANL-6772 MEASUREMENT OF WATER-CHANNEL GAPS IN EBWR CORE-I FUEL ELEMENTS
C. F. Reinke and W. N. Beck

ANL-6799 A SHIELDED ENCLOSURE FOR NEUTRON RADIOGRAPHIC INSPECTION OF ENCAPSULATED, IRRADIATED SPECIMENS
W. N. Beck and H. Berger

ANL-6854 EFFECT OF A TRANSVERSE MAGNETIC FIELD ON VERTICAL TWO-PHASE FLOW THROUGH A RECTANGULAR CHANNEL
Richard J. Thome

ANL-6875 CHEMICAL ENGINEERING DIVISION RESEARCH HIGHLIGHTS, May 1963-April 1964